

AD-A064 911

LIVERPOOL UNIV (ENGLAND) DEPT OF METALLURGY AND MAT--ETC F/G 11/6  
HIGH TEMPERATURE OXIDATION AND CORROSION OF IN-SITU COMPOSITE A--ETC(U)  
OCT 78 D M JOHNSON, D P WHITTLE, J STRINGER AFOSR-75-2785

UNCLASSIFIED

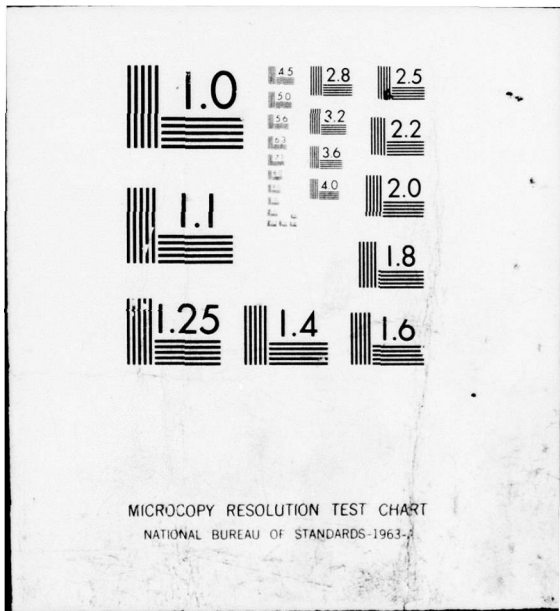
AFML-TR-78-137

NL

1 of 2

AD  
A064911





ADA 064911

DDC FILE COPY

✓

② LEVEL II

AFML-TR-78-137

# HIGH TEMPERATURE OXIDATION AND CORROSION OF IN-SITU COMPOSITE ALLOYS

DEPARTMENT OF METALLURGY AND MATERIALS SCIENCE  
UNIVERSITY OF LIVERPOOL  
LIVERPOOL L69 3BX  
ENGLAND

OCTOBER 1978

TECHNICAL REPORT AFML-TR-78-137  
Final Report - 1 January 1975 - 31 December 1977

DDC  
RECEIVED  
FEB 26 1979  
B

Approved for public release; distribution unlimited.

AIR FORCE MATERIALS LABORATORY  
AIR FORCE WRIGHT AERONAUTICAL LABORATORIES  
AIR FORCE SYSTEMS COMMAND  
WRIGHT-PATTERSON AIR FORCE BASE, OHIO 45433

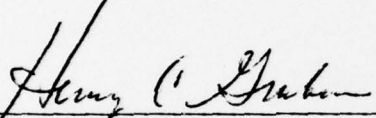
79 02 21 067


NOTICE

When Government drawings, specifications, or other data are used for any purpose other than in connection with a definitely related Government procurement operation, the United States Government thereby incurs no responsibility nor any obligation whatsoever; and the fact that the government may have formulated, furnished, or in any way supplied the said drawings, specifications, or other data, is not to be regarded by implication or otherwise as in any manner licensing the holder or any other person or corporation, or conveying any rights or permission to manufacture, use, or sell any patented invention that may in any way be related thereto.


This report has been reviewed by the Information Office (OI) and is releasable to the National Technical Information Service (NTIS). At NTIS, it will be available to the general public, including foreign nations.

This technical report has been reviewed and is approved for publication.

  
HENRY C. GRAHAM  
Project Engineer

  
NORMAN M. GEYER  
9T Focal Point

FOR THE COMMANDER

  
NORMAN M. GEYER  
ACTING CHIEF  
Processing and High Temperature Materials Branch  
Metals and Ceramics Division

"If your address has changed, if you wish to be removed from our mailing list, or if the addressee is no longer employed by your organization please notify AFML/LLM, WPAFB, OH 45433 to help us maintain a current mailing list."

Copies of this report should not be returned unless return is required by security considerations, contractual obligations, or notice on a specific document.

<b>REPORT DOCUMENTATION PAGE</b>		READ INSTRUCTIONS BEFORE COMPLETING FORM	
1. REPORT NUMBER AFML-TR-78-137	2. GOVT ACCESSION NO.	3. RECIPIENT'S CATALOG NUMBER	
4. TITLE (and Subtitle) High Temperature Oxidation and Corrosion of In-Situ Composite Alloys		5. TYPE OF REPORT & PERIOD COVERED Final Report 1 Jan 1975 - 31 Dec 1977	
7. AUTHOR(s) D.M. Johnson, D.P. Whittle and J. Stringer		6. PERFORMING ORG. REPORT NUMBER	
9. PERFORMING ORGANIZATION NAME AND ADDRESS Department of Metallurgy and Materials Science University of Liverpool Liverpool L69 3BX		8. CONTRACT OR GRANT NUMBER(s) AFOSR-75-2785 <i>new</i>	
11. CONTROLLING OFFICE NAME AND ADDRESS Air Force Materials Laboratory (LLM) Wright-Patterson AFB, Ohio 45433		10. PROGRAM ELEMENT, PROJECT, TASK AREA & WORK UNIT NUMBERS 61102F 2306P304	
14. MONITORING AGENCY NAME & ADDRESS (if different from Controlling Office) European Office of Aerospace Research and Development, 223-231 Old Marylebone Road, London N.W.1 5th, England		12. REPORT DATE October 1978	
16. DISTRIBUTION STATEMENT (of this Report) Approved for public release; distribution unlimited. <i>12 132p.</i>		13. NUMBER OF PAGES <i>17</i>	
17. DISTRIBUTION STATEMENT (of the abstract entered in Block 20, if different from Report)		15. SECURITY CLASS. (of this report) Unclassified	
18. SUPPLEMENTARY NOTES		15a. DECLASSIFICATION/DOWNGRADING SCHEDULE	
19. KEY WORDS (Continue on reverse side if necessary and identify by block number) Directional solidification; delta-lamellae; carbides; in-situ composites; oxidation resistance; hot corrosion sulphidation.			
20. ABSTRACT (Continue on reverse side if necessary and identify by block number) The high temperature oxidation and corrosion behavior of a number of direction- ally solidified eutectic alloys were studied in the temperature range 1600- 2000 Degrees F; these include gamma/gamma prime-delta alloys and alloys con- taining Tantalum Carbide or Cr Sub 7 C sub 3 fibers. With all the alloys the important factor appears to be whether or not a fiber-free zone is established between the surface scale and the alloy eutectic structure, and this in turn depends in a complex way on temperature, the degree of alignment and spacing of the eutectic, and the composition of the alloy. (Over)			

D D C  
RECEIVED  
FEB 26 1979  
B

402618

B

SECURITY CLASSIFICATION OF THIS PAGE(When Data Entered)

Tantalum Carbide fibers are very oxidation prone, and alloys containing this phase have poor overall resistance; Cr sub 7 C sub 3 or delta (Ni sub 3 Nb) are not as detrimental.

SECURITY CLASSIFICATION OF THIS PAGE(When Data Entered)

FOREWORD

This Final Report covers the work performed on the project "High Temperature Oxidation and Corrosion of In-Situ Composite Alloys" and was prepared by the Department of Metallurgy and Materials Science, University of Liverpool, Liverpool L69 3BX, United Kingdom, under Air Force Contract AFOSR-75-2785.

The work was performed under the direction of D.P. Whittle as the Program Manager. Dr. Henry C. Graham, AFML/LLM was the Technical Manager for the Air Force.

ACCESSION for		
NTIS	White Section	<input checked="" type="checkbox"/>
DDC	Buff Section	<input type="checkbox"/>
UNANNOUNCED		<input type="checkbox"/>
JUSTIFICATION		
BY		
DISTRIBUTION/AVAILABILITY CODES		
Dist. A IRL and/or SPECIAL		
A		

TABLE OF CONTENTS

	PAGE
INTRODUCTION	1
Oxidation and Hot Corrosion Mechanisms of the Ni <sub>3</sub> Nb-Ni <sub>3</sub> Al-Based Eutectic Alloys	
(a) Oxidation	2
(b) Hot Corrosion	7
Oxidation and Hot Corrosion Mechanisms of Carbide Strengthened Eutectic Alloys	
(a) Oxidation	
(i) Cr <sub>7</sub> C <sub>3</sub> -Reinforced Co-Base Alloys	7
(ii) TaC or NbC-Reinforced Co & Ni Alloys	9
(iii) Cr <sub>7</sub> C <sub>3</sub> -Reinforced Ni-Base Alloys	11
(b) Hot Corrosion	
(i) Cr <sub>7</sub> C <sub>3</sub> - Reinforced Co-Base Alloys	12
(ii) Co-Cr-TaC	12
(iii) Ni-Cr-Al-C	13
PRESENT INVESTIGATION	
Ni <sub>3</sub> Nb-Ni <sub>3</sub> Al Based Eutectic Alloys	13
Carbide-Based Eutectic Alloys	14
EXPERIMENTAL	14
RESULTS	
Ni <sub>3</sub> Nb-Ni <sub>3</sub> Al Based Eutectic Alloys	
(a) Oxidation	
Ni-23.1Nb-4.4Al	16
Ni-19.7Nb 6Cr-2.5Al	19
(b) Formation of the $\delta$ -Free Zone	20
(c) Hot Corrosion	
Ni-23.1Nb-4.4Al	21
Ni-19.7Nb-6Cr-2.5Al	24
Carbide-Based Eutectic Alloys	
(a) Oxidation	
(i) Co-Cr-C	26
(ii) Co-Cr-TaC	28
(iii) Ni-Cr-Al-C	30
(b) Hot Corrosion	
(i) Co-Cr-C	31
(ii) Co-Cr-TaC	33
(iii) Ni-Cr-Al-C	35
DISCUSSION	
Ni <sub>3</sub> Al-Ni <sub>3</sub> Nb-Based Eutectic Alloys	
(a) Oxidation	37
(b) Hot Corrosion	45
Carbide-Based Eutectic Alloys	
(a) Oxidation	51
(b) Hot Corrosion	53



TABLE OF CONTENTS (cont)

REFERENCES

Page

119

APPENDIX

122

LIST OF TABLES

TABLE		PAGE
I	Growth of the Free Zone	21
I	Summary of the Oxide Scale Structures Formed on Co-41Cr-2.4C Alloys	26
II	Parabolic Rate Constants for the Oxidation of the Various Directionally Solidified Eutectic Alloys	27
III	Depths of Oxide Penetration for the Oxidation of the Various Eutectic Alloys	28
IV	Approximate Parabolic Rate Constants for the Directionally Solidified Eutectic Alloy Co-41Cr-2.4C Cooled at 10.6 cm/h.	32
V	Approximate Parabolic Rate Constants for the Directionally Solidified Eutectic Alloys Co-15Cr-TaC and Co-20Cr-10Ni-13TaC	34
VI	Approximate Parabolic Rate Constants for the Directionally Solidified Eutectic Alloy Ni-12.9Cr-6.9Al-1.8C	36
VII	Depths of Oxide Penetration for the Oxidation of the Various Eutectic Alloy in the Presence of Na <sub>2</sub> SO <sub>4</sub>	36
VIII	Depth of Oxide Penetration for the Hot Corrosion of Various Eutectic Alloys	37
XI	Parabolic Rate Constants for the Oxidation of Various Alloys at 900 Degrees C	37
X	Free Energies of Formation of Oxides	43
XI	Parabolic Rate Constants for the Hot Corrosion of Various Alloys at 900 Degrees C	45

LIST OF FIGURES

FIGURE		PAGE
1	Microstructures of Various Ni-23.1Nb-4.4Al Alloys.	55
2	Microstructures of Various Ni-19.6Nb-6Cr-2.5Al Alloys.	56
3	Microstructures of the Various Co-41Cr-2.4C Eutectic Alloys.	57
4	Microstructures of the Various Co-15Cr-TaC Eutectic Alloys.	58
5	Microstructures of the Various Co-20Cr-10Ni-TaC Eutectic Alloys.	59
6	Microstructures of the Various Ni-12.3Cr-6.9Al-1.8C Eutectic Alloys.	60
7	Cross-Sections of Various Ni-23.1Nb-4.4Al Alloys Oxidized in Air at 900 Degrees C for 50 hours.	61
8	Cross-Section of Ni-23.1Nb-4.4Al (Directionally Solidified) Oxidized in Air at 1000 Degrees C for 96 Hours.	62
9	Cross-Sections of Various Ni-23.1Nb-4.4Al Alloys Oxidized in Air at 1100 Degrees C for 72 Hours.	63
10	Cross-Section of Ni-23.1Nb-4.4Al Directionally Solidified Eutectic Alloy Oxidized for 1 Hour at 800 Degrees C.	64
11	Cross-Section of Ni-23.1Nb-4.4Al Directionally Solidified Eutectic Alloy Oxidized for Various Times at 900 Degrees C.	65
12	Cross-Section of Ni-23.1Nb-4.4Al Directionally Solidified Eutectic Alloy Oxidized for Various Times at 1000 Degrees C.	66
13	Cross-Section of Ni-23.1Nb-4.4Al Directionally Solidified Eutectic Alloy Oxidized for 5 Hours at 1100 Degrees C.	67
14	Aluminum Profiles Across Ni-23.1Nb-4.4Al Directionally Solidified Eutectic Alloy Specimens Which Have Been Oxidized at Various Temperatures.	68
15	Cross-Sections of Various Ni-19.7Nb-6Cr-2.5Al Alloys Oxidized in Air at 900 Degrees for 50 Hours.	69
16	Electron Microprobe X-Ray Images of the Sample Shown in Figure 15(b).	70
17	Cross-Section of Ni-19.7Nb-6Cr-2.5Al (as-cast) Oxidized in Air at 1000 Degrees C for 96 Hours.	71
18	Cross-Section of Ni-19.7Nb-6Cr-2.5Al (Directionally Solidified) Oxidized in Air at 1100 Degrees C for 72 Hours.	72

List of Figures  
(Continued)

Figure		Page
19	Cross-Section of Ni-6Cr-2.5Al Alloy Which Has Been Oxidized for 76 Hours at 900 Degrees C.	73
20	Oxide Map of the Ternary System Ni-Cr-Al at 1000 Degrees C (from C.R. Wallwork and A.Z. Hed, Oxid. Metals, <u>3</u> , 171 (1971)). The points represent data from three different sources. In Ox - internal oxide and the position of the Ni-6Cr-2.5Al is marked by an asterisk.	74
21	Cross-Section of Ni-Nb-6Cr-2.5Al Alloys Which Have Been Oxidized for 76 Hours at 900 Degrees C.	75
22	Cross-Section of Ni-Nb Alloys Which Have Been Oxidized for 95 Hours at 900 Degrees C.	76
23	Cross-Section of Ni-Nb-4.4Al Alloys Which Have Been Oxidized for 95 Hours at 900 Degrees C.	77
24	Graph of the Diffusion Results of $\text{Log}_{10} (x^2/t)$ Against $1/T$ .	78
25	Graph of the Diffusion Results of $\text{Log}_{10} (x^2/t)$ Against $1/T$ .	79
26	Cross-Section of Ni-23.1Nb-4.4Al (as cast) Coated with $1.81 \text{ mg.cm}^{-2} \text{ Na}_2\text{SO}_4$ and Subsequently Oxidized in Air at 900 Degrees C for 24 Hours.	80
27	Cross-Section of Ni-23.1Nb-4.4Al (Directionally Solidified) Coated with $\text{Na}_2\text{SO}_4$ and Subsequently Oxidized in Air for 24 Hours.	81
28	Kinetics for Ni-23.1Nb-4.4Al (Directionally Solidified) Alloy Oxidized under Various Conditions at 900 Degrees C.	82
29	Kinetics for Ni-23.1Nb-4.4Al (Directionally Solidified) Alloy Oxidized under Various Conditions at 1000 Degrees C.	83
30	Kinetics for Ni-23.1Nb-4.4Al (Directionally Solidified) Alloy Oxidized with and without a $\text{Na}_2\text{SO}_4$ Coating at 870 Degrees C.	84
31	Cross-Section of Ni-23.1Nb-4.4Al (Directionally Solidified).	85
32	Cross-Section of Ni-23.1Nb-4.4Al (Directionally Solidified) Alloy.	86
33	Cross-Section of Ni-23.1Nb-4.4Al (Directionally Solidified) Alloy Which Has Been Sulphidized/Oxidized.	87
34	Cross-Section of Ni-19.6Nb-6Cr-2.5Al (Directionally Solidified) Alloy Coated with $2.22 \text{ mg.cm}^{-2} \text{ Na}_2\text{SO}_4$ and Subsequently Oxidized in Air at 900 Degrees C for 24 Hours.	88

List of Figures  
(Continued)

Figure		Page
35	Cross-Section of Ni-19.7Nb-6Cr-2.5Al (Directionally Solidified) Alloy Coated with $2.1\text{y mg.cm}^{-2}$ $\text{Na}_2\text{SO}_4$ and Subsequently Oxidized in Air at 1100 Degrees C for 24 Hours.	89
36	Kinetics for Ni-19.7Nb-6Cr-2.5Al (Directionally Solidified) Alloy Oxidized Under Various Conditions at 900 Degrees C.	90
37	Kinetics for Ni-19.6Nb-6Cr-2.5Al (Directionally Solidified) Alloy Oxidized under Various Conditions at 1100 Degrees C.	91
38	Cross-Section of Ni-19.7Nb-6Cr-2.5Al (Directionally Solidified) Alloy Oxidized at 950 Degrees C in the Dean Apparatus in a $\text{Na}_2\text{SO}_4/10\%$ NaCl Atmosphere for 168 Hours with Thermal Cycling.	92
39	Cross-Section of Ni-19.7Nb-6Cr-2.5Al (Directionally Solidified) Alloy Which Has Been Sulphidized/Oxidized at 1000 Degrees C for 3 Hours.	93
40	Cross-Section of Various Co-41Cr-2.4C Eutectic Alloys Oxidized for 100 Hours in Air Between 900-1100 Degrees C, Illustrating Each Morphological Structure.	94
41	Kinetics for Co-41Cr-2.4C Directionally Solidified Eutectic Alloy Oxidized Under Various Conditions at 900 Degrees C.	95
42	Kinetics for Co-41Cr-2.4C Directionally Solidified Eutectic Alloy Oxidized Under Various Conditions at 1100 Degrees C.	96
43	Cross-Section of Directionally Solidified Co-15Cr-TaC Specimens Oxidized in Air for 100 Hours at Different Temperatures.	97
44	Cross-Section of Various Co-20Cr-10Ni-TaC Specimens Oxidized in Air for 100 Hours at Different Temperatures.	98
45a	Kinetics for Co-15Cr-TaC Directionally Solidified Eutectic Alloy Oxidized Under Various Conditions at 900 Degrees C.	99
45b	Kinetics for Co-20Cr-10Ni-TaC Directionally Solidified Eutectic Alloy Oxidized Under Various Conditions at 900 Degrees C.	100
46a	Kinetics for Co=15Cr-TaC Directionally Solidified Eutectic Alloy Oxidized Under Various Conditions at 1000 Degrees C.	101

List of Figures  
(Continued)

Figure		Page
46b	Kinetics for Co-20Cr-10Ni-TaC Directionally Solidified Eutectic Alloy Oxidized Under Various Conditions at 1000 Degrees C.	102
47	Cross-Section of Various Ni-12.3Cr-6.9Al-1.8C Specimens Oxidized in Air for 100 Hours at Different Temperatures.	103
48	Kinetics for Ni-12.3Cr-6.9Al-1.8C Directionally Solidified Alloy Oxidized Under Various Conditions at 900 Degrees C.	104
49	Kinetics for Ni-12.3Cr-6.9Al-1.8C Directionally Solidified Eutectic Alloy Oxidized Under Various Conditions at 1000 Degrees C.	105
50	Cross-Section of Various Directionally Solidified Co-41Cr-2.4C Eutectic Alloys Coated with $\text{Na}_2\text{SO}_4$ , and Subsequently Oxidized in Air for 100 Hours at Different Temperatures.	106
51	Cross-Section of Directionally Solidified Co-41Cr-2.4C Eutectic Alloy (10.6 cm/h) Specimens Which Have Been Subject to Various Hot-Corrosion Tests.	107
52	Cross-Section of Directionally Solidified Co-15Cr-TaC Eutectic Alloy Specimens Coated with $\text{Na}_2\text{SO}_4$ and Subsequently Oxidized in Air for 100 Hours at Different Temperatures.	108
53	Cross-Section of Directionally Solidified Co-15Cr-TaC Eutectic Alloy Specimens Which Have Been Subject to Various Hot-Corrosion Tests.	109
54	Cross-Section of Directionally Solidified Co-20Cr-10Ni-TaC Eutectic Alloy Specimens Coated with $\text{Na}_2\text{SO}_4$ and Subsequently Oxidized in Air for 100 Hours at Different Temperatures.	110
55	Cross-Section of Directionally Solidified Co-20Cr-10Ni-TaC Eutectic Alloy Specimens Which Have Been Subject to Various Hot-Corrosion Tests.	111
56	Cross-Section of Directionally Solidified Ni-12.3Cr-6.9Al-1.8C Eutectic Alloy Specimens Coated with $\text{Na}_2\text{SO}_4$ and Subsequently Oxidized in Air for 100 Hours at Different Temperatures.	112
57	Cross-Section of Directionally Solidified Ni-12.3Cr-6.9Al-1.8C Eutectic Alloy Specimens Which Have Been Subject to Various Hot-Corrosion Tests.	113
58	Schematic Diagram Showing $\text{Al}_2\text{O}_3$ Formation with the Ni-23.1Nb-4.4Al Directionally Solidified Alloy at 1100 Degrees C.	114

List of Figures  
(Continued)

Figure		Page
59	Schematic Diagram for the Oxidation of Ni-23.1Nb-4.4Al Directionally Solidified Eutectic Alloy at 900 Degrees C and 1000 Degrees C.	115
60	Schematic Mechanism for the Oxidation of the Directionally Solidified Eutectic Alloy Ni-23.1Nb-4.4Al Within the Temperature Range 800-1100 Degrees C.	116
61	Schematic Reaction Mechanism for the Oxidation of the Quaternary Ni-19.7Nb-6C4-2.5Al Alloy.	117
62	Schematic Mechanism Diagram for the Hot-Corrosion of Both the Ternary and Quaternary Alloys.	118

### Introduction

It has long been recognised that increasing the temperature of the turbine inlet gas in aircraft turbines offers attractive advantages in aircraft performance and economy. However, the high temperature characteristics of currently available nickel and cobalt-base superalloys are approaching their limit and continued advancement along conventional alloying lines are not very attractive. Directionally solidified eutectic alloys seem to offer the most promising approach towards increased metal operating temperatures. This class of alloys depends for its high temperature strength on the precipitation of very strong fibres or platelets of a second phase in a more ductile matrix; the fibres or platelets are aligned parallel to the direction of the solidification enhancing the material properties in that direction. Unlike conventional, precipitation-hardened superalloys, the eutectic alloys should show less tendency for the hardening phase to re-dissolve after extended heating at high temperatures. The term "in-situ composites" is now widely used in referring to alloys of this type to differentiate them from metal/matrix composite materials prepared by other means.

Three classes of "in-situ" composite alloys have so far received particular attention:-

- (a) Cobalt-based alloys reinforced by chromium carbide fibres;
- (b) Tantalum carbide or niobium carbide-reinforced nickel or cobalt-based alloys; and
- (c) Nickel alloys based on the  $\text{Ni}_3\text{Nb-Ni}_3\text{Al}$  eutectic.

However, a further alloy has now been developed, based on the Ni-Cr-Al-C system, which consists of  $\text{Cr}_7\text{C}_3$  fibres reinforcing a Ni/ $\text{Ni}_3\text{Al}$  ( $\gamma/\gamma'$ ) matrix.

Over the last few years a number of papers (1-11) and several conferences (12, 13) have demonstrated the attractive mechanical properties of these systems in comparison with conventional cast superalloys.



However, surprisingly little has been published on their corrosion and oxidation resistance. Although in general terms, the chemically less stable component would expect to preferentially oxidise, depleting the alloy of that particular phase, other considerations are also involved. The possible differences in oxidation rates and volume changes of the two phases may produce an accommodation problem at the alloy/scale interface, and the interfaces within the scale; rapid transport along the matrix/fibre interface in the alloy is also a possibility.

The final report examines the oxidation and hot-corrosion behaviour of both the alloys based on the  $\text{Ni}_3\text{Nb-Ni}_3\text{Al}$  ( $\gamma/\gamma' - \delta$ ) eutectic, and those based on the carbide strengthened eutectics.

Oxidation and Hot Corrosion Mechanisms of the  $\text{Ni}_3\text{Nb-Ni}_3\text{Al}$ -based Eutectic Alloys

(a) Oxidation

Until recently very few detailed mechanistic studies of the oxidation behaviour of aligned eutectic alloys have been carried out (14-16). Most of the earlier studies were related to qualitative identification of the oxide phases formed during high temperature mechanical testing (17-20). However, non-directionally solidified alloys have been oxidised at relatively lower temperatures (21).

Thompson (17) found that a Ni-23.1 Nb-4.4 Al alloy oxidised parabolically at  $1800^\circ\text{F}$ ; the oxide was not markedly affected by thermal cycling. A layer denuded in the  $\text{Ni}_3\text{Nb}$  phase was observed at the alloy surface, and consequently the oxidation rate was insensitive to the interlamellar spacings produced by different growth rates in the range 0.5 - 325 cm/h (18). Lemkey (19, 20) carried out isothermal oxidation tests on a Ni-21.8 Nb-2.6 Al alloy and contrary to Thompson found that the scales cracked and spalled on cooling to room temperature. Increase in the oxidation temperature or the length of the exposure tended to increase the severity of the spalling. The oxidation rate was again

parabolic. Thermal cycling caused further spalling of the oxide layer. Arbuzov (21) found that non-directionally solidified alloys were protected by a double-oxide layer, either NiO, Nb<sub>2</sub>O<sub>5</sub> or NiO, Al<sub>2</sub>O<sub>3</sub>, when oxidised at 700-725°C and 800-850°C respectively.

Ternary Ni-Nb-Al alloys, then, have little inherent oxidation resistance, and attempts have been made to improve the oxidation resistance by chromium additions (17). Even 1 atomic % Cr adversely affects the mechanical properties of these alloys. However, the Y/Y<sup>1</sup>-δ alloy, Ni-19.7 Nb-6 Cr-2.5 Al, has received much attention, and has been shown to have an excellent combination of mechanical strength and oxidation resistance (19).

Smeggil and McConnell (15) have studied the oxidation behaviour of directionally solidified Ni-22.1 Nb-4.9 Al eutectic alloy in the temperature range 600-1155°C, using interlamellar spacings of 1.7 and 3.5 μm. Very little spalling was observed during oxidation, but this was considerable on cooling to room temperature, particularly from 990 and 1155°C. The oxidation rate was dependent on the eutectic lamellar spacing at 800 and 990°C but not at 600 and 1155°C. However, at 600°C considerable oxidation occurred down the interphase boundaries, which greatly increased the total oxidising surface area. Preferential oxidation of the Ni<sub>3</sub>Nb phase had occurred but an outer, continuous NiO layer also formed, which was apparently sufficiently protective at this low temperature. There was no evidence of an outer continuous Al<sub>2</sub>O<sub>3</sub> layer, which is not surprising since the aluminium would be unable to laterally diffuse in the alloy at 600°C and interlamellar spacing is not important in determining the oxidation rate.

At 800°C the alloy with the larger inter-lamellae spacing oxidised the slowest, which is somewhat surprising if the results are being interpreted in terms of the ability of the alloys to form a protective Al<sub>2</sub>O<sub>3</sub> layer. However, there is no real evidence that a

continuous  $\text{Al}_2\text{O}_3$  layer did form. Smeggil points out that the oxidation behaviour is complicated by the preferential oxidation of the  $\text{Ni}_3\text{Nb}$  phase, which greatly increases the effective oxidising surface area, and probably produces a very irregular alloy/oxide interface. This behaviour is probably similar to that at  $600^\circ\text{C}$  except due to the higher overall oxidation rate, the fingers of oxidised  $\text{Ni}_3\text{Nb}$  lamellae protruding into the alloy matrix are considerably longer. Furthermore, the smaller the interlamellae spacing, the larger this oxidising surface area becomes, and consequently the overall oxidation rate increases. Inward diffusion of oxygen appears to be involved, since there are no depleted regions within the alloy.

At  $990^\circ\text{C}$  a more conventional oxidation mechanism seems to operate, and a planar alloy/oxide interface is formed. Again, preferential oxidation of the  $\text{Ni}_3\text{Nb}$  lamellae occurred and nickel islands were left isolated in the outer oxide layer. Outward diffusion of aluminium and niobium had been more pronounced at this higher temperature and there was less preferential oxidation down the interphase boundary. In fact a region deficient in the  $\delta$  and  $\gamma'$  phases was present adjacent to the scale layer. Surprisingly, the oxidation rate was smaller the finer the interlamellae spacing, presumably because the aluminium has to diffuse much smaller distances to cover the  $\text{Ni}_3\text{Nb}$  lamellae and form a continuous  $\text{Al}_2\text{O}_3$  layer. At  $1155^\circ\text{C}$ , a similar process occurred, but the rate was independent of the inter-lamellae spacing since the lateral diffusion of the aluminium was sufficient to rapidly form the  $\text{Al}_2\text{O}_3$  layer.

The oxidation mechanism for the Ni-22.1 Nb-4.9 Al alloy at  $1155^\circ\text{C}$  has been investigated more thoroughly (16). Smeggil proposes that a number of steps occur before a sufficiently protective  $\text{Al}_2\text{O}_3$  layer forms. The first step preventing catastrophic oxidation of the  $\text{Ni}_3\text{Nb}$  phase is the formation of a eutectic-free zone between the initial oxide structure and the base alloy. This region consists of a Ni-Nb-Al solid solution, and the rate controlling step at this stage of the

oxidation is the outward diffusion of aluminium and niobium through this layer. However, continuing reaction produces islands of nickel included in the oxide layer, which eventually oxidise, forming an external layer of NiO. Smeggil further suggests that the voids produced by the outward diffusion and subsequent oxidation of nickel from these islands may help in retarding the overall oxidation rate, but more importantly, they apparently cause diffusion parallel to the oxidising interface. As at 990°C, such lateral diffusion results in the eventual formation of a protective Al<sub>2</sub>O<sub>3</sub> layer. However, there is some metallographic evidence to indicate that this process can be repeated a number of times followed by rupture of the Al<sub>2</sub>O<sub>3</sub> layer, before complete protection is achieved.

Pettit (14) investigated the oxidation mechanisms of eutectic alloys in the Ni-Nb-Al, Ni-Nb-Cr, and Ni-Nb-Cr-Al systems at 600-1200°C. At 700 and 1000°C there was no preferential attack of the strengthening phase -  $\delta$ , Ni<sub>3</sub>Nb. At 700°C the oxide morphology consisted of an outer NiO layer separated from the internally oxidised zone by a layer of virtually pure nickel. The texture and composition of the internally oxidised zone depends on the alloy composition and which phase has been internally oxidised. In the Ni-21.7Nb-2.5Al alloy, the Ni<sub>3</sub>Nb phase has been oxidised producing coarse Nb<sub>2</sub>O<sub>5</sub> particles and nickel, whereas in the more aluminium-rich alloy, Ni-23.1 Nb-4.4 Al the Ni<sub>3</sub>Al has been attacked producing a fine oxide dispersion of Nb<sub>2</sub>O<sub>5</sub> and AlNbO<sub>4</sub>.

At 1000°C the oxidised structure consisted of an outer NiO layer, and intermediate layer of NiNb<sub>2</sub>O<sub>6</sub> and an internal oxidation zone of nickel, Nb<sub>2</sub>O<sub>5</sub>, and AlNbO<sub>4</sub>. Unlike at 700°C, the texture of this zone is less dependent on the alloy composition since it is separated from the bulk alloy by a continuous layer of the  $\Upsilon$ -phase (Ni). The outer NiO layer grows by outward diffusion of nickel, whereas Nb<sub>2</sub>O<sub>5</sub> is formed by inward oxygen diffusion, the volume fraction of precipitated aluminium-containing oxide, either AlNbO<sub>4</sub> or Al<sub>2</sub>O<sub>3</sub>, is insufficient

to form a continuous layer, and the overall oxidation rate depends on the external NiO layer.

Comparison of the results of Pettit and Smeggil presents general agreement at 1000°C, but not at the lower temperatures, 700 and 800°C. At these latter temperatures, both authors indicate that there is no single phase (Y) region in the alloy adjacent to the scale, but the alloy/scale interface was irregular in Smeggil's alloys as opposed to the relatively planar interface observed by Pettit. It should be pointed out that the alloys varied slightly in composition: Pettit used Ni-21.7Nb-2.5Al and Ni-23.1Nb-4.4Al whereas Smeggil used Ni-22.1Nb-4.9Al. Smeggil's observations seem perhaps the most understandable, since inward diffusion of oxygen seems to be important and preferential oxidation of the Ni<sub>3</sub>Nb phase might thus be expected.

The other alloys studied by Pettit (14) (Ni-Nb-Cr and Ni-Nb-Cr-Al) formed more protective oxide layers than the NiO on the Ni-Nb-Al alloys, namely CrNbO<sub>4</sub> and (Cr,Al)NbO<sub>4</sub> or Al<sub>2</sub>O<sub>3</sub> respectively. However, as indicated earlier (15) Ni-Nb-Al alloys can eventually form a protective Al<sub>2</sub>O<sub>3</sub> layer at 1155°C, although not at 600°C and 990°C. The Ni-Nb-Cr and Ni-Nb-Cr-Al alloys develop protective layers quite rapidly, and these remain stable. The layer forms initially over the matrix and then grows by lateral diffusion over the strengthening phase. As the temperature decreases, the time for the protective oxide layer to form increases, since it is a diffusion controlled process. Al<sub>2</sub>O<sub>3</sub> layers were found to be more protective than either CrNbO<sub>4</sub> or (Cr,Al)NbO<sub>4</sub> layers, although both these alloys oxidised more slowly than the Ni-Nb-Al alloy. Again the alloys with larger δ-lamellae spacing oxidised more severely at both 700 and 1000°C, since the lateral diffusion required to form the protective layer was greater. However, as shown by Smeggil (16), if sufficient oxidation of the δ-lamellae occurs, the surface area of the matrix exposed for oxidation increases, and this area increases with decreasing spacing of the lamellae. Such a process could cause severe

Cr and Al depletion of the matrix and a protective  $\text{CrNbO}_4$  or  $\text{Al}_2\text{O}_3$  layer would become unstable over the matrix phase.

(b) Hot-Corrosion

There have been few detailed studies of the hot corrosion behaviour of these  $\gamma/\gamma' - \delta$  alloys. Thompson (17) found that the presence of a sodium sulphate ( $\text{Na}_2\text{SO}_4$ ) coating increased the oxidation rate of a  $\text{Ni}_3\text{Nb-Ni}_3\text{Al}$  alloy at  $1652^\circ\text{F}$  ( $900^\circ\text{C}$ ), although the increase was not as great as that observed with low-chromium bearing nickel-base alloys. The addition of 4 or 8.5% Cr greatly increased the hot-corrosion resistance at  $1832^\circ\text{F}$  ( $1000^\circ\text{C}$ ) for the  $\text{Ni}_3\text{Nb-Ni}_3\text{Al}$  alloy, which in itself is far more resistant than the commercial nickel-base superalloy B1900 (also an  $\text{Al}_2\text{O}_3$  former). Presumably the mixed, complex oxide layers on the eutectic alloys are more resistant to acidic fluxing than  $\text{Al}_2\text{O}_3$  alone.

Lemkey (19,20) exposed the  $\gamma/\gamma' - \delta$  alloy, Ni-20.2Nb-9.1Cr-1Al to a cyclic burner rig test, together with various nickel-base superalloys (B1900, TRW NASA VI A, IN 738). The specimens were subjected to cycles of  $954^\circ\text{C}$  for 3 min., followed by heating to  $1121^\circ\text{C}$  for 2 min., and then cooling to  $315^\circ\text{C}$ , whilst rotating in a Mach 0.3 jet burner using JP-5R fuel containing 3-5 ppm synthetic sea salt. Subsequent microstructural examination indicated that this  $\gamma/\gamma' - \delta$  alloy ranked with the best superalloys in terms of resistance to hot-corrosion.

Oxidation and Hot Corrosion Mechanisms of Carbide Strengthened Eutectic Alloys

(a) Oxidation

(i)  $\text{Cr}_7\text{C}_3$ -reinforced Co-base Alloys

The only alloy in this group is Co-41Cr-2.4C (73C), which consists of  $\text{Cr}_7\text{C}_3$  strengthening fibres in a Co-28.5Cr matrix. Very few detailed studies of the oxidation behaviour of this alloy have been carried out; some incidental observations on the behaviour of specimens during high temperature mechanical testing have been reported.

During creep testing in air at 1000°C, a thin, protective Cr<sub>2</sub>O<sub>3</sub> layer was formed, accompanied by significant carbide depletion near the alloy surface at least parallel to the fibres (8). Vandermousen (22) found similar carbide depletion following stress-rupture tests in air at 1093°C for 1483 h. In a more detailed study of the oxidation behaviour of both conventionally cast and directionally solidified Co-41Cr-2.4C Fritscher et al (23) found that the parabolic rate constant for oxidation of the directionally solidified material was about half an order of magnitude less than that of the conventionally cast alloy in the temperature range 1000-1200°C. Decarburization occurred and in addition there was some preferential internal oxidation of the carbides.

El Dahshan et al (24) have studied the oxidation behaviour of a number of Co-Cr-C alloys in the temperature range 900-1150°C. Carbon had only a small effect on the overall oxidation rate of Co-25Cr-(0.5-2.0)C alloys. In some respects this seems surprising since the formation of Cr-rich carbide, M<sub>23</sub>C<sub>6</sub>, would diminish the chromium content of the matrix, and hence the chromium activity (1 wt. % C reduces the chromium content of the matrix by approximately 12.5 wt. % Cr). However, the reduction in the chromium activity does not appear to affect the ability of the alloy to form a continuous Cr<sub>2</sub>O<sub>3</sub> layer. Of course, the chromium-carbide is much less stable than the oxide, and there is no difficulty in the exchange reaction, but this does not imply that there is a mechanism capable of raising the chromium activity near the interface. Furthermore, the accumulation of carbon below the interface will reduce the chromium activity of the alloy still further, at least until the oxide breaks down at long times, or high temperatures, and decarburization can occur. This demonstrates that it is the chromium availability at the alloy/oxide interface which is important, and not the chromium activity. Consequently, the ability of a two-phase alloy to form a protective oxide will not necessarily be less than that of single phase alloy having the same overall content of the protective scale-forming element, but it would

seem likely that it would depend on the mean spacing between the areas of the phase richer in the scale-forming element. If these are large and widely separated the areas poor in the element will tend to oxidise in a non-protective manner, giving a heterogeneous scale, with the more protective regions being overgrown and possibly disrupted; the critical spacing is probably a function of temperature, increasing with increasing temperature.

(ii) TaC or NbC-reinforced Co and Ni alloys

The main alloy in this group, Co-15Cr-13TaC, consists of TaC fibres in a Co-15Cr matrix. However, a more recent development has been to increase the matrix chromium content to 20% and to add 10% Ni: Co-10Ni-20Cr-13TaC. This modification is intended to improve the oxidation resistance.

Benz et al (7) oxidised a series of directionally solidified alloys based on the Co-TaC system, but containing additions of Cr, Mo, V, Al, Hf, Si, W, Ta, Ti, and Nb. Additions of Ni, Cr, Fe and Ti were beneficial and reduced the oxidation rate in static air at 2000°F (1093°C), whereas Nb, Y, Mo and W had an adverse effect; Al, Hf and Si additions had little effect. The best compromise between oxidation resistance and stress rupture behaviour was achieved with a Co-15Cr-9.5Ni-3W-13TaC alloy, which showed a weight gain of around 12-18 mg.cm.<sup>-2</sup> after 100 h exposure, in comparison to the conventional nickel-base superalloy René 80 of 6 mg.cm.<sup>-2</sup>. The alloy was also slightly less oxidation resistant than René 80 under dynamic thermal cycling conditions.

Lemkey and Thompson (2) compared the behaviour of TD-nickel and a conventionally cast Ni-NbC eutectic at 700°C and 900°C. The eutectic alloy did not form a protective oxide layer and continuous decarburization took place. They suggested that a protective coating, or the addition of up to 25-30% Cr to the matrix, would be required for high temperature service. Boiks and Moroz (25) also reported that nickel containing carbide dispersions were less oxidation resistant at 1000°C than pure nickel.



Bibring et al (26) measured the oxidation resistance of a number of directionally solidified eutectic alloys strengthened by NbC and TaC at 1000°C in still air. The weight gains after 20 h were approximately 5, 2 and 1 mg.cm.<sup>-2</sup> for Co-20Cr-10Ni-13NbC, Co-15Cr-13TaC and Co-20Cr-10Ni-13TaC respectively. The presence of as little as 1% Al decreased the rate further. Alloys containing TaC rather than NbC are more oxidation resistant. In thermal cycling tests (5 h cycles in air at 1000°C followed by rapid cooling to room temperature) only the Co-15Cr-13TaC alloy suffered significant spallation. The presence of Nb in conventionally cast Co-Cr alloys has been found to increase the oxidation rate quite considerably, whereas Ta had little effect (27), which may well explain the generally better oxidation resistance of alloys containing TaC as opposed to NbC.

Felten and Pettit (14) observed preferential oxidation of TaC from a directionally solidified Co-TaC eutectic alloy at temperatures below 900°C, but more uniform oxidation at higher temperatures; cyclic oxidation above 900°C also produced preferential oxidation of the carbide phase. The oxidation resistance of a conventionally cast Ni-Co-Cr-TaC alloy was poor in the temperature range 1000-1200°C (28), with rapid oxidation of the TaC phase causing fragmentation of the alloy.

Smeggil (29) in a comprehensive study of the oxidation of a Co-15Cr-8.5Ni-6W-20TaC alloy between 600 and 1155°C found contrasting behaviour to that reported above. Between 600°C and 800°C the alloy showed simple parabolic oxidation kinetics and the TaC fibres apparently oxidised at a much slower rate than the matrix causing the unoxidised fibres to protrude into the scale. In the temperature range 850-900°C an oxide subscale penetrated into the alloy along the matrix/fibre interface producing a depletion in chromium; the kinetics were initially parabolic but subsequently changed to a linear rate law. At higher temperatures still, 1080 and 1155°C, a rapid, non-parabolic oxidation rate occurred with substantial oxidation of the fibres, particularly

when the matrix had been depleted in chromium. Smeggil explained the difference in behaviour in terms of a competition between chromium in the matrix and the TaC fibres for the available oxygen. At low temperatures, where the oxidation rate is slow, there was little chromium depletion, and consequently the oxygen activity is not sufficient to oxidise the TaC fibres. As the temperature was increased, the extent of the chromium depletion in the matrix was also increased, and oxidation of the fibres proceeded, initially only along the interface with the matrix. However, eventually at 1080°C and 1155°C, a more general degradation of the TaC fibres occurred.

The orientation of the TaC fibres was also found to significantly affect the oxidation rate. When the TaC fibres and their oxidised remnants were perpendicular to the surface they prevented crack propagation by pore coalescence in the oxide scale, thus maintaining protection of the underlying alloy substrate. However, in the case of TaC fibres parallel to the oxidising interface, both the fibres and their oxidised remnants lie parallel both to the oxidising interface, and, more importantly, to the propagating cracks. Consequently, there is no barrier against crack propagation, and the oxide scales were non-protective, particularly at high temperatures. due to pore coalescence.

Smeggil (30) has also investigated the effect of thermal cycling on the oxidation behaviour of the same alloy at 800°C and 1000°C. Parabolic behaviour was observed at 1000°C, but not at the lower temperature. Rather strikingly, at 800°C, the scale layers showed very irregular morphologies, unlike those formed under isothermal conditions, and it was suggested that the chemical heterogeneities in the neighbourhood of the TaC fibres, caused by the thermal cycling, was largely responsible.

(iii) Cr<sub>7</sub>C<sub>3</sub>-reinforced Ni-base alloys

The main alloy in this group is Ni-12.3Cr-6.9Al-1.8C, which consists of Cr<sub>7</sub>C<sub>3</sub> fibres in a Ni(Ni<sub>3</sub>Al(γ/γ')) matrix. However, its

oxidation behaviour does not appear to have been studied.

(b) Hot-corrosion

(i) Cr<sub>7</sub>C<sub>3</sub>-reinforced Co-base alloys

There have been few detailed studies of the hot-corrosion of this alloy. Staub and Erdős (31) observed preferential attack of the carbides (Cr<sub>7</sub>C<sub>3</sub>) in preliminary studies using a combustor rig. Nevertheless, the alloy was considered to be more resistant to attack than the highly rated commercial superalloy IN 738 (8). According to Sahn (8), the rate of corrosion was determined initially only by the matrix, which is very resistant since it represents the nearly ideal Co : Cr ratio of 70 : 30; however, as soon as the surface has been depleted in chromium the carbides are preferentially attacked.

El Dahshan et al (32-35) have studied the hot-corrosion behaviour of various conventionally cast Co-25Cr-(0.5-2.0)C alloys at temperatures in the range 800 - 1000°C. As in the oxidation of these alloys (24), carbon has only a small effect on the overall hot-corrosion rate, due to it not affecting the ability of the alloy to form a protective Cr<sub>2</sub>O<sub>3</sub> layer. However, the carbide network does provide an easy diffusion path for the ingress of sulphur and oxygen into the alloy.

(ii) Co-Cr-TaC

Benz (7) subjected various Co-Cr-TaC, Co-Cr-Ni-TaC, and Co-Cr-Ni-W-TaC alloys to burner rig tests under the following conditions: temperature 1700°F (927°C); time 310-348 h with a cooling cycle every 24 h; fuel JP-5; air/fuel ratio 30 : 1; salt 5 p.p.m. as sea water (ASTM 665-60), atomised and injected into the combustion zone. Little accelerated attack occurred, although there was a little preferential oxidation of the TaC fibres; penetration depths ranged from 6-9 mils with the Co-Cr-TaC and Co-Cr-Ni-TaC alloys to about 1 mil with the Co-Cr-Ni-W-TaC alloy. These values compare favourably with those obtained under similar exposure conditions with MAR-M 509 (1 mil), X-40 (1 mil), and René 80 (7-8 mils).

Bibring (26) exposed a Co-20Cr-10Ni-13TaC alloy to a combustion gas atmosphere containing 0.12% S with 100 p.p.m. NaCl at 1000°C, with thermal shocks being introduced every 8 h. Weight losses of around 6 mg.cm.<sup>-2</sup> were noted after 200 h exposure, comparing favourably with 19 mg.cm.<sup>-2</sup> for IN 100 after a similar test.

(iii) Ni-Cr-Al-C

There have been no previous reported studies of the hot-corrosion behaviour of this alloy system.

Present Investigation

Ni<sub>3</sub>Nb-Ni<sub>3</sub>Al Based Eutectic Alloys

Following the three oxidation mechanistic studies (14-16) discussed in detail, it is clear that the oxidation of these eutectic alloys is a very complex process, and two alloys were chosen for further study in the present investigation: Ni-23.1Nb-4.4Al and Ni-19.7Nb-6Cr-2.5Al. The former represents the basic Ni<sub>3</sub>Nb-Ni<sub>3</sub>Al eutectic system containing a high volume fraction of the δ-phase (0.44), and the latter is modified by chromium (0.33) to improve its oxidation resistance. No detailed studies of the mechanisms of hot-corrosion of these alloys have previously been reported.

As cast, slowly cooled and directionally solidified alloys of each composition were examined in order to study the effects of various degrees of alignment of the δ-lamellae. There is virtually no alignment in the as-cast Ni-23.1Nb-4.4Al alloy (Figure 1a), whereas slow cooling produces a relatively coarse grained structure with good alignment in each grain (Figure 1b). The microstructure of the directionally solidified alloy is shown in Figure 1c, revealing good alignment of the lamellae. The corresponding microstructures for the Ni-19.7Nb-6Cr-2.5Al alloy are shown in Figure 2; essentially similar features to the ternary alloy are apparent.

### Carbide-Based Eutectic Alloys

It seems likely then, that decarburization or oxidation of the carbide network may well occur during oxidation and hot-corrosion, and consequently a detailed study has been carried out. Samples of each of the various alloys in three different conditions were again used: as cast, slowly cooled, and directionally solidified. In addition the carbide spacing in the directionally solidified Co-41Cr-2.4C material was varied by varying the cooling rates: 3.4, 10.6 and 31.5 cm/h. Also both the basic and modified alloys in the Co-TaC system, Co-15Cr-13TaC and Co-20Cr-10Ni-13TaC respectively were included. The microstructures of all the various samples are shown in Figures 3-6; as the cooling rate decreases, the carbide particles increase in size, and their alignment improves.

### Experimental

The alloys were prepared from high purity elements by vacuum induction melting and casting into 25 mm square sectioned moulds. The slowly cooled alloys were left in the cylindrical alumina crucibles and allowed to cool in the induction furnace, producing cylindrical alloy bars. The directionally solidified alloys were first cast into cylindrical bars in a conventional way and subsequently directionally solidified. Acknowledgement is due to Dr. M. McClean, N.P.L., Teddington, Middlesex (Co-Cr-C); Dr. H. Bibring, O.N.E.R.A., Chatillon, France (Co-TaC); and Dr. P. Cowley, N.G.T.E., Pyestock, Farnborough, Hampshire (Ni-Cr-Al-C and  $Ni_3Nb-Ni_3Al$ ) for supplying the various directionally solidified samples.

Specimens of approximately 10 x 10 x 1 mm. were then cut from the alloy samples using a carborundum cutting machine. Each specimen was ground on metallographic silicon carbide papers through 600 grit, degreased and cleaned using carbon tetrachloride.

Oxidation experiments were carried out at 900, 1000 and 1100°C in static air, the samples being supported in recrystallized alumina boats. These temperatures were chosen since they represent the current turbine

operating temperatures (900-1000°C), and the proposed increased temperature (1100°C) with the use of eutectic alloys. Oxidation was commenced by pushing the cleaned samples quickly into the hot muffle furnace. After oxidation the samples were removed slowly from the furnace in an attempt to minimize spalling. Oxidation kinetics were measured by suspending the specimen in a conventional thermobalance.

As will be described later, the formation of a  $\delta$ -free zone at the alloy/oxide interface is decisive in determining which type of oxidation occurs with the  $\text{Ni}_3\text{Nb-Ni}_3\text{Al}$  alloys, and it seemed appropriate to assess the likely rate of formation of this zone under more closely defined conditions. To this end diffusion couples consisting of pure nickel and the  $\text{Ni-23.1Nb-4.4Al}$  alloy were prepared and subjected to diffusion anneals in an inert atmosphere at various temperatures. Mating surfaces of the couples were polished to 6  $\mu\text{m}$  diamond and bound together by wrapping with platinum wire. The couples were then sealed into evacuated quartz capsules and annealed in a vacuum furnace for appropriate times. Subsequently, the couples were sectioned, metallographically prepared and etched allowing the width of the  $\delta$ -free zone to be measured in the microscope.

Three types of hot-corrosion tests were carried out on the various alloys:-

(i) A  $\text{Na}_2\text{SO}_4$ -coating was applied to the sample surface by spraying with a saturated aqueous solution. The exact details of the coating application have been described previously (36). The coated sample was then oxidised, either suspended in a conventional thermobalance, or placed in an alumina boat in a horizontal muffle furnace.

(ii) The corrosion of the samples in the Dean rig has also been studied. In the Dean test, the contaminating salt ( $\text{Na}_2\text{SO}_4$  or  $\text{Na}_2\text{SO}_4/\text{NaCl}$  mixture) is introduced into the atmosphere by passing the gas stream over the heated salt in an auxiliary furnace before passing it over the samples; the temperature conditions are arranged such that the salt condenses onto the samples. The exact details of the apparatus have been described previously (37).

(iii) Samples were given a brief pre-sulphidation treatment in  $H_2/H_2S$  (90:10) mixtures prior to oxidation in a conventional thermobalance.

Oxidised samples were prepared for metallographic examination, electron probe microanalysis, and X-ray diffraction in the usual way. When necessary, etching was carried out using a mixture consisting of equal parts of glacial acetic acid, conc. nitric acid, and water.

### Results

#### $Ni_3Nb-Ni_3Al$ Based Eutectic Alloys

##### (a) Oxidation

##### Ni-23.1Nb-4.4Al

Samples of the as-cast, slowly cooled, and directionally solidified alloys were oxidised for various times at 900, 1000, and 1100°C. A typical cross-section of the as-cast alloy oxidised for 50h. at 900°C is shown in Figure 7 (a). There is an outer NiO layer overlying a region containing oxidised and unoxidised metal, essentially pure nickel. The etching process has removed most of the nickel in the mixed layer, since it reveals the eutectic structure by dissolving the nickel ( $\Upsilon$ ) phase away. The oxides in the intermediate layer were identified as  $Nb_2O_5$  and  $AlNbO_4$ .  $Al_2O_3$  was also identified as a discontinuous layer at the alloy/scale interface. At the surface of the alloy, there is a single phase region of  $\Upsilon$ -phase (nickel-rich). The distribution of the nickel islands in the inner oxide layer does not bear any obvious relationship to the structure of the eutectic. The morphology of the scale after 168h is very similar, and it is clear that no protective  $Al_2O_3$  layer has formed since there are still islands of metallic nickel in the scale.

The slowly cooled alloy oxidised in a similar manner to the as-cast sample in regions where the lamellae were not aligned. However, in contrast, where there was appreciable alignment normal to the surface, the  $Ni_3Nb(\delta)$  lamellae were oxidised preferentially: Figure 7 (b). Furthermore, in these aligned regions no single phase  $\Upsilon$ -zone is formed at the interface. Aligned lamellae which are parallel to the alloy surface

are not preferentially oxidised direct from the surface unless oxygen can gain access via the normal lamellae, see Figure 7 (b).

Rather surprisingly the directionally solidified alloy did not show any preferential attack of the  $\delta$ -lamellae, and a more or less planar alloy/scale interface was observed, Figure 7 (c). Again a zone of  $\gamma$ -phase denuded in aluminium and niobium was present at the alloy/scale interface, and the surface scale composition was similar to that shown in Figure 7 (a).

At 1000°C there is little difference in oxidation behaviour between the as-cast, slowly cooled and directionally solidified alloys. Figure 8 shows a typical cross-section. The outer layer is again NiO, overlying an intermediate layer in which  $\text{NiNb}_2\text{O}_6$ ,  $\text{NiAl}_2\text{O}_4$  and  $\text{AlNbO}_4$  have been identified. The inner layer has  $\text{Nb}_2\text{O}_5$ ,  $\text{AlNbO}_4$  and nickel-rich islands, suggesting that this layer is being oxidised to form the mixed oxide layer, and the metal/oxide phase propagates into the alloy at a more or less constant thickness.

The three alloys behave similarly at 1100°C also and most of the oxide structure is similar to that at 1000°C. However, in some areas around the cross-section a continuous  $\text{Al}_2\text{O}_3$  layer has developed at the base of the scale, isolating the nickel-rich islands, Figure 9 (a). In other areas, Figure 9 (b), there are short lengths of  $\text{Al}_2\text{O}_3$  but oxidation has been able to proceed around these. The formation of the continuous  $\text{Al}_2\text{O}_3$  layer does not appear to be related to the microstructure of the alloy, since the directionally solidified alloy also produces an  $\text{Al}_2\text{O}_3$  layer at the base of the scale, Figure 9 (c).

However, both at 1000°C and 1100°C the  $\gamma$ -phase zone (or  $\delta$ -free zone) is again present at the alloy/oxide interface, and its thickness increases with increasing temperature.

With these heterogeneous alloys the initial stages of oxidation are perhaps even more important than with conventional alloys in determining



subsequent oxidation behaviour. Thus, samples of the directionally solidified alloy Ni-23.1Nb-4.4Al were oxidised for 1, 2 and 5 h in the temperature range 800-1100°C; representative cross-sections are shown in Figures 10-13.

At 800°C preferential attack of the Ni<sub>3</sub>Nb fibres occurs, (Figure 10) and this continues even after long exposure times, as was shown in the earlier reports (1). Presumably, the ratio of scale growth rate to alloy interdiffusion rate is sufficiently high that there are virtually no local compositional changes in the alloy, and a heterogeneous scale results; there is preferential attack of the Ni<sub>3</sub>Nb-fibres, in comparison to the more oxidation-resistant Ni/Ni<sub>3</sub>Al matrix phase.

Initial behaviour is similar at 900°C (Figure 11a). However, diffusion in the underlying alloy must start to be involved since a Ni<sub>3</sub>Nb-free zone does form after an exposure of 2H (Figure 11b). The scale formed during these early stages is quite heterogeneous and remains at the scale/atmosphere interface. However, once the Ni<sub>3</sub>Nb-free zone has been established, it acts as a 'randomiser' and the subsequent oxide layers which develop are more uniform in composition, particularly in a direction parallel to the alloy/scale interface.

The Ni<sub>3</sub>Nb-free zone forms more rapidly at 1000°C and 1100°C, with no internal attack of the Ni<sub>3</sub>Nb fibres. The overall extent of corrosion during these initial stages also increases as the temperature increases with thicker surface scales, and also a greater thickening of the Ni<sub>3</sub>Nb-free zone (Figures 12 and 13).

With this Ni-Nb-Al alloy, protection is only going to be afforded by the development of a continuous Al<sub>2</sub>O<sub>3</sub> layer. Obviously, this is going to involve aluminium diffusing from the Ni/Ni<sub>3</sub>Al phase, and spreading laterally along the alloy/scale interface as rapidly as possible, thus preventing excessive oxidation of the alloy. Increasing the temperature will favour this process, and indeed continuous Al<sub>2</sub>O<sub>3</sub> formation only occurs at 1100°C

as shown in Figure 14, which illustrates the aluminium profiles across samples oxidised at 900, 1000 and 1100°C. However, the  $\text{Al}_2\text{O}_3$  layer does not form rapidly even at 1100°C, and quite extensive oxidation does occur beforehand.

Ni-19.7Nb-6Cr-2.5Al

A typical cross-section of this alloy in the as-cast condition oxidised for 50h at 900°C is shown in Figure 15 (a). The oxide is very thin all around the section and there are no obvious signs of any preferential attack of the niobium-rich  $\delta$ -phase. However, there is a single phase region in the alloy at the scale interface. In the directionally solidified alloy preferential attack of the  $\delta$ -phase does occur before a continuous, protective layer of  $\text{Al}_2\text{O}_3$  developed, Figure 15 (b). The preferential attack seems to be the more extensive the wider the  $\delta$ -lamellae. The electron image and X-ray distribution pictures for the directionally solidified alloy are shown in Figure 16; the outer discontinuous layer is niobium-rich ( $\text{Nb}_2\text{O}_5$ ) which is associated with chromium ( $\text{CrNbO}_4$ ) above the  $\delta$ -lamellae, whilst at the alloy surface is a continuous aluminium-rich layer ( $\text{Al}_2\text{O}_3$ ) which affords protection to the alloy. There is little change in the morphological features after oxidation for longer times except presumably for a thickening of the  $\text{Al}_2\text{O}_3$  layer. Certainly there is no noticeable increase in the amount of niobium-rich oxide outside the alumina.

The directionally solidified alloy behaved similarly at 1000°C, with slight thickening of the outer oxide layer. However, continuous, less protective oxides were formed on the as-cast and slowly cooled alloys, and some internal precipitation of  $\text{Al}_2\text{O}_3$  has taken place, as shown in Figure 17.

At 1100°C the directionally solidified alloy suffered more severe internal oxidation, as shown in Figure 18, and as a consequence  $\text{Cr}_2\text{O}_3$  formed the main external oxide. There is no evidence of niobium-rich oxides forming during the initial stages of oxidation, unless they have spalled from the surface; however, there is a depletion of the  $\delta$ -lamellae

near to the interface. The other two alloys behaved similarly at this temperature, except that internal penetration of  $\text{Al}_2\text{O}_3$  was not as great.

To investigate the role of niobium, the alloy under investigation was cast without the niobium: a ternary Ni-6Cr-2.5Al alloy. A cross-section of this alloy oxidized at  $900^\circ\text{C}$  is shown in Figure 19, and clearly there has been extensive oxidation. There is a discontinuous, non-protective layer of  $\text{Al}_2\text{O}_3$  and internal oxide particles of both  $\text{Cr}_2\text{O}_3$  and  $\text{Al}_2\text{O}_3$ ; spalling of the outer NiO layer seems to have occurred. This type of behaviour agrees with that reported previously, and as shown in Figure 20. It seems, therefore, that at these fairly low chromium and aluminium levels, there is no development of a protective oxide layer.

However, the addition of only 5% Nb to the ternary Ni-6Cr-2.5Al alloy improves its oxidation resistance at  $900^\circ\text{C}$ , as shown in Figure 21; the depth of internal oxidation is considerably reduced; 10% Nb decreases the oxidation rate further, and it has been shown earlier that 19.7 Nb greatly improves the oxidation resistance primarily due to encouraging the formation of  $\text{Al}_2\text{O}_3$ .

However, niobium is not beneficial in improving the oxidation resistance of Ni and Ni-Al alloys, as shown in Figures 22 and 23 respectively. In pure nickel, the presence of niobium causes internal oxidation and  $\text{Nb}_2\text{O}_5$  platelets form in the alloy; in addition an intermediate layer of the spinel ( $\text{NiNb}_2\text{O}_6$ ) forms beneath the outer NiO layer. Equally in the Ni-Nb-4.4Al alloys, no protective oxide forms, at 5% Nb the intermediate spinel layer contains  $\text{AlNbO}_4$  and there is no internal oxidation, whilst at 15% Nb there are in addition to the spinel layer internal oxides containing  $\text{AlNbO}_4$  and  $\text{Al}_2\text{O}_3$ . The eutectic alloy containing 23.1% Nb also does not form a protective oxide layer, except at high temperatures, as has been shown earlier.

(b) Formation of the  $\delta$ -free Zone

The formation of a zone depleted in the  $\delta$ -phase at the surface of the alloy by the selective removal of niobium during high temperature

oxidation is clearly important. This was studied under more closely defined conditions using the diffusion couples referred to earlier. Clearly, the rate of growth of the  $\delta$ -free layer is governed by diffusion and thus the ratio of (thickness)<sup>2</sup>/time represents a rate constant of growth. This is shown as a function of temperature in Table I.

TABLE I. Growth of the  $\delta$ -free Zone

<u>Temperature</u> °C.	<u>Thickness</u> $\mu\text{m}$	<u>Time</u> h.	<u>Rate Constant</u> $\text{cm}^2/\text{s}$
900	11	138	$2.4 \times 10^{-12}$
1000	42	150	$3.3 \times 10^{-11}$
1100	102	136.5	$2.1 \times 10^{-10}$

The activation energy for the diffusion-controlled process has been calculated from Figure 24 as 300 kJ/mole.

However, this does not accurately simulate the process which occurs during oxidation, where niobium loss to the external oxide scale produces the depletion zone. Thus electron probe microanalysis was used to measure the  $\text{Ni}_3\text{Nb}$ -free zone thickness, of alloys which had been oxidised at 900, 1000 and 1100°C. Again, the rate of growth of the depletion zone showed an Arrhenius-type dependence on temperature as shown in Figure 25, giving an apparent activation energy of approximately 345 kJ/mole. This would suggest that the formation of the depletion zone is a diffusion-controlled process, at least in the very early stages. During the later stages of oxidation, if a protective oxide layer of  $\text{Al}_2\text{O}_3$  develops, then no further Nb is lost to the oxide and the growth of the depletion zone ceases; Lemkey (19) in fact has shown that the thickness of the depletion zone reaches a limiting value after long exposures, particularly at the higher temperatures.

(c) Hot-Corrosion

Ni-23.1Nb-4.4Al

After coating with  $\text{Na}_2\text{SO}_4$  the as-cast and slowly cooled samples behaved very similarly at 900 and 1000°C, both materials oxidising at a

faster rate than uncoated samples. Figure 26 (a) shows a typical cross-section. There is an outer NiO layer overlying a mixed metal/oxide region in which  $\text{NiNb}_2\text{O}_6$  and  $\text{AlNbO}_4$  have been identified; the metal islands are essentially pure nickel. A further feature of the corroded structure evident in Figure 26 (b) is the presence of NiS particles in the alloy where it has been depleted of the  $\delta$ -lamellae. These sulphides have a similar distribution to the original  $\delta$ -lamellae, and consequently the mixed oxide/metal region above the sulphides also has a similar appearance to the original alloy structure; it represents areas where the nickel sulphide phase has been preferentially oxidised.

Rather surprisingly, accelerated attack of the directionally solidified was confined to a few isolated areas as shown in Figure 27; the scale in these areas had a similar appearance to that described above. However, sulphides were formed in the alloy behind both types of scale, although they had different distributions in the two cases and also were present in a higher concentration in the more heavily attacked areas. Where heavy corrosion had taken place, the sulphides connected the  $\delta$ -lamellae with the oxide scale, whereas in regions of slight corrosion this was not so, and a denuded zone remained separating the lamellae, and the sulphides, from the external scale. As noted in the previous section, the presence of a  $\delta$ -free zone assists  $\text{Al}_2\text{O}_3$  formation. At  $1000^\circ\text{C}$  some areas of heavy attack on the directionally solidified alloy had healed, presumably due to the formation of a denuded zone beneath the nodule. Figure 27 (b) shows such a nodule in which the outer portion is typical of a rapidly formed scale and the inner portion is similar to that formed in the slightly attacked areas.

All three alloys behave similarly at  $1100^\circ\text{C}$  and the scale is similar to that formed in the absence of  $\text{Na}_2\text{SO}_4$  described previously: an outer NiO layer, an intermediate layer containing  $\text{NiNb}_2\text{O}_5$ ,  $\text{NiAl}_2\text{O}_4$ , and  $\text{AlNbO}_4$ , and an inner layer of  $\text{AlNbO}_4$ ,  $\text{Nb}_2\text{O}_5$ , and nickel-rich metallic

islands underneath which is an  $\text{Al}_2\text{O}_3$  layer. There are no sulphides in the  $\delta$ -free zone.

The kinetics of the oxidation of the directionally solidified alloy, with and without a  $\text{Na}_2\text{SO}_4$  coating, are shown in Figure 28 at  $900^\circ\text{C}$ , and in Figure 29 at  $1000^\circ\text{C}$ . The presence of the salt only slightly increases the oxidation rate at  $900^\circ\text{C}$ , whereas the increase is greater at  $1000^\circ\text{C}$ . However, the oxidation rate is lower at  $1000^\circ\text{C}$  than at  $900^\circ\text{C}$ , since protective  $\text{Al}_2\text{O}_3$  layers are more easily formed at the higher temperatures (16).

Kinetic measurements were also carried out at  $870^\circ\text{C}$  with and without a salt coating, and are shown in Figure 30. The presence of the  $\text{Na}_2\text{SO}_4$  coating significantly reduces the oxidation rate. The reason for this becomes apparent on examining the scales formed in cross-section, as shown in Figure 31. The uncoated alloy shows preferential attack of the  $\delta$ -lamellae producing fingers of oxide ( $\text{Nb}_2\text{O}_5$  and  $\text{AlNbO}_4$ ) penetrating into the alloy. However, in the presence of the salt a  $\delta$ -free zone is formed which results in a lower oxidation rate; sulphides are present beneath the  $\delta$ -free zone, but since they do not bridge the zone they have no effect as shown earlier.

Samples of each material were also corroded in the Dean apparatus with the  $\text{Na}_2\text{SO}_4$  maintained at  $1050^\circ\text{C}$  and the samples at  $950^\circ\text{C}$ , conditions which previously had given good correlation with practical experience for more conventional alloys (37). Little heavy corrosion was observed in any of the samples and the oxide morphology strongly resembled that formed in uncontaminated atmospheres. Figure 32 (a) shows a typical cross-section, and apart from the surface scale, sulphide formation ( $\text{NiS}$ ) has occurred below the  $\delta$ -free zone, again the sulphides being associated with the  $\delta$ -lamellae.

Samples were also exposed in the Dean apparatus to a salt mixture of  $\text{Na}_2\text{SO}_4 + 10\% \text{NaCl}$  and in some cases this produced complete attack of the 1 mm. thick coupons after 168h exposure (samples were thermally cycled to room temperature every 30h. approximately). This result was not

entirely reproducible, and Figure 32 (b) shows a heavily attacked area of a similar sample but where some underlying alloy remains. The outer oxide layer is similar to that formed during ordinary oxidation, and the  $\delta$ -phase is depleted at the alloy surface with both internal oxides ( $\text{NiAl}_2\text{O}_4$ ) and sulphides present in the  $\delta$ -free zone.

To examine the influence of the sulphides on the oxidation behaviour, samples of the directionally solidified alloys were pre-sulphidised in a  $\text{H}_2$ - $\text{H}_2\text{S}$  (90:10) mixture for 6 min. prior to oxidation at 900 and 1000°C; the kinetics are included in Figures 12 and 13. Pre-sulphidation produced a very rapid initial oxidation rate, which after approximately 4h. decreased to a level similar to that of un-presulphidized samples. Surprisingly, the weight gain was larger at 900°C than at 1000°C.

Typical cross-sections of the samples corroded at 900°C and 1000°C are compared in Figure 33. Severe corrosion has occurred and the surface scale is typical of that described earlier: an outer NiO layer, an intermediate layer of  $\text{NiNb}_2\text{O}_6$ ,  $\text{NiAl}_2\text{O}_4$  and  $\text{AlNbO}_4$ , and an inner layer containing  $\text{AlNbO}_4$ ,  $\text{Nb}_2\text{O}_5$  and nickel-rich islands. Many NiS particles are present across the  $\delta$ -free zone connecting the outer oxide layer to the  $\delta$ -lamellae in a manner similar to samples coated with  $\text{Na}_2\text{SO}_4$  before oxidation.

#### Ni-19.7Nb-6Cr-2.5Al

The influence of a  $\text{Na}_2\text{SO}_4$  coating is not very marked at 900°C, and all three alloys behave very similarly. In each case most of the alloy is relatively unattacked, Figure 34 (a). The outer layer mainly consists of  $\text{NiNb}_2\text{O}_6$ , and underneath this, there is a continuous  $\text{Al}_2\text{O}_3$  layer protecting the alloy. In the  $\delta$ -free zone there are some internal  $\text{Cr}_2\text{O}_3$  and  $\text{Al}_2\text{O}_3$  particles, and nickel sulphides next to the  $\text{Ni}_3\text{Nb}(\delta)$  lamellae. There are, however, a few random areas where severe oxidation has taken place, presumably by breakdown of the protective,  $\text{Al}_2\text{O}_3$  layer. A cross-section of this nodular attack is shown in Figure 34 (b). The nodules consist of  $\text{NiNb}_2\text{O}_6$  and  $\text{NbCrO}_4$  and metallic islands of virtually

pure nickel, the distribution of the phases reflecting the original eutectic structure; a semi-continuous  $\text{Al}_2\text{O}_3$  layer is present at the base of the nodules. As observed earlier, in the alloy behind the nodules  $\text{NiS}$  has been formed, bridging across the  $\delta$ -free zone; behind the protective scale the sulphide precipitates lie behind the  $\delta$ -free zone.

At 1000 and 1100°C oxidation of the  $\text{Na}_2\text{SO}_4$ -coated alloys is more uniform as shown in Figure 35. The outer oxide layer is mainly  $\text{NiCr}_2\text{O}_4$ , whilst underneath there is a layer of  $\text{Cr}_2\text{O}_3$ , containing particles of  $\text{NbCrO}_4$ . Internal oxides of  $\text{Al}_2\text{O}_3$  are also present, together with nickel-rich sulphides on the inside of the  $\delta$ -free zone, adjacent to the  $\text{Ni}_3\text{Nb}$  lamellae. However, chromium-rich sulphides have also been formed deeper in the alloy. Surprisingly similar sulphides are observed in the samples oxidised at 1100°C.

The oxidation kinetics of this alloy oxidised with and without a  $\text{Na}_2\text{SO}_4$  coating at 900 and 1000°C are shown in Figures 36 and 37: The coating has produced only a marginal increase in the overall oxidation rate.

Samples were oxidised in the Dean apparatus under similar conditions to the ternary eutectic alloys. When the condensing salt was  $\text{Na}_2\text{SO}_4$ , there was no evidence of sulphide formation and the oxide morphology was identical to that produced by direct oxidation. However, on addition of 10%  $\text{NaCl}$  to the salt mixture, as with the ternary alloys, the severity of the attack was considerably increased and some samples were completely oxidised after 168h. Figure 38 shows a typical cross-section with  $(\text{AlCr})\text{NbO}_4$  formed internally and copious amounts of sulphide ( $\text{NiS}$ ).

Presulphidation at 900°C had little effect on the oxidation kinetics of this quaternary alloy, as shown in Figure 36. However, at 1000°C a similar treatment had a catastrophic effect: Figure 37. Figure 39 shows a typical cross-section of the scale: an outer  $\text{NiO}$  layer, an intermediate layer of  $\text{NiNb}_2\text{O}_6$ ,  $\text{NiAl}_2\text{O}_4$ , and  $\text{NbCrO}_4$ , and an



inner layer containing nickel-rich metallic islands,  $\text{AlNbO}_4$ ,  $\text{Nb}_2\text{O}_5$  and  $\text{NbCrO}_4$ . There is heavy internal sulphidation with the sulphides bridging the  $\delta$ -free zone.

Carbide-Based Eutectic Alloys

(a) Oxidation

(i) Co-Cr-C

Four main types of oxide morphology are produced, and Table I summarises the detailed observations.

TABLE I

SUMMARY OF THE OXIDE SCALE STRUCTURES FORMED ON Co-41Cr-2.4C ALLOYS

<u>Condition of Alloy</u>	<u>Type of Scale</u>		
	<u>900°C</u>	<u>1000°C</u>	<u>1100°C</u>
As cast	I	II	III
Slowly cooled	I + III	II + III	III
3.4 cm/h )	Directionally solidified	III	IV
10.6 cm/h )		III	IV
31.5 cm/h )		III	IV

Key :-

- I - Surface scale consisting largely of  $\text{Cr}_2\text{O}_3$ , a zone depleted in carbide, and no internal oxidation.
- II - Surface scale consisting largely of  $\text{Cr}_2\text{O}_3$ , with a zone depleted in carbide containing internal oxide particles of  $\text{Cr}_2\text{O}_3$ .
- III - Surface scale consisting largely of  $\text{Cr}_2\text{O}_3$ , and internal attack of the carbide network to form  $\text{Cr}_2\text{O}_3$ .
- IV - Surface scale containing both chromium and cobalt-rich oxides, and heavy attack of the carbide network, again forming largely chromium-rich oxides.

Scale of types I-III usually occur at the lower temperatures and with the least aligned structures, whereas type IV occurs more extensively at the higher temperatures and with the more aligned structures. Representative cross-sections are shown in Figure 40, and it is clear that types I-III are

the more oxidation-resistant.

The oxidation kinetics of the three directionally solidified eutectic alloys at 900°C and 1000°C are shown in Figures 41 and 42. There is no systematic variation in the oxidation rates with the alloy cooling rate (eutectic spacing) or with temperature. The alloy with the slowest cooling rate (most widely spaced carbide fibres) oxidises faster at 900°C than at 1000°C. Furthermore, the alloy of intermediate carbide spacing oxidises at the fastest rate at both temperatures. Table II summarizes the approximate parabolic rate constants. However, the depth of penetration of the carbide network is probably the more critical factor, and these values are shown in Table III. Increasing both the fibre alignment and the temperature generally causes a greater depth of attack.

TABLE II  
PARABOLIC RATE CONSTANTS FOR THE OXIDATION OF THE  
VARIOUS DIRECTIONALLY SOLIDIFIED EUTECTIC ALLOYS

<u>Alloy</u>	<u>Parabolic Rate Constant</u>	
	<u>(g. <sup>2</sup>m. <sup>-4</sup>s. <sup>-1</sup>)</u>	
	<u>900°C</u>	<u>1000°C</u>
Co-41Cr-2.4C (3.4)	0.002	0.022
Co-41Cr-2.4C (10.6)	0.091	0.111
Co-41Cr-2.4C (31.5)	0.061	0.011
Co-15Cr-13TaC	0.114	0.059
Co-20Cr-10Ni-13TaC	0.001	0.014
Ni-12.3Cr-6.9Al-1.8C	0.142	0.036

TABLE III

DEPTHS OF OXIDE PENETRATION FOR THE OXIDATION  
OF THE VARIOUS EUTECTIC ALLOYS

<u>Alloy</u>	<u>Depth of Penetration (<math>\mu\text{m}</math>)</u>		
	<u>900°C</u>	<u>1000°C</u>	<u>1100°C</u>
Co-41Cr-2.4C (as cast)	17	33	30
Co-41Cr-2.4C (slow cool)	27	43	60
Co-41Cr-2.4C (D.S. 3.4)	20	70	$\infty$
Co-41Cr-2.4C (D.S. 10.6)	33	110	167
Co-41Cr-2.4C (D.S. 31.5)	23	60	120
Co-15Cr-13TaC (as cast)	17	13	50
Co-15Cr-13TaC (slow cool)	20	17	53
Co-15Cr-13TaC (D.S.)	13	33	33
Co-20Cr-10Ni-13TaC (as cast)	0	17	40
Co-20Cr-10Ni-13TaC (slow cool)	10	40	100
Co-20Cr-10Ni-13TaC (D.S.)	10	27	47
Ni-12.3Cr-6.9Al-1.8C (as cast)	0	0	0
Ni-12.3Cr-6.9Al-1.8C (slow cool)	0	0	0
Ni-12.3Cr-6.9Al-1.8C (D.S.)	0	33	113

(ii) Co-Cr-TaC

Each of the three Co-15Cr-13TaC alloys behaves quite similarly at 900°C; the scale consists of an outer CoO layer and underneath this is a spinel layer containing  $\text{CoCr}_2\text{O}_4$  and  $\text{CoTa}_2\text{O}_6$ ; at the alloy interface there are areas rich in  $\text{Ta}_2\text{O}_5$  and  $\text{Cr}_2\text{O}_3$ , and there is only slight internal oxidation of the TaC carbide network forming  $\text{Ta}_2\text{O}_5$ . Improving the alignment of the TaC fibres only has a small effect, causing a slight increase in the overall outer oxide thickness, the  $\text{Cr}_2\text{O}_3$ -rich areas, and the amount of internal oxidation of the fibres themselves. The  $\text{CoTa}_2\text{O}_6$  particles within the spinel layer tend to resemble the original shape of the TaC fibres.

Similar features are also evident at 1000°C, except that there is a tendency for the outer oxide layer to spall, particularly with the

directionally solidified alloy; there is also more internal oxidation of the TaC fibre network. At 1100°C the outer oxide layer (CoO + spinel) is very thick in each case, and prone to spalling, particularly with the directionally solidified alloy. A  $\text{Cr}_2\text{O}_3$  layer attempts to form at the alloy interface, beneath which is a zone depleted in the TaC fibres, and containing internal  $\text{Cr}_2\text{O}_3$  and  $\text{Ta}_2\text{O}_5$  particles.

Representative cross-sections of the various oxidised structures, at each of these three temperatures, for the ternary alloy are shown in Figure 43, illustrating the features which have been described in detail above.

The quaternary alloys (Co-20Cr-10Ni-13TaC) are more oxidation resistant than the ternary alloy; the as-cast alloy rapidly forms a protective  $\text{Cr}_2\text{O}_3$  layer at 900°C, and there is virtually no attack of the fibres. However, as the alignment of the TaC fibres improves, the alloy apparently has more difficulty in forming a protective  $\text{Cr}_2\text{O}_3$  layer; internal oxidation of the TaC fibres occurs producing internal  $\text{Ta}_2\text{O}_5$  oxides. In some areas there is considerable oxidation of the matrix producing scale nodules containing CoO and  $\text{CoCr}_2\text{O}_4$ ,  $\text{NiCr}_2\text{O}_4$ ,  $\text{CoTa}_2\text{O}_6$ , although eventually an underlying protective  $\text{Cr}_2\text{O}_3$  protective  $\text{Cr}_2\text{O}_3$  layer develops.

Similar behaviour is also seen at 1000°C, but the overall attack is more extensive. Again the as-cast alloy rapidly forms a protective  $\text{Cr}_2\text{O}_3$  layer, but adjacent to the alloy/oxide interface there is a zone depleted in the TaC fibres and containing  $\text{Cr}_2\text{O}_3$  and  $\text{Ta}_2\text{O}_5$  internal oxides. The furnace cooled and directionally solidified alloys show similar features as at 900°C, except that the oxide nodules are larger and internal oxidation of the TaC fibres is more extensive. The nodules also tend to be larger on the directionally solidified alloy substrate.

At 1100°C each of the alloys is subject to scale spallation, at least on cooling from the reaction temperature. The as-cast alloy has a fairly thin outer oxide layer, consisting of the Ni- and Co-containing spinels based on Cr and Ta ( $\text{CoCr}_2\text{O}_4$ ,  $\text{NiCr}_2\text{O}_4$ ,  $\text{CoTa}_2\text{O}_6$ ,  $\text{NiTa}_2\text{O}_6$ ). There is also a layer depleted in the TaC fibres containing internal oxides ( $\text{Cr}_2\text{O}_3$  and  $\text{Ta}_2\text{O}_5$ ). In some areas these internal oxides are inter-connected, thus isolating metal particles within the outer oxide scale. The thick outer CoO layer has spalled on cooling. Similar behaviour occurs with the furnace cooled alloy, except that the internal oxidation is more extensive, and also with the directionally solidified alloy, where again the outer CoO layer has spalled after cooling, but there is less internal oxidation. Microstructures illustrating these various features at each of the three temperatures are shown in Figure 44.

Weight gain/time curves for the ternary and quaternary directionally solidified alloys at 900°C and 1000°C are shown in Figures 45 and 46 respectively. Approximately parabolic behaviour is observed in each case, with the parabolic rate constants being shown in Table II. The depth of oxide penetration is shown in Table III, indicating that as the alignment of the fibres and temperature increases so does the amount of attack.

(iii) Ni-Cr-Al-C

At 900°C all of the alloys rapidly form a protective  $\text{Al}_2\text{O}_3$  layer, and there is virtually no attack of the carbide network. With the as-cast and slowly cooled alloys at 1000°C internal oxidation of the carbide network is not apparent, although slight blistering of the protective  $\text{Al}_2\text{O}_3$  is evident, suggesting some oxidation of the carbides has occurred, but insufficient for complete scale failure. However, with the directionally solidified alloy significant oxidation of the  $\text{Cr}_7\text{C}_3$  fibres occurs,  $\text{Al}_2\text{O}_3$  forms internally, and a non-protective scale of  $\text{Cr}_2\text{O}_3$  forms externally.

Each of the three alloys has considerably more difficulty in forming a protective oxide layer at 1100°C. The as-cast and slowly cooled alloys form a convoluted outer  $\text{Al}_2\text{O}_3$  layer. Presumably formation of gaseous

oxides of carbon have some disrupting influence on the protective oxide layer, although there is no obvious evidence of gross-oxidation of the carbides in the cross-sections; possibly spalling has occurred on cooling. The directionally solidified alloy does not form a protective  $\text{Al}_2\text{O}_3$  layer, and suffers severe internal oxidation. The structure consists of an outer discontinuous  $\text{Cr}_2\text{O}_3$  layer, beneath which is an internal dispersion of  $\text{Al}_2\text{O}_3$  particles and  $\text{Al}_2\text{O}_3$  platelets in a (Ni, Cr) matrix, and below which is the unaffected  $\text{Ni}_3\text{Al/Cr}_7\text{C}_3$  matrix. Figure 47 illustrates each of these morphological features.

The oxidation kinetics at  $900^\circ\text{C}$  and  $1000^\circ\text{C}$  are shown in Figures 48 and 49, indicating parabolic behaviour, with the parabolic rate constants being shown in Table II. The depth of oxide penetration is shown in Table III, again demonstrating that both improved fibre alignment and temperature accelerate the oxidation rate.

(b) Hot-corrosion

(i) Co-Cr-C

Generally, the presence of a  $\text{Na}_2\text{SO}_4$  coating barely affects the oxidation behaviour at  $900^\circ\text{C}$  of the various Co-41Cr-2.4C alloys. A protective  $\text{Cr}_2\text{O}_3$  scale develops on the as-cast and slowly cooled alloys, as well as those which have been directionally solidified, and there is no evidence of a zone depleted in carbides beneath the scale. The carbide network suffers some internal oxidation, and chromium-rich sulphides (CrS) are precipitated within the matrix ahead of the internal oxidation zone.

Similar behaviour also occurs at  $1000^\circ\text{C}$ , although the extent of surface scaling and penetration of the carbide network is greater. The oxidation kinetics of the directionally solidified alloy cooled at  $10.6 \text{ cm/h}$ , with and without a  $\text{Na}_2\text{SO}_4$  coating are presented in Figures 41 and 42 for  $900^\circ\text{C}$  and  $1000^\circ\text{C}$  respectively; the presence of the salt coating has apparently decreased the rate at both temperatures.

At  $1100^\circ\text{C}$  no outer, cobalt-rich oxides are formed as in the absence of the  $\text{Na}_2\text{SO}_4$  coating, which suggests that again the coating

assists in the rapid establishment of a  $\text{Cr}_2\text{O}_3$  layer. Representative cross-sections of these various coated specimens are shown in Figure 50, for each of the three temperatures.

Presulphidation increases the subsequent oxidation rate at both  $900^\circ\text{C}$  and  $1000^\circ\text{C}$ , as shown in Figures 41 and 42. However, the rate tends to decrease after about three hours to a level similar to that of direct oxidation. Furthermore, the increase in rate is greater at  $900^\circ\text{C}$  than at  $1000^\circ\text{C}$ , as in the initial oxidation rate without any pre-sulphidation. Table IV compares the approximate parabolic rate constants for oxidation with and without a  $\text{Na}_2\text{SO}_4$  coating and following pre-sulphidation, for the directionally solidified alloy cooled at 10.6 cm/h. There is no real systematic variations in the rate constants with either the type of test or temperature. However, the depth of penetration of the carbide network is probably the critical factor. Figure 51 (a) shows a typical cross-section for an alloy pre-sulphidised prior to oxidation at  $1000^\circ\text{C}$ ; the total depth of internal oxidation is greater than that for alloys not given a pre-sulphidation treatment.

TABLE IV  
APPROXIMATE PARABOLIC RATE CONSTANTS FOR THE DIRECTIONALLY  
SOLIDIFIED EUTECTIC ALLOY Co-41Cr-2.4C COOLED AT 10.6 cm/h.

<u>Test</u>	<u>Approximate Rate Constant</u> <u>(g. m. <sup>-4</sup> s. <sup>-1</sup>)</u>	
	<u>900°C</u>	<u>1000°C</u>
Oxidation	0.09	0.11
$\text{Na}_2\text{SO}_4$ coating (1 mg.cm. <sup>-2</sup> )	0.003	0.01
Sulphidation/oxidation	0.47	0.28

Since sodium sulphate has little effect on these alloys a  $\text{Na}_2\text{SO}_4/10\%$  NaCl mixture was used in the Dean Test. However, the salt condensing onto the samples is richer in NaCl because of its higher

volatility. After 24 h exposure in the Dean Test, all the directionally solidified alloys have a rather loose, outer, non-protective oxide layer consisting of  $\text{CoO}$ ,  $\text{CoCr}_2\text{O}_4$ , and  $\text{Cr}_2\text{O}_3$ , as shown in Figure 51 (b). Internal voids are observed within the alloy and also chromium-rich particles at even deeper locations. The presence of the voids suggest participation of a volatile species at the reaction temperature.

Catastrophic oxidation of the alloys occurs under similar exposure conditions, but after 4 x 24 h cycles, as shown in Figure 51 (c). A thick, porous scale is formed and the carbide network within the alloy has been severely attacked.

(ii) Co-Cr-TaC

The main effect of the presence of a  $\text{Na}_2\text{SO}_4$  coating on the oxidation of the Co-15Cr-TaC alloys is to increase the extent of internal oxidation of the TaC fibres at each of the three temperatures, resulting in internal oxides containing  $\text{Cr}_2\text{O}_3$  and  $\text{Ta}_2\text{O}_5$ , ahead of which are CrS particles associated with unaffected TaC fibres. The only effect of the degree of alignment of the fibres is in the appearance of the internal oxides, which they resemble. At  $1000^\circ\text{C}$  -  $1100^\circ\text{C}$  the outer oxide is more porous, which coincides with the formation of sodium chromate. Furthermore at  $1100^\circ\text{C}$ , the internal oxides formed within the directionally solidified alloy coalesce and leave metal islands (virtually pure cobalt) isolated in the outer oxide scale. Representative morphologies are shown in Figure 52.

The kinetics at  $900^\circ\text{C}$  and  $1000^\circ\text{C}$  (Figures 45 and 46) indicate that the presence of a  $\text{Na}_2\text{SO}_4$  coating initially increases the oxidation rate, although during the later stages it decreases to that of ordinary oxidation, with the overall weight gain being slightly less.

Pre-sulphidation also increases the oxidation rate, both at  $900^\circ\text{C}$  and  $1000^\circ\text{C}$ , as shown in the kinetics (Figures 45 and 46). This coincides with severe internal oxidation of the TaC fibre network, as illustrated in



Figure 53 (a), with sulphides (CrS) again being present ahead of the oxides associated with the TaC fibres.

Exposure in the Dean Rig causes even more extensive internal oxidation and sulphidation of the TaC fibres, and also the formation of an outer porous, non-protective oxide layer containing CoO,  $\text{CoCr}_2\text{O}_4$ ,  $\text{Cr}_2\text{O}_3$ , and  $\text{Na}_2\text{CrO}_4$  (Figure 53 (b)).

The presence of a  $\text{Na}_2\text{SO}_4$  coating has a similar effect on the quaternary alloy (Co-20Cr-10Ni-TaC) as with the ternary alloy; representative cross-sections are shown in Figure 54.

Oxidation kinetics with and without a salt coating are shown in Figures 45 and 46 at  $900^\circ\text{C}$  and  $1000^\circ\text{C}$  respectively, indicating that the  $\text{Na}_2\text{SO}_4$  layer has a similar effect as with the ternary alloy.

The effect of pre-sulphidation again increases the oxidation rate at both temperatures as shown in Figures 45 and 46, but not as greatly as does the salt coating. However, extensive internal oxidation, accompanied by sulphidation, occurs as seen in Figure 55 (a). Approximate parabolic rate constants for the various kinetics curves shown for each directionally solidified alloy are given in Table V.

TABLE V  
APPROXIMATE PARABOLIC RATE CONSTANTS FOR THE DIRECTIONALLY  
SOLIDIFIED EUTECTIC ALLOYS Co-15Cr-TaC AND Co-20Cr-10Ni-13TaC

(Figures for quaternary alloy in brackets)

<u>Test</u>	<u>Approximate Rate Constant</u> ( $\text{g.}^2\text{m.}^{-4}\text{s.}^{-1}$ )	
	<u><math>900^\circ\text{C}</math></u>	<u><math>1000^\circ\text{C}</math></u>
Oxidation	0.114 (0.001)	0.059 (0.014)
$\text{Na}_2\text{SO}_4$ coating (1 mg.cm. <sup>-2</sup> )	0.127 (0.144)	0.069 (0.018)
Sulphidation/Oxidation	0.333 (0.008)	0.027 (0.004)

The Dean Test severely corrodes the alloy resulting in an outer porous, non-protective oxide layer containing CoO,  $\text{Cr}_2\text{O}_3$ ,  $\text{CoCr}_2\text{O}_4$  and  $\text{Na}_2\text{CrO}_4$ , accompanied by internal oxides and sulphides similar to those

formed during the coating test (Figure 55 (b)).

(iii) Ni-Cr-Al-C

With the  $\text{Na}_2\text{SO}_4$  coating test, the general morphology is similar for each of the alloys at the three temperatures studied, and is shown in Figure 56. Essentially, the scale consists of an outer oxide layer ( $\text{NiO}$ ,  $\text{NiCr}_2\text{O}_4$  and  $\text{NiAl}_2\text{O}_4$ ), an intermediate mixed metal and oxide layer ( $\text{Ni}$ ,  $\text{Al}_2\text{O}_3$ ,  $\text{Cr}_2\text{O}_3$ ), and an inner layer, consisting of virtually pure nickel and chromium-rich sulphides; these latter are not obviously associated with the  $\text{Cr}_7\text{C}_3$  fibres. Generally, the thickness of each layer increases with temperature and degree of alignment of the fibres, except at  $1100^\circ\text{C}$ , when there is less overall attack; at this temperature the salt coating is quickly lost by evaporation. Fibre alignment only seems to play a critical part in influencing the rate of attack when  $\text{Al}_2\text{O}_3$  forms a continuous layer, as seen previously during ordinary oxidation; this is apparently not the case in the presence of a  $\text{Na}_2\text{SO}_4$  coating.

The kinetic curves for the oxidation of the directionally solidified alloy, with and without a salt coating are shown in Figures 48 and 49; the presence of the  $\text{Na}_2\text{SO}_4$  coating greatly increases the oxidation rate.

Pre-sulphidation also greatly increases the oxidation rate, both at  $900^\circ\text{C}$  and  $1000^\circ\text{C}$ , as shown in Figures 48 and 49. Typical cross-sections are shown in Figure 57 (a), which strongly resembles that produced by the  $\text{Na}_2\text{SO}_4$  coating although the effect is much greater at  $1000^\circ\text{C}$ . This suggests that the primary role of  $\text{Na}_2\text{SO}_4$  is to supply sulphur for sulphidation, and any oxide fluxing is of secondary importance. The approximate parabolic rate constants for the various tests are shown in Table VI.

TABLE VI

APPROXIMATE PARABOLIC RATE CONSTANTS FOR THE DIRECTIONALLY  
SOLIDIFIED EUTECTIC ALLOY Ni-12.9Cr-6.9Al-1.8C

<u>Test</u>	<u>Approximate Rate Constant</u> ( $\text{g.}^2 \text{m.}^{-4} \text{s.}^{-1}$ )	
	<u>900°C</u>	<u>1000°C</u>
Oxidation	0.142	0.036
Na <sub>2</sub> SO <sub>4</sub> coating (1 mg.cm. <sup>-2</sup> )	0.156	0.181
Sulphidation/Oxidation	0.185	2.407

Thermal cycling in the Dean's Test in the presence of Na<sub>2</sub>SO<sub>4</sub>/10% NaCl condensing onto the surface has not greatly affected the rate of attack; Figure 57 (b) shows a typical cross-section. The surface scale is somewhat thinner than that on samples subjected to the Na<sub>2</sub>SO<sub>4</sub> coating test, but the inner oxide/alloy layer is correspondingly thicker. This could be due to the thermal cycling causing spallation of any outer oxide layer. Surprisingly, the NaCl has not caused excessive attack of the carbide fibres, as it did with the Co-41Cr-2.4 alloy, which also contains Cr<sub>7</sub>C<sub>3</sub> fibres.

For each of these alloy systems the presence of a Na<sub>2</sub>SO<sub>4</sub> coating increases the depth of attack during oxidation as can be seen from comparing Tables VII and III.

TABLE VII

DEPTHS OF OXIDE PENETRATION FOR THE OXIDATION OF THE VARIOUS  
EUTECTIC ALLOY IN THE PRESENCE OF Na<sub>2</sub>SO<sub>4</sub>

<u>Alloy</u>	<u>Depth of Penetration (µm)</u>		
	<u>900°C</u>	<u>1000°C</u>	<u>1100°C</u>
Co-41Cr-2.4C (as cast)	27	40	53
Co-41Cr-2.4C (slow cooled)	33	50	70
Co-41Cr-2.4C (D.S. 3.4)	17	70	130
Co-41Cr-2.4C (D.S. 10.6)	27	73	83
Co-41Cr-2.4C (D.S. 31.5)	20	70	80
Co-15Cr-13TaC (as cast)	50	83	133
Co-15Cr-13TaC (slow cool)	33	100	167
Co-15Cr-13TaC (D.S.)	70	133	116
Co-20Cr-10Ni-13TaC (as cast)	30	47	70
Co-20Cr-10Ni-13TaC (slow cool)	50	40	113
Co-20Cr-10Ni-13TaC (D.S.)	27	37	233
Ni-12.3Cr-6.9Al-1.8C (as cast)	70	167	300
Ni-12.3Cr-6.8Al-1.8C (slow cool)	70	100	400
Ni-12.3Cr-6.8Al-1.8C (D.S.)	70	167	160

Both the sulphidation/oxidation treatment and the Dean's test also greatly increase the overall depth of attack, as can be seen by comparing Tables VIII and III.

TABLE VIII  
DEPTH OF OXIDE PENETRATION FOR THE HOT CORROSION  
OF VARIOUS EUTECTIC ALLOYS

<u>Alloy</u>	<u>Depth of Penetration (<math>\mu\text{m}</math>)</u>	
	<u>S/O (1000°C)</u>	<u>Deans (950°C)</u>
Co-41Cr-2.4C (D.S. 10.6)	100	$\infty$
Co-15Cr-13TaC	25	133
Co-20Cr-10Ni-TaC	25	200
Ni-12.3Cr-6.9Al-1.8C	40	113

Discussion

Ni<sub>3</sub>Al-Ni<sub>3</sub>Nb Based Eutectic Alloys

(a) Oxidation

Table IX compares the oxidation rates (in terms of the approximate parabolic rate constant) of these eutectic alloys with those of more conventional superalloys (38): B-1900 and IN713LC are nickel-base alloys which form  $\text{Al}_2\text{O}_3$  scales, and IN-738 and X-40 are nickel and cobalt-base alloys respectively which form  $\text{Cr}_2\text{O}_3$  scales.

TABLE IX  
PARABOLIC RATE CONSTANTS FOR THE OXIDATION OF VARIOUS ALLOYS AT 900°C

<u>Alloy</u>	<u><math>K_p, \text{g}^2\text{m}^{-4}\text{s}^{-1}</math></u>
B-1900	$3.3 \times 10^{-3}$
IN-738	$8.5 \times 10^{-3}$
IN-713LC	$1.6 \times 10^{-2}$
X-40	$5.8 \times 10^{-3}$
Ni-23Nb-4.4Al	$4.7 \times 10^{-2}$
Ni-19.7Nb-6Cr-2.5Al	$4.6 \times 10^{-3}$

The quaternary alloy compares favourably with that of the more conventional alloys, whilst the ternary alloy is considerably less

resistant. However, at higher temperatures the rates are more compatible.

The scale morphologies and compositions observed are in reasonable agreement with those of previous investigations (14-16). The important factor appears to be whether or not a  $\delta$ -free zone is established between the surface scale and the alloy eutectic structure. This in turn depends in a complex way on: (i) temperature, (ii) the degree of alignment and spacing of the eutectic and (iii) the composition of the alloy.

Generally, preferential oxidation of the  $\delta$ -phase only occurs at low temperatures, 800°C and below (15), and at all higher temperatures, a  $\delta$ -free zone is formed at the surface of the alloy. However, in the present work, preferential attack did occur at 900°C, but only with the slowly-cooled alloy; the structure of this alloy may best be described as partially aligned, in that the eutectic shows good alignment within the large, individual grains; but the grains are randomly orientated one with another. Both the completely random alloy, and the completely aligned alloys developed  $\delta$ -free zones at 900°C.

The interphase boundaries presumably can act as preferential paths for oxygen diffusion inwards, but also for niobium and aluminium outwards. The limited alignment in the slowly cooled alloy may limit the latter process, resulting in fingers of oxide penetrating from the surface scale into the alloy.

Under most other conditions, especially at the higher temperatures, the attack of the alloys was relatively uniform and a zone of depletion of the  $\delta$ -lamellae was produced at the alloy surface, through which aluminium and niobium diffused into the scale where they were oxidised to  $Nb_2O_5$ ,  $AlNbO_4$  and  $Al_2O_3$ . As the zone of  $\gamma$ -phase receded into the alloy, nickel-rich islands were incorporated into this mixed oxide layer. As oxidation continues, nickel diffuses from the nickel-rich islands and forms an external NiO layer. Surprisingly, this process occurs relatively

slowly at 900°C as presumably all the inward diffusing oxygen must react with the aluminium and niobium. At 1000°C, the nickel-rich islands are more readily oxidized, making the outer NiO layer correspondingly thicker than at the lower temperatures.

At 1100°C, a protective Al<sub>2</sub>O<sub>3</sub> layer develops at the interface between the δ-free zone and the mixed metal/oxide layer, reducing the overall oxidation rate. This is probably related to the relatively higher diffusion rate of aluminium at this higher temperature which permits sufficient lateral diffusion to support the continued growth of Al<sub>2</sub>O<sub>3</sub>, as suggested by Smeggil (16). At the lower temperatures, only a discontinuous Al<sub>2</sub>O<sub>3</sub> layer forms and, as observed, the oxidation rate is more dependent on the structure of the eutectic.

Clearly, the establishment of a Ni<sub>3</sub>Nb-free zone at the surface of the alloy is critical and implies that Nb is selectively oxidised from the alloy in the early stages. If it is assumed that only Nb<sub>2</sub>O<sub>5</sub> is formed during the initial stages of oxidation then a weight gain of 10 mg/cm<sup>2</sup> would correspond approximately to a Ni<sub>3</sub>Nb-free zone thickness of 55 μm. (These figures neglect the gamma-phase in the matrix, and assume a density for the alloy of 8,62 g/cm<sup>3</sup>; the volume % of Ni<sub>3</sub>Nb is 44). If Al<sub>2</sub>O<sub>3</sub> forms a continuous layer after this weight gain and selective oxidation of niobium ceases, the thickness of the Ni<sub>3</sub>Nb-free zone would be expected to contract. However, the zone contains sufficient aluminium for continued growth of the Al<sub>2</sub>O<sub>3</sub> at the measured rate for approximately 6 x 10<sup>4</sup> days. Thus, it is not surprising that no contraction in the thickness of the Ni<sub>3</sub>Nb-free zone is observed.

These figures agree reasonably well with those observed for the directionally solidified samples oxidised at 1100°C, which forms a depletion zone about 50 μm wide, following relatively extensive oxidation before the protective Al<sub>2</sub>O<sub>3</sub> layer forms. There is some aluminium depletion within this zone, but not sufficient to make the protective

$\text{Al}_2\text{O}_3$  layer unstable. Once the continuous  $\text{Al}_2\text{O}_3$  layer has formed above the  $\text{Ni}_3\text{Nb}$ -free zone, the oxidation-prone  $\text{Ni}_3\text{Nb}$  lamellae are separated from the oxidising atmosphere. Thus, the alloy in effect behaves as a single phase material, and retains this configuration providing the  $\text{Al}_2\text{O}_3$  layer does not fail. Spallation of the  $\text{Al}_2\text{O}_3$  layer would cause further aluminium consumption and a narrowing of the depletion zone. A rapid increase in oxidation rate might be expected, particularly if the fibres again become exposed to the oxidising atmosphere.

During the early stages of oxidation when the  $\text{Ni}_3\text{Nb}$ -free zone, if formed, is very thin, the aluminium concentration will vary along the alloy/scale interface, being low directly above the  $\text{Ni}_3\text{Nb}$  fibres. However, as oxidation continues and the zone widens, lateral diffusion of aluminium can be expected to even out these concentration differences. Eventually, the lateral diffusion will be sufficient to allow the continuous  $\text{Al}_2\text{O}_3$  scale to form (Figure 58). This final step only seems to occur at  $1100^\circ\text{C}$ , presumably when the lateral diffusion is sufficiently rapid, and the depletion zone wide enough, for the aluminium concentration to reach a high enough level all along the alloy/scale interface. At lower temperatures, the depletion zone is too narrow preventing  $\text{Al}_2\text{O}_3$  formation and this allows continued oxidation of the Nb-rich phase and the matrix, resulting in the heterogeneous scale structures typified in Figure 59.

The relative thicknesses of the various layers varies with temperature, and presumably this is related to the changes in relative diffusion rates through the scale. Once the protective  $\text{Al}_2\text{O}_3$  layer is formed, the scaling rate is very much reduced and oxidation of the nickel-rich islands in the outer oxide layer takes place as has been shown earlier; this produces a more homogeneous outer oxide scale.

Because of the randomizing effect of the depletion zone, the degree of alignment of the fibres does not affect the oxidation rate,

unless it interferes with the outward diffusion process. This latter point has been demonstrated earlier with slowly cooled alloys, when adjacent grains of differently orientated fibres near the alloy/scale interface prevented a sufficiently wide depletion zone forming. Thus, the aluminium concentration at the alloy surface was insufficient for the protective oxide to form along the entire interface; this was particularly noticeable above the  $Ni_3Nb$  fibres.

During the initial stages of oxidation, fibre spacings are clearly important: the larger they are, the less uniform will be the aluminium concentration near the alloy surface. Thus, with widely spaced fibres a wide depletion zone is required in order to achieve a uniform concentration of aluminium at the alloy surface for protective oxide formation. Consequently, the overall weight gain would be larger for the more widely spaced fibres. Smeggil (15) and Thompson (18) have both shown that the fibre size is not critical to the oxidation kinetics, once  $Al_2O_3$  has formed.

In conclusion then, it seems appropriate to summarise the mechanism of oxidation of the directionally solidified eutectic alloy Ni-23.1Nb-4.4Al within the temperature range 800 - 1100°C; this is illustrated schematically in Figure 60.

- (a) Initially, preferential oxidation of the less-resistant  $Ni_3Nb$  fibres occurs; an outer NiO layer is formed, the nickel, for the most part, coming from the fibres, rather than the oxidation-resistant Ni/ $Ni_3Al$  matrix phase.
- (b) This process continues at temperatures below 900°C. At higher temperatures, the outward diffusion of Nb becomes more significant, and a depletion zone devoid of fibres is formed. Remnants of the oxidised  $Ni_3Nb$  lamellae can often be seen in the scale next to the outer NiO layer. Ni-rich metallic islands are also incorporated into the scale.



- (c) As oxidation continues, the mixed metal/oxide layer thickens, although the metallic islands are converted into oxide when they are pushed out into the outer regions of the scale.
- (d) No further changes in scale structure occur at 900 and 1000°C. However, at 1100°C, the depletion zone is wide enough for a uniform concentration of aluminium to be produced at the alloy/scale interface and thus a continuous and protective  $\text{Al}_2\text{O}_3$  scale forms. No further nickel or niobium enters the scale and the metallic islands are soon converted to oxide.

The presence of chromium in the quaternary alloy assists development of a continuous  $\text{Al}_2\text{O}_3$  layer even at 900°C. Initially, however, at 900°C the  $\delta$ -lamellae in the directionally solidified alloy are attacked preferentially, resulting in a depletion of the fibres; the thicker the fibres, the more extensive the preferential oxidation forming  $\text{Nb}_2\text{O}_5$ . At 1000°C, the directionally solidified alloy behaved in a similar manner to 900°C. However, with the other alloy structures the aluminium was oxidized internally and an external scale of  $\text{Cr}_2\text{O}_3$  was formed; the unaligned fibres hindered the outward diffusion of aluminium. At 1100°C aluminium is oxidized internally even with the aligned structure, and again the surface scale is primarily  $\text{Cr}_2\text{O}_3$ .

This beneficial effect of chromium to the oxidation resistance of the ternary Ni-Nb-Al alloy suggests the possibility of a gettering-type action as in, for example, Ni-Cr-Al alloys where the addition of chromium also greatly improves the oxidation resistance in comparison to binary Ni-Al alloys. Pettit and Giggins (39) found that chromium and aluminium are initially complementary in providing the oxidation resistance of Ni-Cr-Al alloys. Chromium allows a continuous, external layer of  $\text{Al}_2\text{O}_3$  to be formed on Ni-Cr-Al alloys at lower aluminium concentrations than would be the case in the absence of chromium, by contributing to the volume fractions of the precipitated oxide, which reduces the initial transport of oxygen into the alloy. In addition, aluminium promotes the

formation of continuous  $\text{Cr}_2\text{O}_3$  layers on some Ni-Cr-Al alloys for similar reasons. Thus, depending on the relative amounts of aluminium and chromium in the alloy, the oxidation resistance is increased for either of these reasons. Stott et al (40) also investigated the oxidation behaviour of Ni-Cr-Al alloys, and obtained similar results to Pettit and Giggins (39), in that aluminium and chromium act together in establishing a protective oxide layer of  $\text{Cr}_2\text{O}_3$  or  $\text{Al}_2\text{O}_3$  depending on the detailed alloy composition. They explained their results in terms of either chromium or aluminium "gettering" oxygen, thus suppressing the formation of NiO during the initial, transient stages and allowing a compact protective external oxide to form. With low aluminium contents (0.9-1.3%) the aluminium "getters" the oxygen, forming internal oxide particles, with an external  $\text{Cr}_2\text{O}_3$  scale forming by the usual outward diffusion of chromium ions. Eventually, these internal  $\text{Al}_2\text{O}_3$  particles link-up forming a continuous, protective  $\text{Al}_2\text{O}_3$  layer at the  $\text{Cr}_2\text{O}_3$ /alloy interface. Conversely, with high aluminium contents (4.3-5.7%), the chromium "getters" oxygen forming  $\text{Cr}_2\text{O}_3$  particles on the alloy surface, while a continuous  $\text{Al}_2\text{O}_3$  layer rapidly forms on the alloy surface which is free from chromium or nickel impurities.

However, the addition of Nb to the Ni-6Cr-2.5Al alloy reduces the oxidation rate significantly, and this would seem to suggest that niobium can act as a "getter" in promoting  $\text{Al}_2\text{O}_3$  formation. The stabilities of the various oxides, see Table X, are such that this is a possibility with  $\text{Nb}_2\text{O}_5$  being more stable than either  $\text{Al}_2\text{O}_3$  or  $\text{Cr}_2\text{O}_3$ .

TABLE X

FREE ENERGIES OF FORMATION OF OXIDES

<u>Oxide</u>	$\Delta G^\circ$ (Kcal/mole) at 900°C
$\text{Al}_2\text{O}_3$	-312.34
$\text{Cr}_2\text{O}_3$	-194.91
$\text{Nb}_2\text{O}_5$	-338.18

This seems unlikely, since the Ni-Nb-Al alloys cannot readily form protective layers of any form, as has been shown in the results section previously.

Thus, it would seem that niobium additions to Ni-Al alloys are unable to produce this "gettering action", and this may well relate to the relatively rapid growth rate of the oxide  $Nb_2O_5$ . Spinel is also formed, but these also seem to have little influence in retarding the oxidation rate. When chromium is present in the alloy, in addition to the niobium and aluminium, then an  $Al_2O_3$  scale does develop, which seems to point to the spinel phase  $CrNbO_4$  being involved.

Felton and Pettit (14) have shown that after 16 hours at  $1000^\circ C$ , a Ni-20Nb-10Cr alloy formed a thin layer of  $CrNbO_4$  over the surface, with a  $\gamma$ -Ni layer beneath containing no  $\sigma$ -phase; this scale afforded protection to the alloy substrate. Equally, this phase has been identified in the oxidation of Ni-19.7 Nb-6Cr-2.5Al, when an outer NiO layer,  $Nb_2O_5$  layer,  $CrNbO_4$  layer, and again an inner  $Al_2O_3$  were formed. However, when the interlamellae spalling was large, then there tended to be substantially more oxidation prior to the formation of the protective oxide and this was related to the increased lateral diffusion necessary. Thus the formation of a continuous  $CrNbO_4$  layer is apparently necessary, and thus prevents the rapid oxidation of the alloy during the initial stages, except of course, over large  $\delta$ -fibres when appreciable oxidation can occur before sufficient chromium diffuses laterally from the adjacent  $\gamma/\gamma'$  (Ni/Ni<sub>3</sub>Al,Cr) phase. During the formation of this  $CrNbO_4$  layer, aluminium oxidises internally, but eventually the  $Al_2O_3$  particles can link up producing a continuous, protective  $Al_2O_3$  layer. This schematic reaction mechanism is summarised in Figure 61.

At the higher temperatures ( $1100^\circ C$  and above) a protective  $CrNbO_4$  layer cannot form rapidly enough to prevent extensive growth of the faster growing oxides in the initial stages. When it does eventually form, the aluminium concentration at the alloy/oxide interface is too low

to form  $Al_2O_3$ , and  $Cr_2O_3$  eventually develops accompanied by internal  $Al_2O_3$  formation. This layer affords reasonable protection to the alloy.

(b) Hot-Corrosion

It seems appropriate to compare the influence of a  $Na_2SO_4$ -coating on the oxidation rate of these alloys, with its effect on more conventional superalloys (38). Table XI presents the approximate parabolic rate constants together with their ratio normalized to a  $1 \text{ mg/cm}^2$  coating of  $Na_2SO_4$ , which has been shown previously to give a good indication of the hot corrosion resistance (38).

TABLE XI  
PARABOLIC RATE CONSTANTS FOR THE HOT CORROSION OF VARIOUS ALLOYS  
AT 900°C

Alloy	Kp (in the presence of $Na_2SO_4$ ) $g^2 m^{-4} s^{-1}$	Kp (oxidation) $g^2 m^{-4} s^{-1}$	Kp <sup>SO<sub>4</sub></sup> /Kp <sup>oxid.</sup> normalized to unit coating thickness
B1900	1.72	0.003	604
IN738	0.008	0.008	1
IN713LC	3.5	0.016	150
X-40	0.002	0.005	0.4
Ni-23Nb-4.4Al	0.06	0.05	1.2
Ni-20Nb-6Cr-2.5Al	0.009	0.004	2.3

It is clear that the presence of  $Na_2SO_4$  does not produce markedly accelerated attack. However, it must be remembered that the values in Table XI refer to overall attack and not the nodular-type observed in some instances with the present alloys. In the nodular alloys, the  $Na_2SO_4$  coatings have produced considerable structural damage. Generally, similar rates are produced at  $1000^\circ C$ , but not at  $1100^\circ C$ ; most of the sulphate would be expected to volatilize very quickly from the surface at this latter, higher temperature.

As in the oxidation studies, behaviour is critically dependent on the presence of a  $\delta$ -free zone: if it is present, the alloys oxidize relatively slowly; if it is absent, then more rapid oxidation takes place. During the rapid oxidation, the  $\delta$ -lamellae are sulphidised essentially to NiS by the rapid inward transport of sulphur; the sulphides are then oxidised and the released sulphur diffuses further into the alloy repeating the process. Thus, the overall appearance of the resulting scale is similar to that of the original eutectic structure: alternate lamellae of oxide and a nickel-rich phase ( $\gamma$ ).

An apparently essential requirement for rapid oxidation to occur is that the sulphides "bridge" the  $\delta$ -free zone, connecting the unattacked  $\delta$ -lamellae and the oxide columns in the mixed metal/oxide layer. Similar relatively rapid rates of oxidation have been observed in the absence of sulphides when at lower temperatures, no  $\delta$ -free zone was formed (15).

The reaction mechanism is summarised in Figure 62. Essentially this is a sulphidation rather than an acidic fluxing mechanism, although it has been shown that  $Nb_2O_5$  has a high affinity for oxide ions and can influence the fluxing of oxide scales by molten  $Na_2SO_4$  deposits (38). Furthermore, aluminium-containing alloys are known to be very susceptible to accelerated attack via an acid fluxing mechanism (41,42). However, the morphologies of the scales produced on the present alloys were not consistent with a fluxing mechanism. As shown in Figure 62, initially an oxide scale forms on the surface of the alloy consisting of an outer layer of NiO and a mixed inner layer of  $Nb_2O_5$ ,  $AlNbO_4$ , and islands of nickel-enriched metal. A zone free of the  $\delta$ -phase ( $Ni_3Nb$ ) is formed at the surface of the alloy. Sulphur can then apparently diffuse through this oxide layer from the salt layer into the alloy where it reacts with the  $\delta$ -lamellae and precipitates nickel sulphide, the released niobium being oxidised. Sulphides can form at this alloy/scale interface because

the oxygen activity there will be very small; however, it is surprising that nickel sulphide forms in preference to aluminium sulphides. Continued reaction proceeds by oxidation of the sulphides and the surrounding matrix with the released sulphur penetrating deeper into the alloy along the  $\delta$ -lamellae. The rapid oxidation is apparently associated with this build up of sulphur in the heavily oxidised areas causing the  $\delta$ -free zone to be bridged by the sulphides, and thus rendered ineffective. Even during direct oxidation, under conditions where a  $\delta$ -free zone was established, the attack was relatively very much smaller than in conditions where this zone did not form.

The reaction mechanism tended to be independent of the alloy structure, although the morphology of the intermediate metal/oxide layer was related to the original eutectic structure, because of the preferential oxidation of the  $\delta$ -lamellae. The as-cast and slowly cooled samples were heavily attacked all over their surfaces, whereas the directionally solidified alloy only showed localized areas of accelerated attack. Possibly the alignment of the lamellae assisted the outward diffusion of aluminium and a protective  $\text{Al}_2\text{O}_3$  film was able to develop over parts of the surface. Certainly at  $1000^\circ\text{C}$ , some areas of rapid attack of the directionally solidified alloy reverted to a slow rate of attack by forming a  $\delta$ -free zone beneath the oxide nodule.

Presumably the initial stages of the reaction are important. In coating tests, the molten  $\text{Na}_2\text{SO}_4$  layer is in direct contact with the alloy surface immediately and sulphur can enter the alloy at an early stage in the overall process. However, in the Dean test with the  $\text{Na}_2\text{SO}_4$  condensing on the sample surface during the course of oxidation, a substantial thickness of oxide can form before sulphur enters the alloy. Thus, a  $\delta$ -free zone can be established before any sulphide precipitation occurs and the sulphides do not link the surface oxide with the unoxidized lamellae. The presence of chloride in the Dean test somehow prevents the

$\delta$ -free zone from forming, presumably by retarding the formation of any protective oxide. This allows rapid sulphidation and then oxidation of the alloy to occur.

Pre-sulphidation prior to oxidation exaggerates the effects of the sulphides and many sulphide bridges are formed across the  $\delta$ -free zone. A very rapid oxidation rate results.

The addition of chromium to the  $\gamma/\gamma'$  -  $\delta$  alloys appears to have a two-fold beneficial effect in reducing accelerated oxidation in the presence of  $\text{Na}_2\text{SO}_4$  or sulphides. These alloys show much fewer areas of heavy localised attack when coated with  $\text{Na}_2\text{SO}_4$  at  $900^\circ\text{C}$ . and particularly at  $1000^\circ\text{C}$ . Firstly, the presence of chromium appears to promote the formation of a continuous  $\text{Al}_2\text{O}_3$  layer, acting as a secondary getter in the now well established manner. The  $\text{Al}_2\text{O}_3$  limits inward sulphur penetration and fewer sulphides are formed in the alloy beneath the  $\delta$ -free zone. Where the heavier attack has occurred, there is no continuous  $\text{Al}_2\text{O}_3$  scale, and the surface scale is connected directly to the  $\delta$ -lamellae by sulphides bridging the  $\delta$ -free zone as discussed in the previous section. The second factor responsible for the reduction in attack is the preferential formation of chromium-rich sulphides as opposed to nickel sulphides, which minimizes the tendency for bridging of the  $\delta$ -free zone. This zone is generally severely depleted in chromium, as well as in the  $\delta$ -phase.

After the Dean test, no sulphides were formed within the alloy. This is somewhat surprising and implies that the  $\text{Al}_2\text{O}_3$  scale which developed was impervious to sulphur. However, other  $\text{Al}_2\text{O}_3$ -forming alloys have shown similar behaviour in the Dean test (37). The presence of chloride, however, can cause disruption of this protective layer and subsequent rapid attack.

Chromium has a less dramatic effect on the oxidation behaviour following pre-sulphidation, except at  $900^\circ\text{C}$ , and the quaternary alloy behaves in a similar manner to the ternary alloy, with nickel-rich

sulphides forming bridges across the  $\delta$ -free zone allowing rapid oxidation to continue. Presumably, at  $900^{\circ}\text{C}$  the inward diffusion rate of sulphur is insufficient to form the NiS bridges across the  $\delta$ -free zone, before it becomes too wide.

The analysis of the sulphides and the adjacent metallic region is shown below in terms of X-ray counts per second.

<u>Element</u>	<u>Sulphides</u>	<u>Metallic Region</u>
S	2083	131
Nb	1394	642
Al	7183	6161
Ni	18536	12166

Therefore, it seems that the sulphides are nickel-rich, but with an enrichment of aluminium compared to the metallic phase, which is not surprising since aluminium has a high affinity for sulphur (43). The niobium count is low compared to the unaffected  $\delta$ -phase, which suggests that it is rejected by the sulphur, perhaps forming NiNb, which would be expected to oxidise quite rapidly.

A piece of niobium was unaffected when sulphidised in a 90:10  $\text{H}_2/\text{H}_2\text{S}$  mixture, indicating that it has no affinity for sulphur, which could explain its rejection from the sulphidised areas of the lamellae.

The NiS particles are molten at these temperatures ( $900^{\circ}\text{C}$  -  $1100^{\circ}\text{C}$ ), and so it can rapidly penetrate into the alloy, thus advancing the corrosion front, particularly down the matrix/fibre interface, where oxygen can also rapidly diffuse causing oxidation of the prone  $\text{Ni}_3\text{Nb}$  fibres. Some of the sulphides are within the oxidised fibres, implying that the  $(\text{Ni},\text{Al})_{\text{x}}\text{S}_{\text{y}}$  sulphides are oxidised releasing the sulphur for further ingress into the alloy, while the  $(\text{Ni},\text{Al},\text{Nb})_{\text{x}}\text{O}_{\text{y}}$  oxides are left behind in the same shape as the pristine  $\text{Ni}_3\text{Nb}(\delta)$  fibres.

Moreover, when the AlS oxidise they release  $\text{SO}_2$ (44), which would further increase the oxidation rate by hindering any protective oxide formation due to scale blistering occurring.



Only in the sulphidation/oxidation experiments, where the fibres are extensively oxidised in the initial stages, does uniform attack occur. In the presence of sodium sulphate coatings non-uniform attack occurs, with nodules forming where rapid sulphidation/oxidation occurs, as described previously. However, in the lightly attacked areas sulphides are still formed, but behind the depletion zone, associated with the  $\delta$ -fibres. Sulphur has a high affinity for sulphur (43), and so the sulphides tend to form down the fibre/matrix interface, where they are more stable than in the  $\delta$ -free zone itself, which is virtually pure nickel ( $\gamma$ ) phase. Why the sulphides do not form across the depletion zone as before would seem to depend on the initial stages: if the zone forms rapidly the sulphur does not have time to bridge, and so is attracted to the inside, adjacent to the  $\delta$ -fibres, where there is a high aluminium concentration. Alternatively, this could occur if there is only a small sulphur concentration on the alloy surface. Conversely, if there is a high sulphur concentration, the depletion zone cannot form before sulphidation occurs, and so extensive sulphidation/oxidation can occur as described previously. These situations could occur easily in the salt coating test, where with molten salt it is easy to get significant variations in the surface concentration of sodium sulphate, ranging from high to low values. The Dean's test results support this type of behaviour, since the specimen is immediately exposed to a mildly sulphidising/oxidising atmosphere, which gives time for a depletion zone to form before appreciable sulphidation occurs, resulting in the sulphides forming adjacent to the  $\delta$ -fibres behind the depletion zone.

Some of these nodules "heal", with the oxide-sulphide fibre link being broken, and a depletion zone being established between the outer oxide and the sulphides. Presumably, this occurs because the inward diffusion rate of oxygen decreases to such an extent that it cannot drive the sulphides inwards, and so the depletion zone forms as above, with the sulphides on the inside, causing outward diffusion of niobium and aluminium

to become the rate controlling step.

These alloys do not appear to be attacked by a salt fluxing mechanism in the presence of sodium sulphate. Niobium would be expected to move the sodium sulphate in an acidic direction (like molybdenum does) due to the formation of the stable sodium niobate, and alumina scales are known to be susceptible to acidic fluxing (42), so that the alloys should have been rapidly attacked. However, these alloys form complex oxides during ordinary oxidation ( $\text{NiO}$ ,  $\text{AlNbO}_4$ ,  $\text{NiNb}_2\text{O}_6$ ,  $\text{Al}_2\text{O}_3$  and  $\text{Nb}_2\text{O}_5$ ) which presumably are not affected by acidic fluxing. Furthermore, the rapid sulphidation which occurs has the effect of balancing the salt chemistry, thus preventing acidic fluxing of the scale.

The addition of chromium, which notably reduces the oxidation rate, also reduces the hot-corrosion; there are fewer areas of heavy attack, and when sulphidation attack does develop, it appears coarse chromium sulphides are formed with less of the fine lamellar sulphides formed in the ternary alloy. Presumably,  $\text{CrNbO}_4$  is resistant to both acidic fluxing and sulphidation, at least to some extent, since sulphur can gain access to the alloy forming fine "NiS" and coarse CrS particles, the latter reducing the rapid inward diffusion of sulphur. In lightly attacked areas the sulphides are again behind the depletion zone, whereas in the more heavily attacked nodules they bridge the depletion zone, although there are far fewer of the latter areas in the quaternary alloy than in the ternary alloy. The CrS particles also form at the fibre/matrix interface, presumably for similar reasons as the "NiS" particles.

#### Carbide-Based Eutectic Alloys

##### (a) High Temperature Oxidation

The type of oxide morphology, and consequently the overall oxidation-resistance of these carbide-strengthened alloys depends on whether a protective oxide layer of either  $\text{Cr}_2\text{O}_3$  or  $\text{Al}_2\text{O}_3$ , can be established in the early stages of oxidation. In the absence of such a protective layer,

gross oxidation of the carbides occurs and attack continues to penetrate deep into the alloy.

A critical factor affecting the formation of the protective oxide is the spacing and alignment of the carbide fibres. Small, randomly orientated fibres, as are present in the as cast alloys, tend to favour the early establishment of a protective oxide, presumably because they interfere less with the lateral spreading of the oxide from the matrix over the fibres. Lower temperatures, also favour protective oxide formation, which was not the case with the  $\gamma/\gamma'-\delta$  alloys. At the higher temperatures, however, 1000 and particularly 1100°C, the fibre spacing is not as critical, since invariably a carbide-depleted zone is formed between the scale and the bulk alloy. Formation of this fibre-denuded zone apparently has a retarding influence on protective oxide formation: with the  $\gamma/\gamma'-\delta$  alloys it was a pre-requisite for  $\text{Al}_2\text{O}_3$  formation.

The constitution of the fibres is also important. Oxidation of the  $\text{Cr}_7\text{C}_3$  fibres would be expected to form  $\text{Cr}_2\text{O}_3$  and thus not be particularly prone to oxidation: it might be expected that in their presence in a Co-Cr matrix would not be critical. Nevertheless, the evidence seems to suggest that the fibres can oxidize more rapidly than the matrix and this may be related to the simultaneous formation of gaseous oxides of carbon which disrupt the scale. With the Ni-Cr-Al-C alloys, the situation is somewhat different, since these alloys rely on the development of  $\text{Al}_2\text{O}_3$ . This is accomplished on all the alloys at 900°C, but not at the higher temperatures with the aligned structures, when in some cases it is  $\text{Cr}_2\text{O}_3$  which eventually forms a continuous layer and the aluminium oxidizes internally. Surprisingly, the internal  $\text{Al}_2\text{O}_3$  platelets resemble the  $\text{Cr}_7\text{C}_3$  fibres in shape, which suggests that there could have been some form of exchange reaction between aluminium and chromium before oxidation occurred with the liberated chromium entering the matrix.

TaC fibres are oxidation-prone: however, they have very little detrimental effect on the oxidation behaviour of the Co-15Cr-13TaC alloy.

The matrix, Co-15Cr, has a low oxidation resistance as it is unable to develop  $\text{Cr}_2\text{O}_3$ . The presence of the fibres does not seem to affect oxide adherence as was suggested by Smeggil (29).

Improving the oxidation-resistance of the matrix, as in the quaternary Co-20Cr-10Ni-13TaC alloy, improves the alloy, however, the orientation of the fibres then becomes important. Even at  $900^\circ\text{C}$ , rapidly growing oxide nodules form over the TaC fibres, retarding the establishment of the protective  $\text{Cr}_2\text{O}_3$  layer. Nodular growth is more extensive at  $1000^\circ\text{C}$ , but the alloy still develops a protective scale. At  $1100^\circ\text{C}$ , the depth of the fibre-depleted zone is apparently independent of fibre orientation. In addition, substantial amounts of internal oxide are formed and these can sometimes link together causing relatively unoxidized metal, largely cobalt, to be incorporated into the scale. A similar phenomenon was observed by Smeggil (29).

(b) Hot-Corrosion

The behaviour of the three types of alloy is somewhat differently affected by the presence of sodium salts and/or sulphur. In the relatively mild conditions of the coating test, the presence of the  $\text{Na}_2\text{SO}_4$  does not have a particularly dramatic effect, except with the  $\text{Al}_2\text{O}_3$ -forming Ni-Cr-Al-C alloy. With the Co-Cr-C alloy, a protective  $\text{Cr}_2\text{O}_3$  layer develops, if anything, somewhat easier below the  $\text{Na}_2\text{SO}_4$  coating than when it is absent. It has been suggested (36,42) that this is related to the  $\text{Na}_2\text{SO}_4$  layer being able to maintain an oxygen potential gradient across itself, resulting in a low oxygen activity at the alloy/scale interface, which favours  $\text{Cr}_2\text{O}_3$  formation (45); the low oxygen activity there may also prevent decarburization. Sulphidation is observed, but with only a limited supply of salt, this is not extensive, and does not lead to catastrophic attack.

The already rapid oxidation rate of the TaC-strengthened Co-15Cr alloy is virtually unaffected by a  $\text{Na}_2\text{SO}_4$  coating. It does increase the

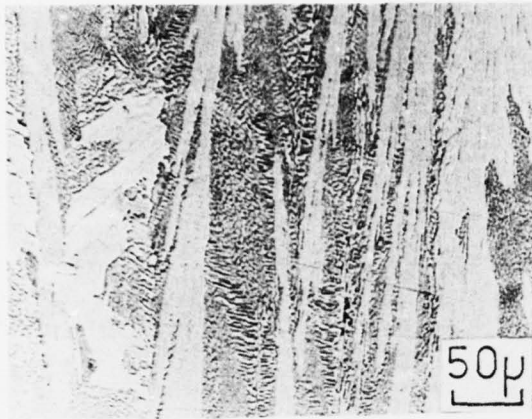
oxidation rate of the Co-20Cr-10Ni-TaC alloy and this may be related to limited fluxing of the scale and sulphide formation causing a surface depletion of chromium. The oxidation rate is more sensitive to change in chromium content in the 15-20% range than at lower levels (46).

As indicated earlier, the Ni-Cr-Al-C alloy is most affected by the  $\text{Na}_2\text{SO}_4$  layer since  $\text{Al}_2\text{O}_3$  is readily fluxed to aluminate by the sulphate (47). The alloy thus behaves like an alloy of lower Al content and substantial amounts of rapidly growing nickel-rich oxides are formed.

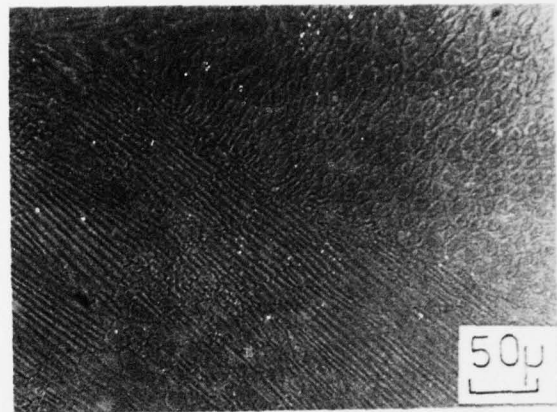
In the pre-sulphidation tests, a higher level of sulphur is introduced into the alloy prior to oxidation. However, with the  $\text{Cr}_7\text{C}_3$ -reinforced materials only chromium-rich sulphides are formed and whilst this delays the formation of a continuous  $\text{Cr}_2\text{O}_3$  scale, the effect is not catastrophic. Although only chromium-rich rather than aluminium-rich sulphides are observed in the Ni-Cr-Al-C alloy, they have much the same effect. Depleting the matrix chromium content means that there is no longer sufficient aluminium to form a protective  $\text{Al}_2\text{O}_3$  scale.

Again pre-sulphidation has little effect on the TaC-containing alloys, except for increasing the depth of apparent internal oxidation.

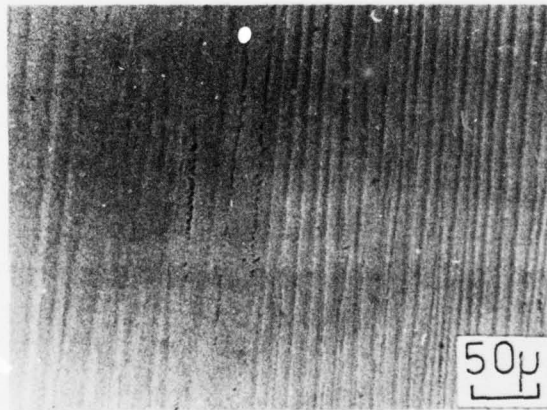
The Dean test using thermal cycling and NaCl additions to the sulphate is much more severe. The presence of chloride causes severe disruption of normally protective  $\text{Cr}_2\text{O}_3$  layers (38) and this is exaggerated by the thermal stresses induced by cycling. Thus, the Co-Cr-C alloys are catastrophically destroyed, with the carbide network acting as an easy path for the inward diffusion of the deleterious elements. It also serves to segregate the chromium to the fibre network where it reacts with the chloride-containing species. The TaC fibres in the Co-Cr-TaC alloy are much more resistant in this respect, presumably since Ta does not form a volatile chloride species. However, the presence of a  $\text{Al}_2\text{O}_3$  layer prevents catastrophic oxidation of the  $\text{Cr}_7\text{C}_3$  fibre network, as has been found previously using conventional alloys without carbides in the Dean test (37).



(a).



(b).



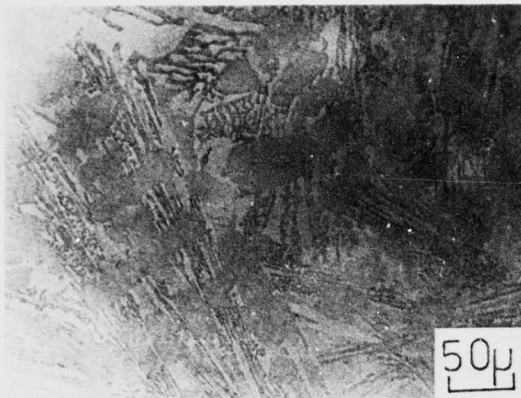
(c).

Figure 1. Microstructures of various Ni-23.1Nb-4.4Al alloys.

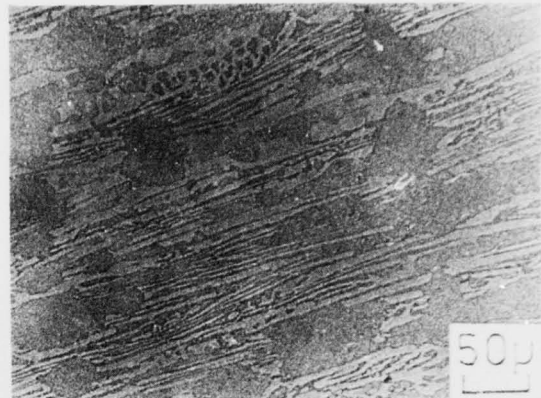
(a) as-cast.

(b) slow cooled.

(c) directionally solidified.



(a).



(b).



(c).

Figure 2. Microstructures of various Ni-19.7Nb-6Cr-2.5Al alloys.

(a) as-cast.

(b) slow cooled.

(c) directionally solidified.

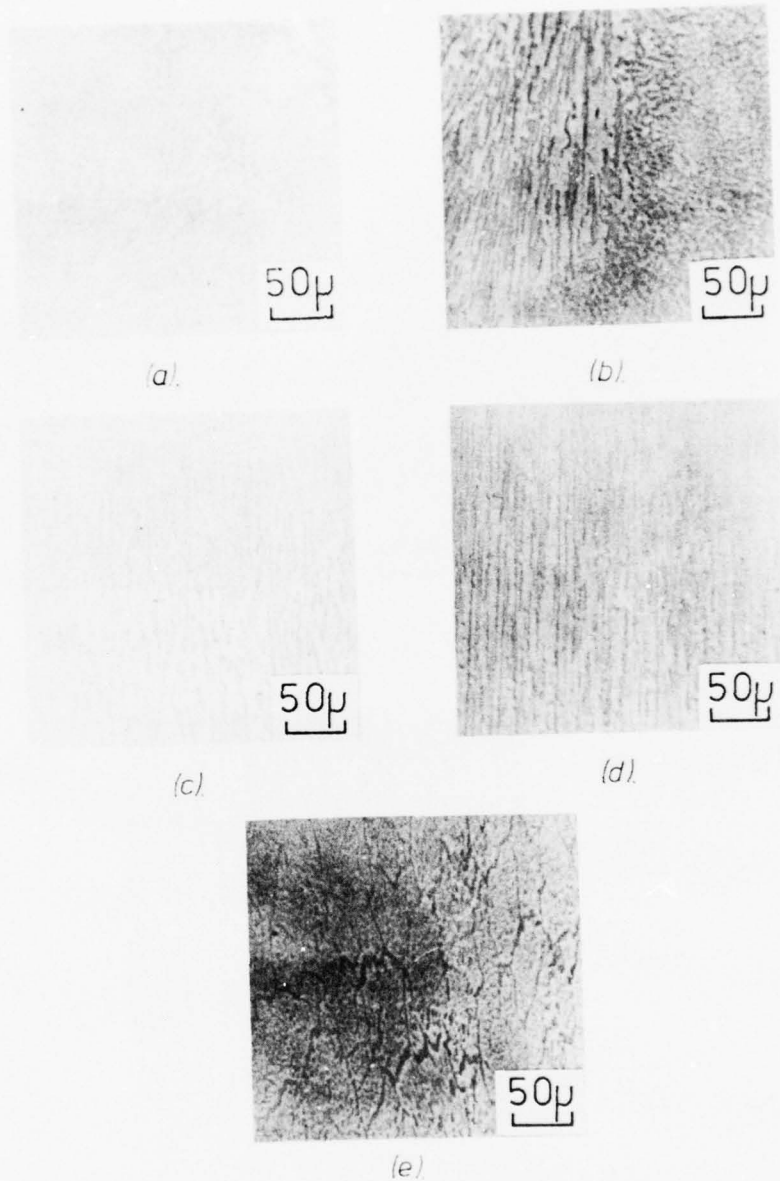


Figure 3. Microstructures of the various Co-41Cr-2.4C eutectic alloys.

- |  |  |
|--|--|
| (a) as-cast                                  | (b) furnace-cooled                           |
| (c) directionally solidified<br>(3.4 cm/hr)  | (d) directionally solidified<br>(10.6 cm/hr) |
| (e) directionally solidified<br>(31.5 cm/hr) |  |



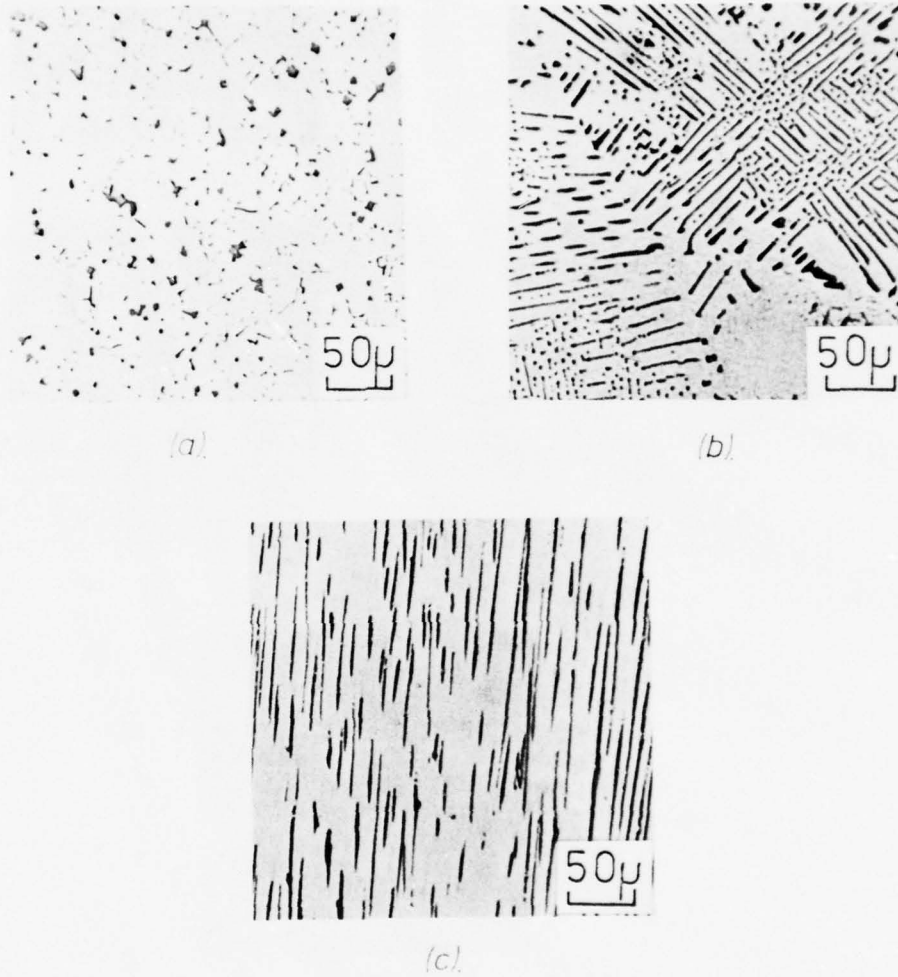


Figure 4. Microstructures of the various Co-15Cr-TaC eutectic alloys.

- (a) as-cast.
- (b) furnace-cooled.
- (c) directionally solidified.

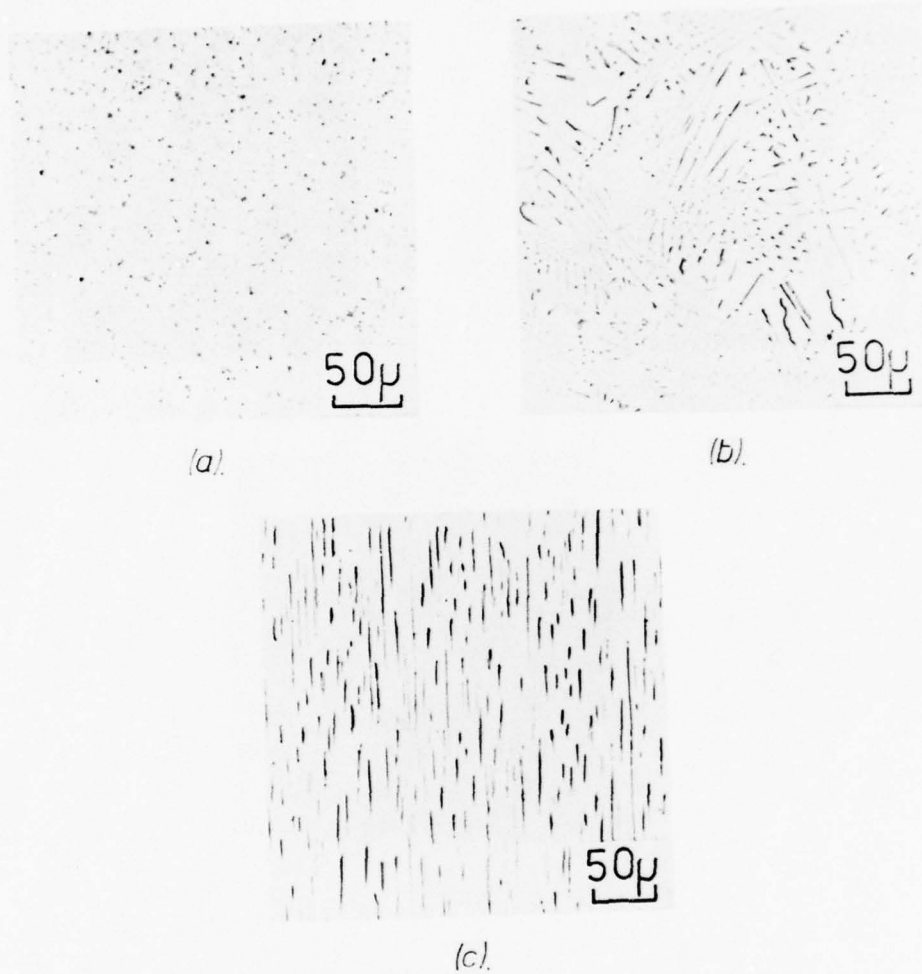


Figure 5. Microstructures of the various Co-20Cr-10Ni-TaC eutectic alloys.

(a) as-cast.

(b) furnace-cooled.

(c) directionally solidified.

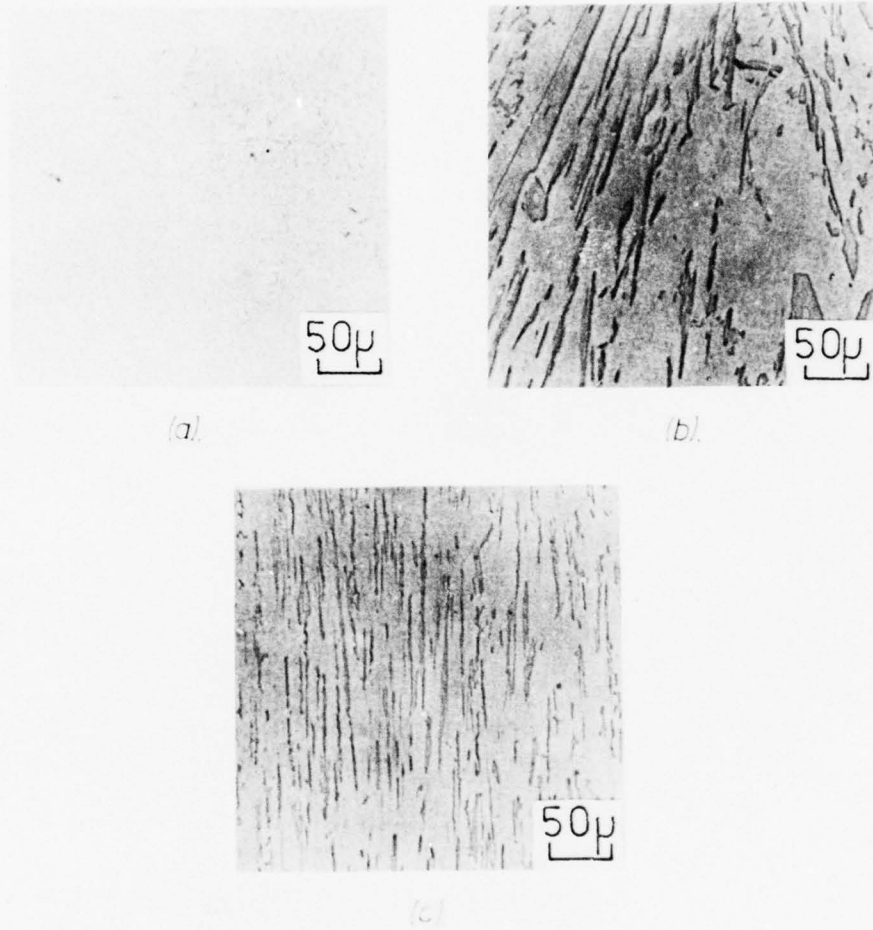
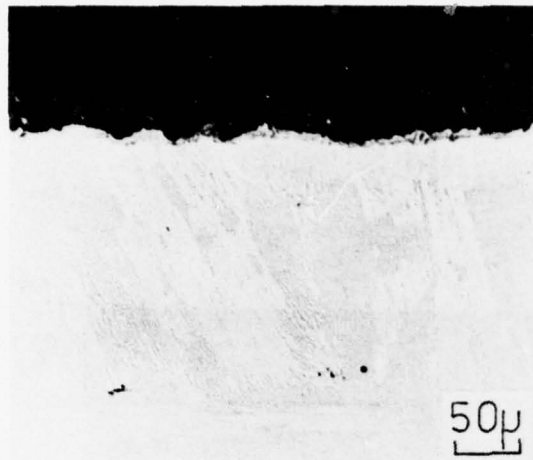
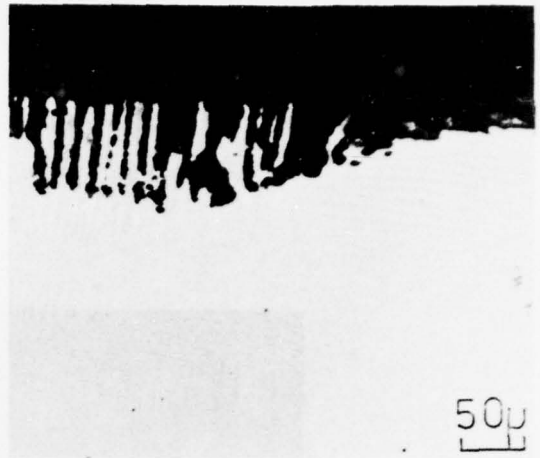


Figure 6. Microstructures of the various Ni-12.3Cr-6.9Al-1.8C eutectic alloys.

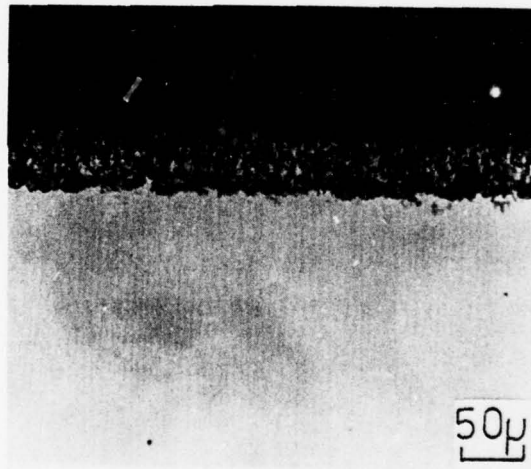
- (a) as-cast.
- (b) furnace-cooled.
- (c) directionally solidified.



(a).



(b).



(c).

Figure 7. Cross-sections of various Ni-23.1Nb-4.4Al alloys oxidised in air at 900°C for 50 hours.

(a) as-cast.

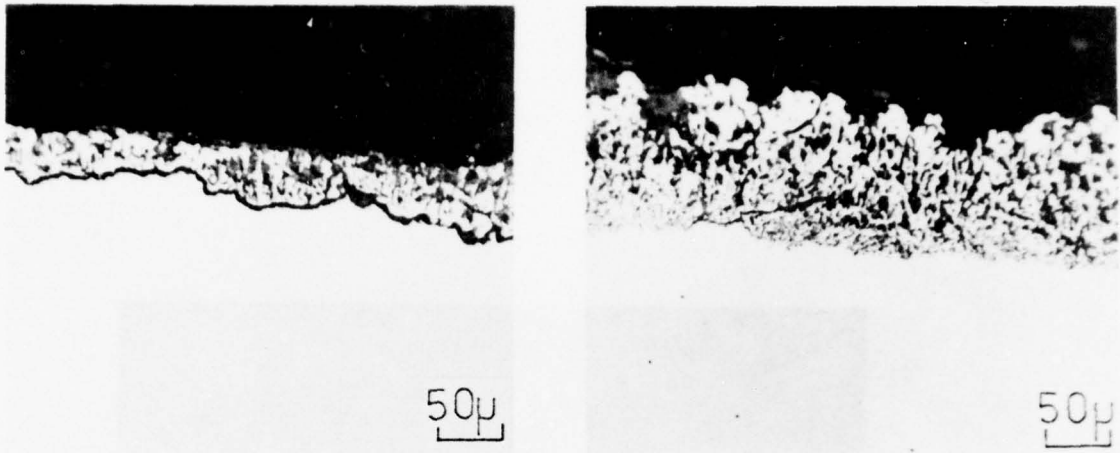
(b) slow cooled.

(c) directionally solidified.



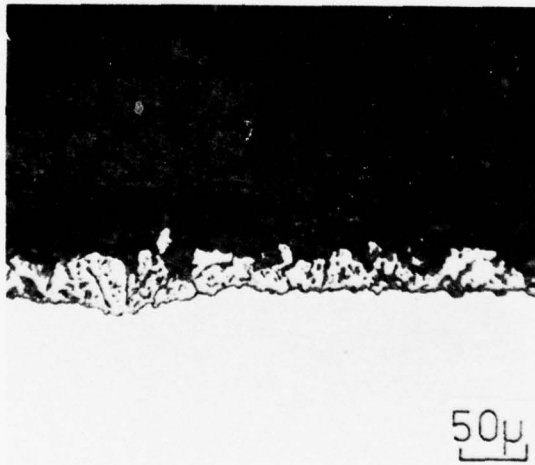
50μ

Figure 8. Cross-section of Ni-23.1Nb-4.4Al (directionally solidified) oxidised in air at 1000°C for 96 hours.



(a).

(b).



(c).

Figure 9. Cross-sections of various Ni-23.1Nb-4.4Al alloys oxidised in air at 1100°C for 72 hours.

- (a) as-cast.
- (b) slow cooled.
- (c) directionally solidified.

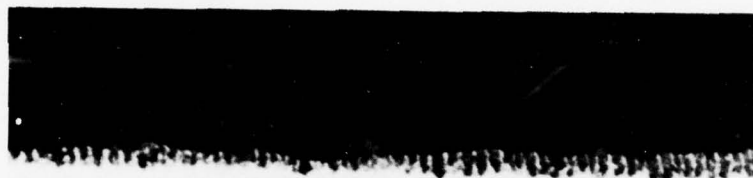
25 $\mu$ 

Figure 10. Cross-section of Ni-23.1Nb-4.4Al directionally solidified eutectic alloy oxidised for 1h at 800°C.

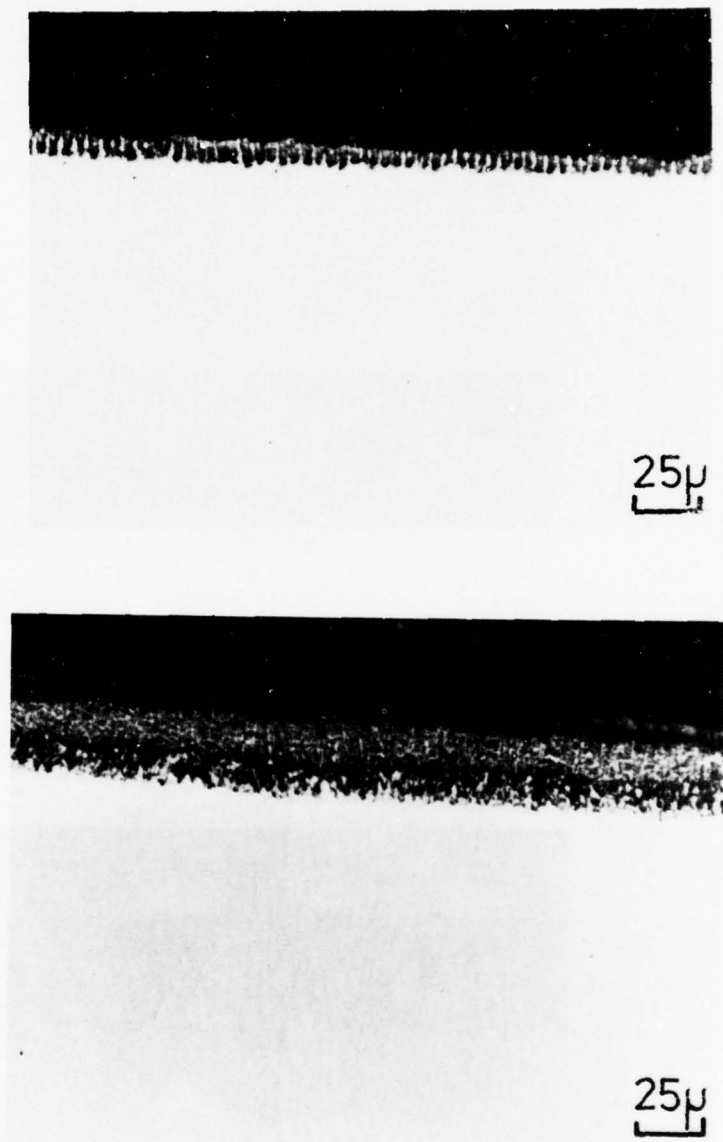


Figure 11. Cross-section of Ni-23.1Nb-4.4Al directionally solidified eutectic alloy oxidised for various times at 900°C.

(a) 1h.

(b) 2h.



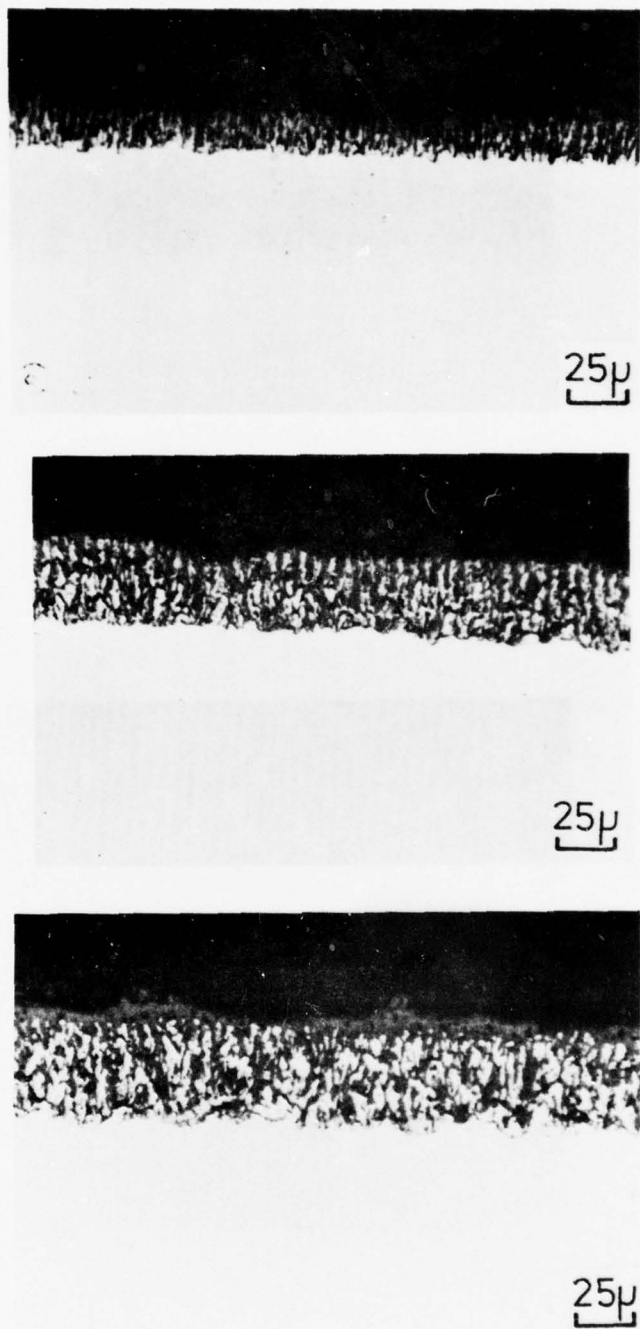


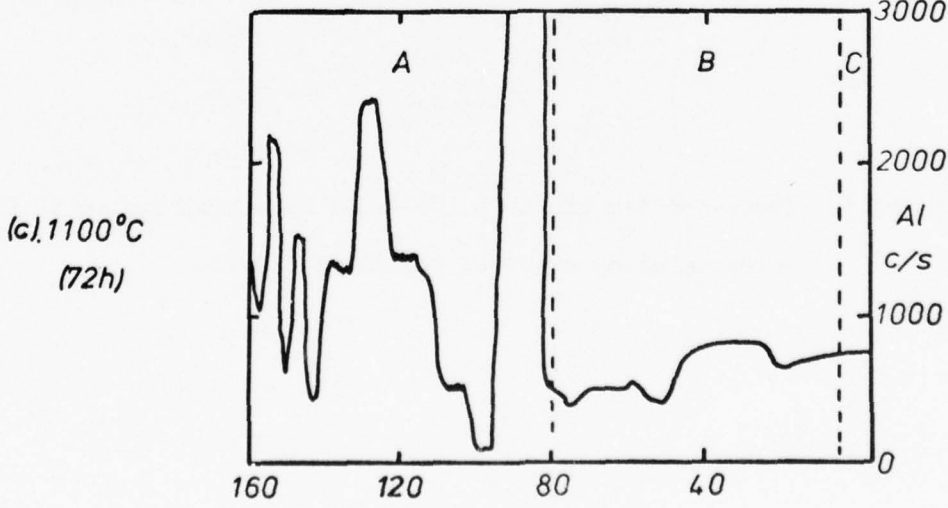
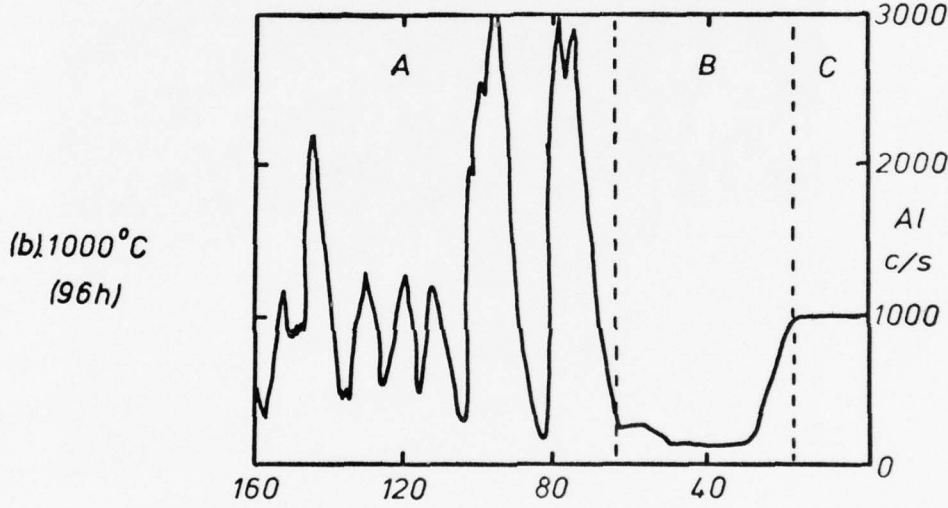
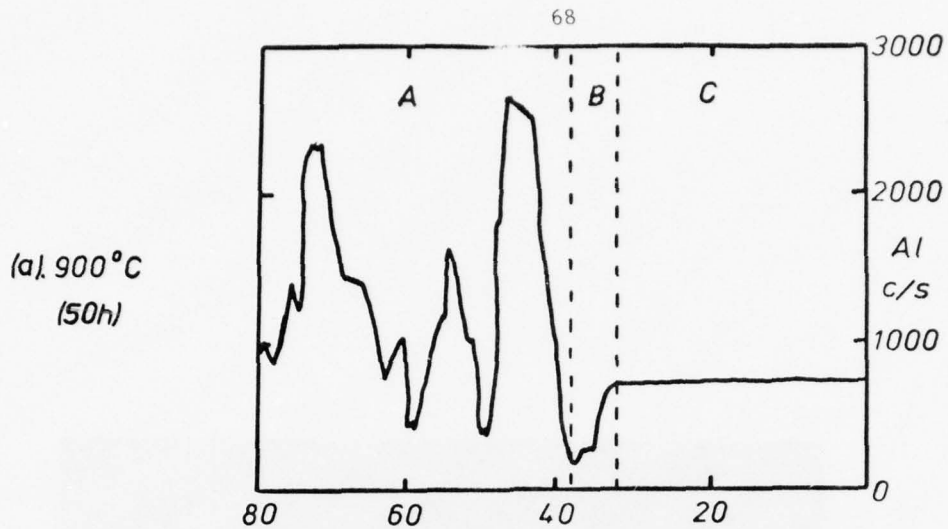
Figure 12. Cross-section of Ni-23.1Nb-4.4Al directionally solidified eutectic alloy oxidised for various times at 1000°C.

- (a) 1h.
- (b) 2h.
- (c) 5h.



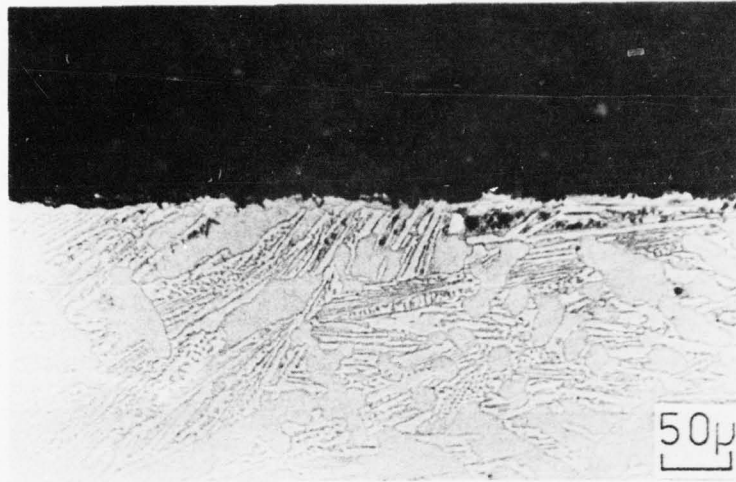
25μ

Figure 13. Cross-section of Ni-23.1Nb-4.4Al directionally solidified eutectic alloy oxidised for 5h at 1100°C.

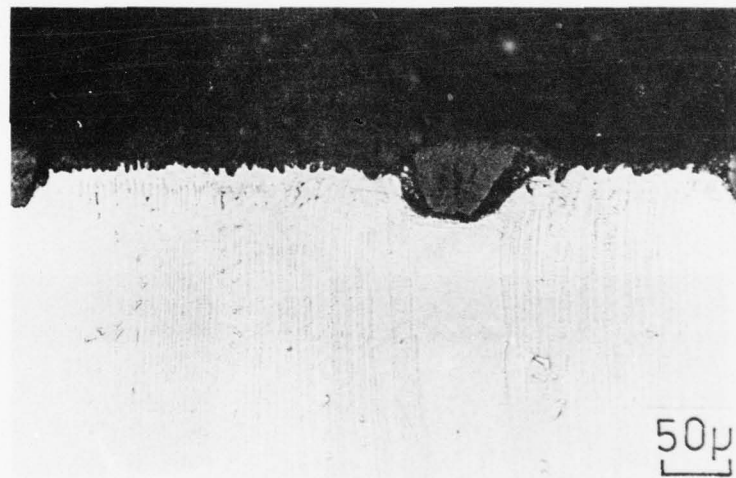


Distance ( $\mu\text{m}$ ).  
 A - Oxide Scale.    B - Depletion Zone.    C - Alloy.

Figure 14. Aluminum profiles across Ni-23, INb-4.4Al directionally solidified eutectic alloy specimens which have been oxidised at various temperatures.



(a).

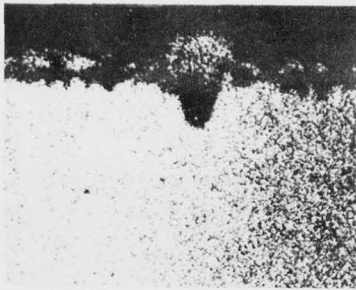
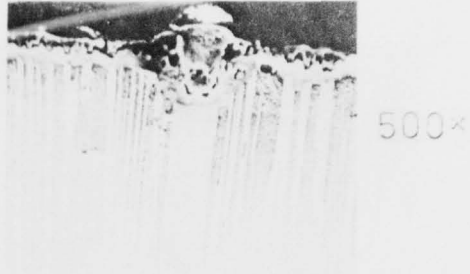


(b).

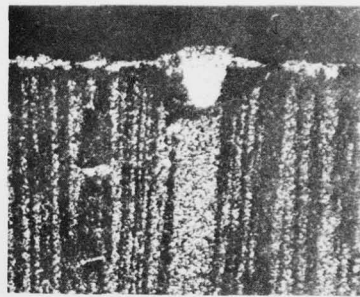
Figure 15. Cross-sections of various Ni-19.7Nb-6Cr-2.5Al alloys oxidised in air at 900°C for 50 hours.

(a) as-cast.

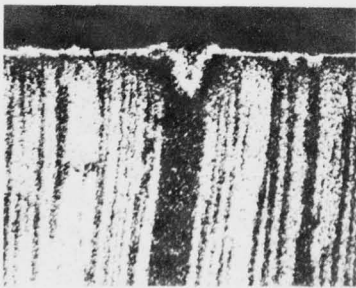
(b) directionally solidified.



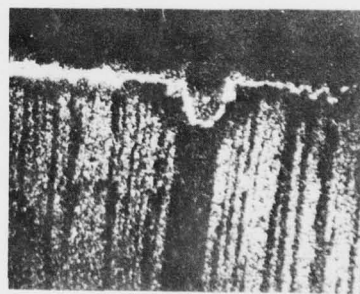
Ni(K $\alpha$ )



Nb(K $\alpha$ )



Cr(K $\alpha$ )



Al(K $\alpha$ )

Figure 16. Electron microprobe X-ray images of the sample shown in Figure 15(b).

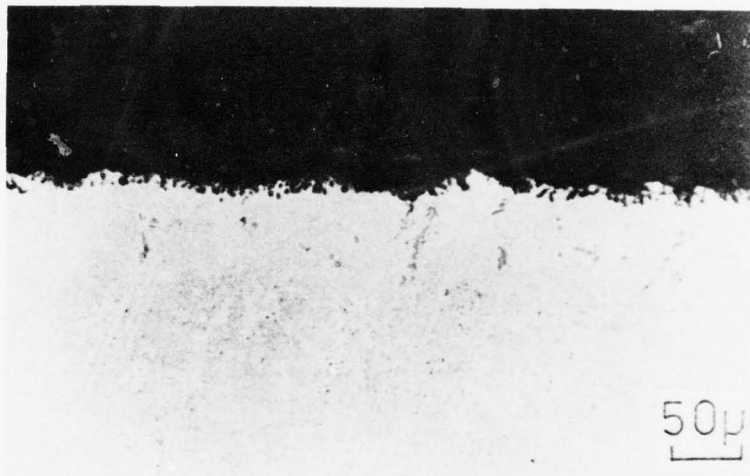


Figure 17. Cross-section of Ni-19.7Nb-6Cr-2.5Al (as-cast) oxidised in air at 1000°C for 96 hours.



Figure 18. Cross-section of Ni-19.7Nb-6Cr-2.5Al (directionally solidified) oxidised in air at 1100°C for 72 hours.



25μ

Figure 19. Cross-section of Ni-6Cr-2.5Al alloy which has been oxidised for 76h at 900°C.



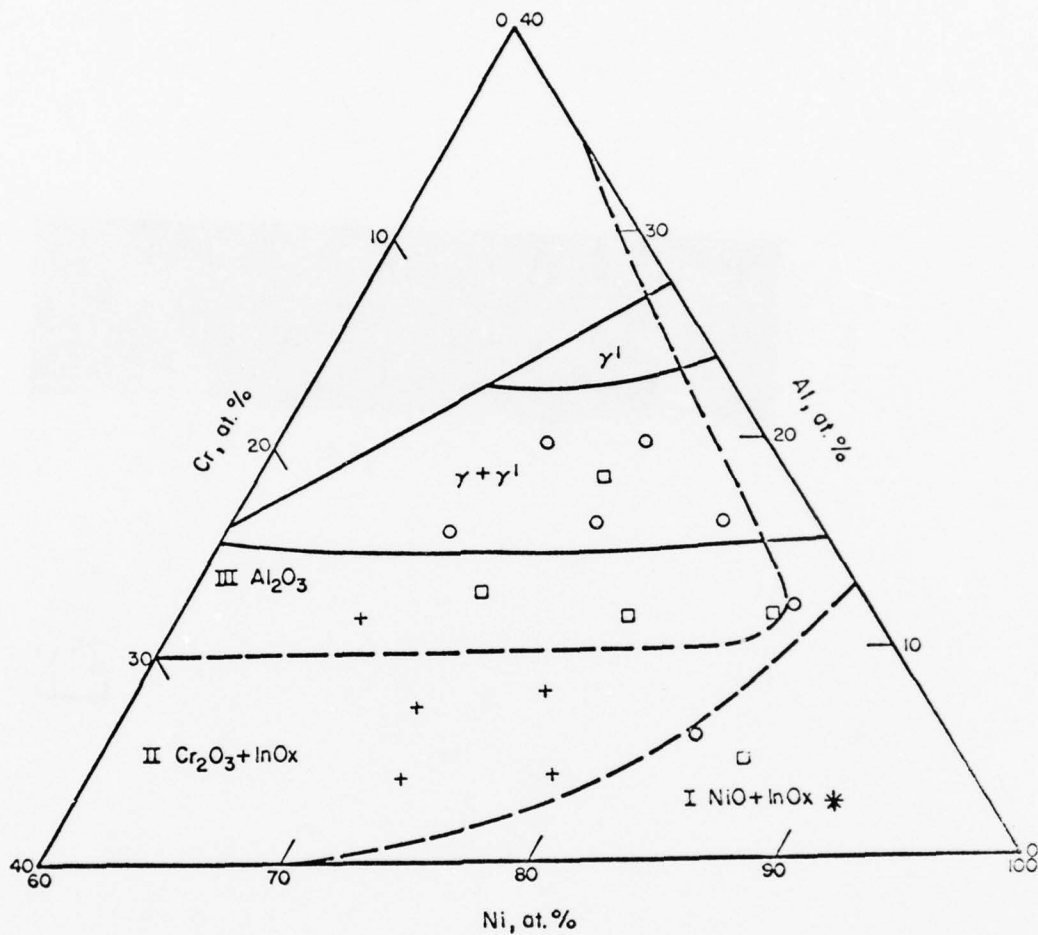
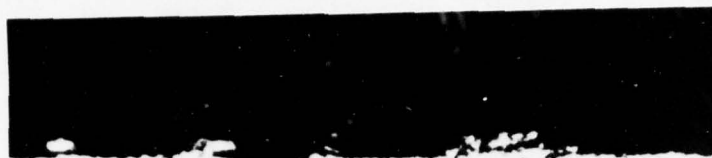
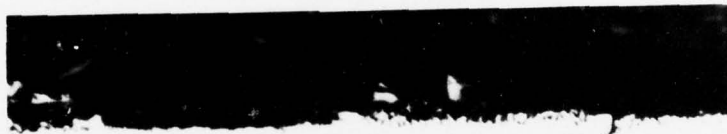


Figure 20. Oxide map of the ternary system Ni-Cr-Al at 1000°C (from G.R. Wallwork and A.Z. Hed, *Oxid. Metals*, **3**, 171 (1971)). The points represent data from three different sources. In Ox = internal oxide and the position of the Ni-6Cr-2.5Al is marked by an asterisk.



25μ



25μ

Figure 21. Cross-section of Ni-Nb-6Cr-2.5Al alloys which have been oxidised for 76h at 900°C.

(a) Ni-5Nb-6Cr-2.5Al.

(b) Ni-10Nb-6Cr-2.5Al.

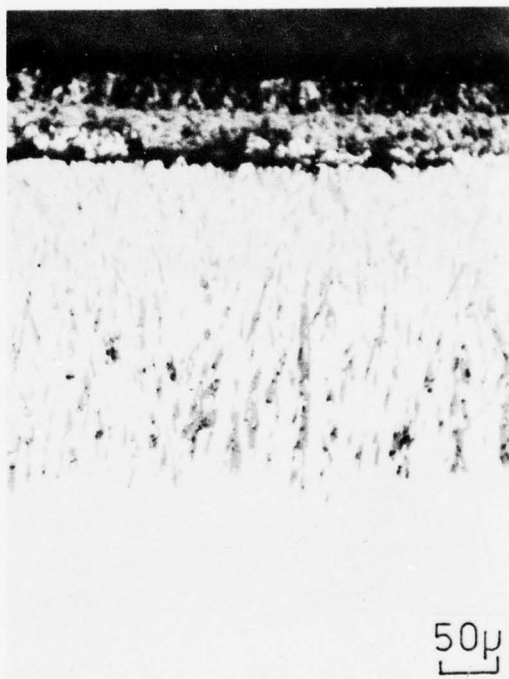
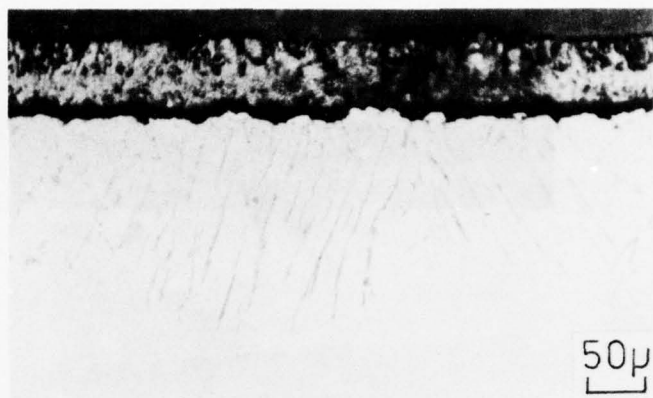


Figure 22. Cross-section of Ni-Nb alloys which have been oxidised for 95h at 900°C.

(a) Ni-5Nb.

(b) Ni-15Nb.

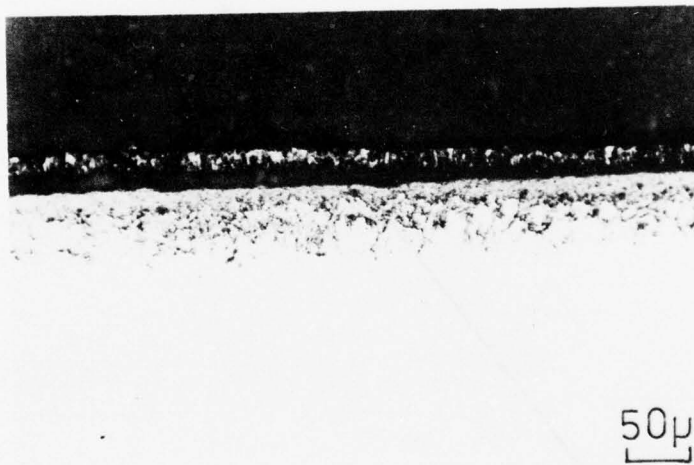
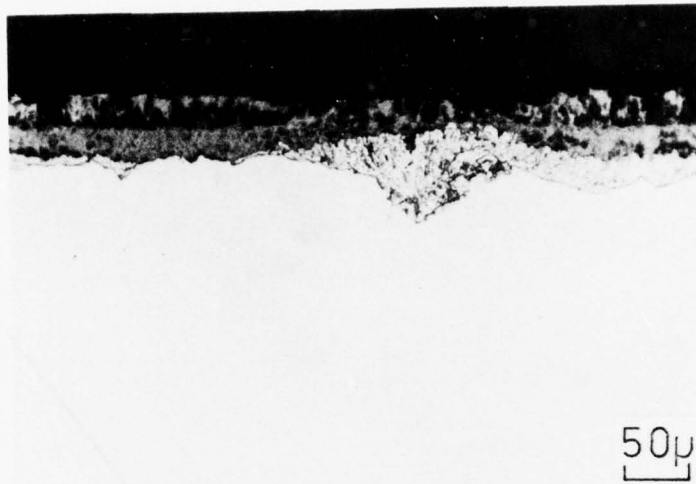


Figure 23. Cross-section of Ni-Nb-4.4Al alloys which have been oxidised for 95h at 900°C.

(a) Ni-5Nb-4.4Al.

(c) Ni-15Nb-4.4Al.

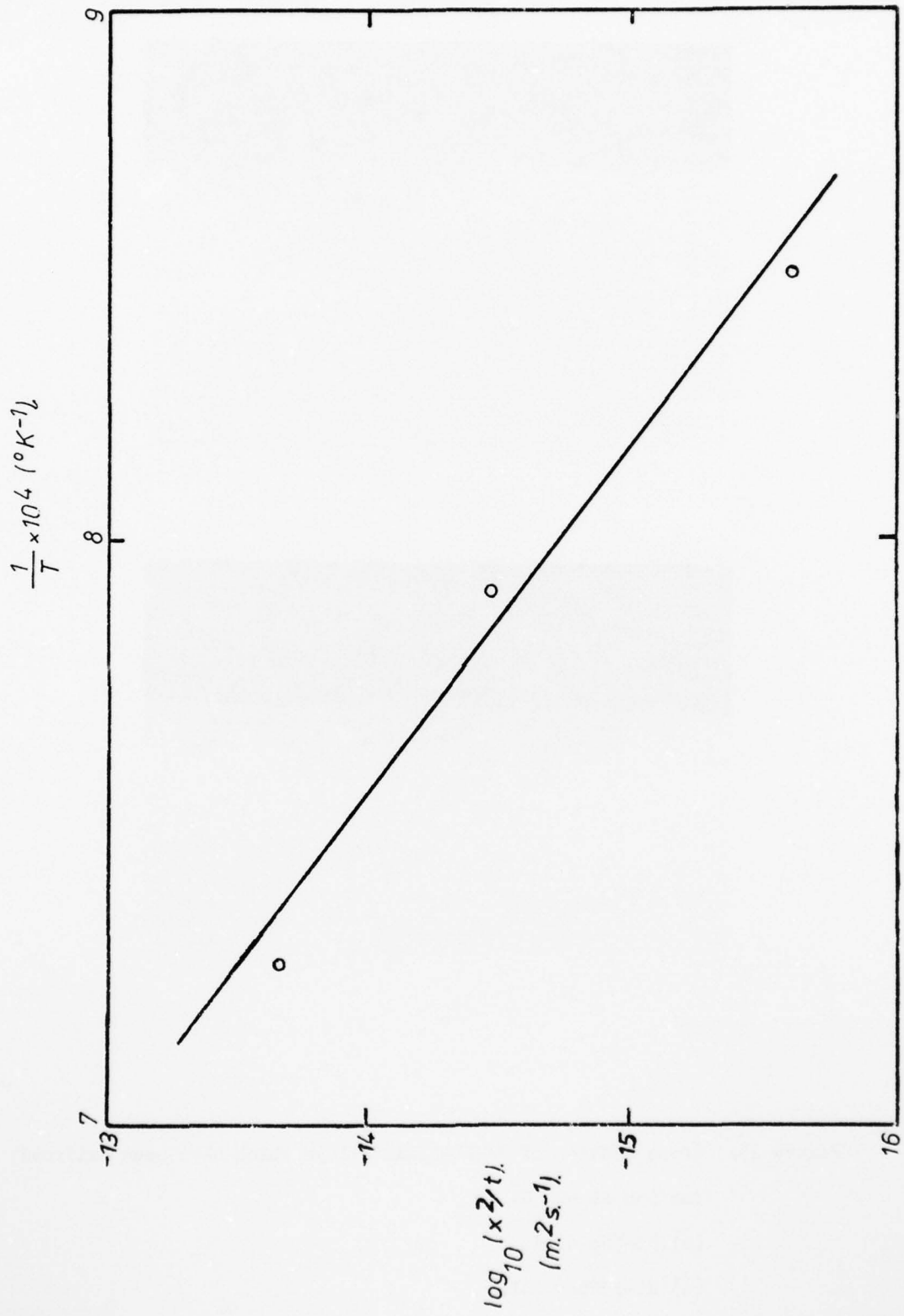


Figure 24. Graph of the diffusion results of  $\log_{10}(x^2/t)$  against  $1/T$ .

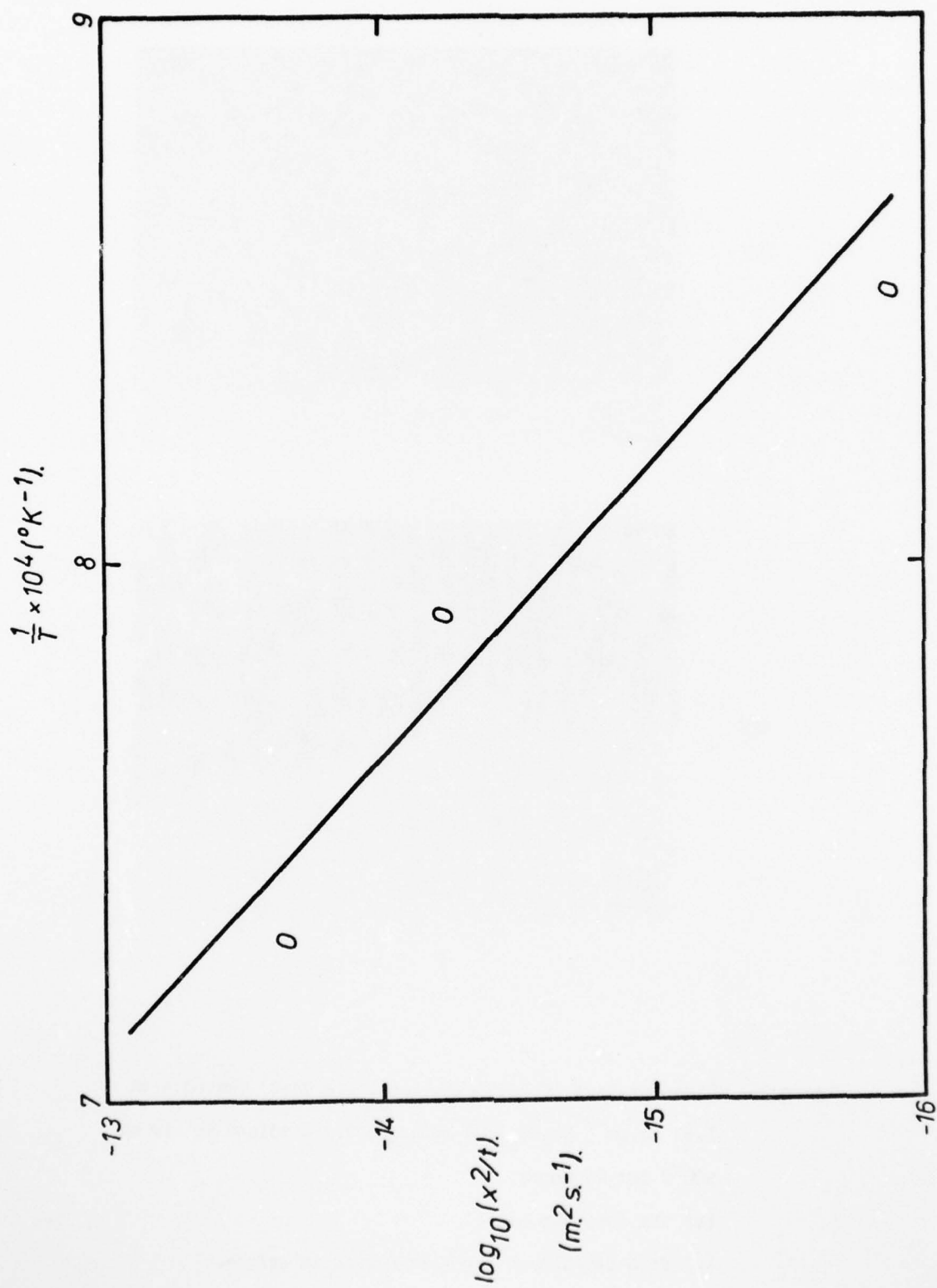


Figure 25. Graph of the diffusion results of  $\log_{10}(x^2/t)$  against  $1/T$ .

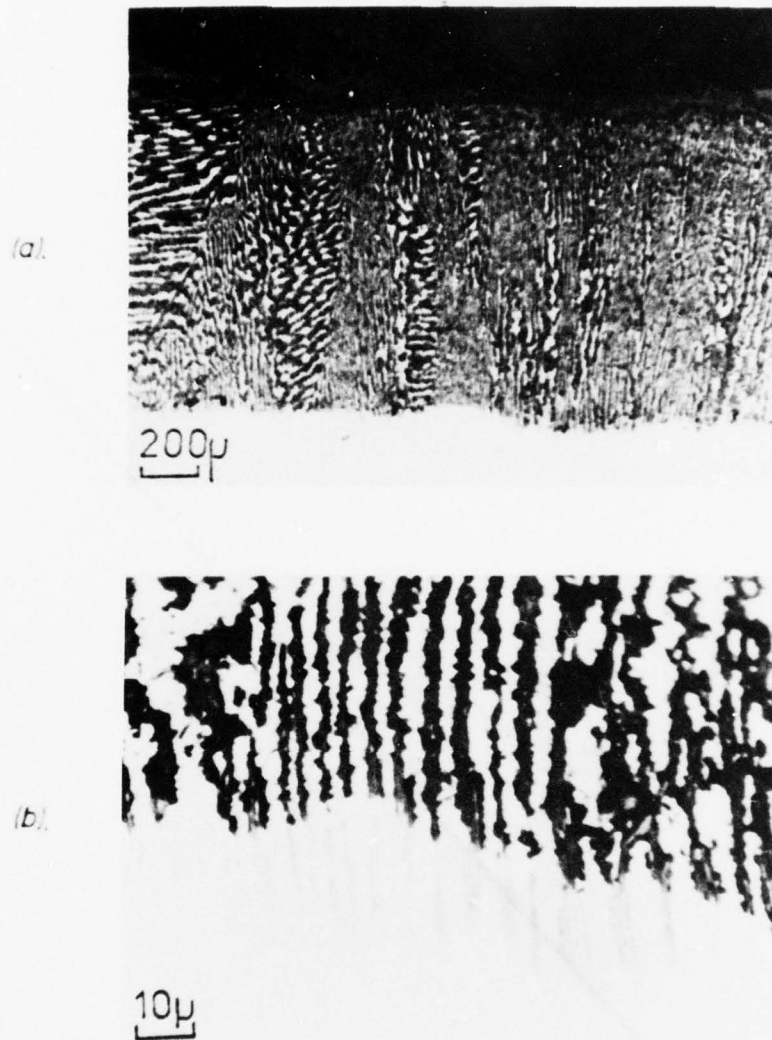


Figure 26. Cross-section of Ni-23.1Nb-4.4Al (as cast) coated with  $1.81 \text{ mg}\cdot\text{cm}^{-2}$   $\text{Na}_2\text{SO}_4$  and subsequently oxidised in air at  $900^\circ\text{C}$  for 24 hours.

(a) the complete scale

(b) fine details of the alloy/oxide interface.

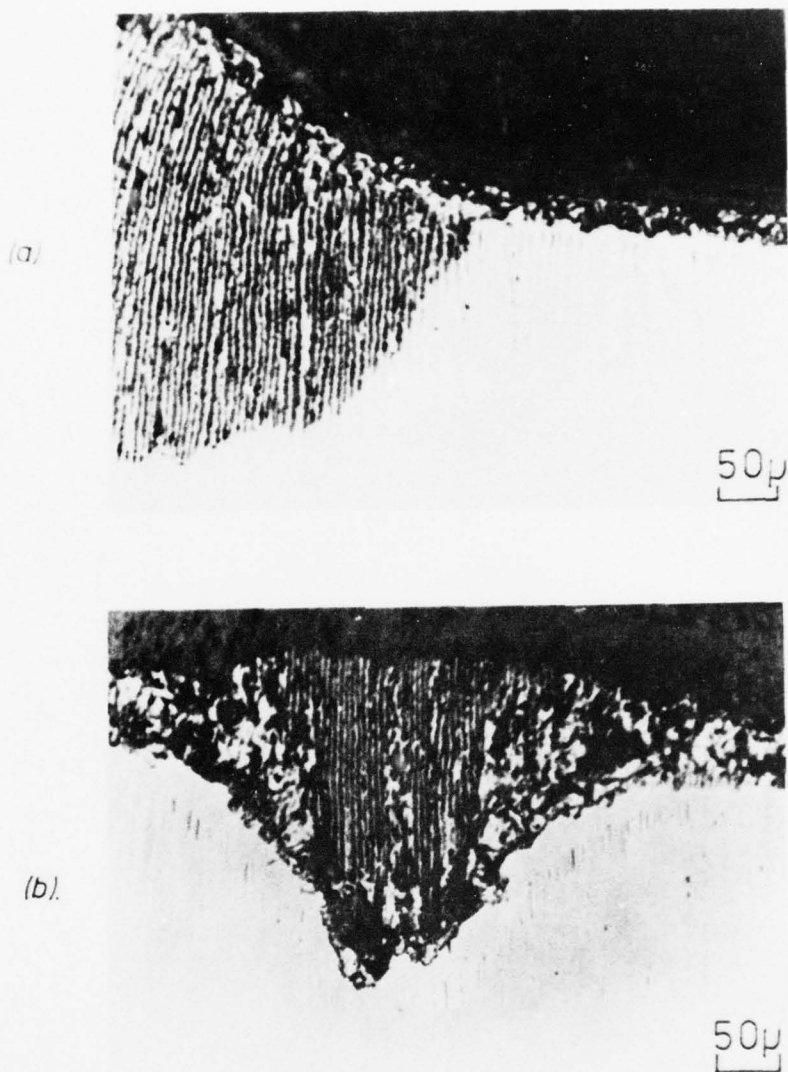


Figure 27. Cross-section of Ni-23.1Nb-4.4Al (directionally solidified) coated with  $\text{Na}_2\text{SO}_4$  and subsequently oxidised in air for 24 hours.

(a)  $900^\circ\text{C}$  ( $3.58 \text{ mg}\cdot\text{cm}^{-2} \text{ Na}_2\text{SO}_4$ ).

(b) close-up of healed nodule at  $1000^\circ\text{C}$  ( $1.92 \text{ mg}\cdot\text{cm}^{-2} \text{ Na}_2\text{SO}_4$ ).



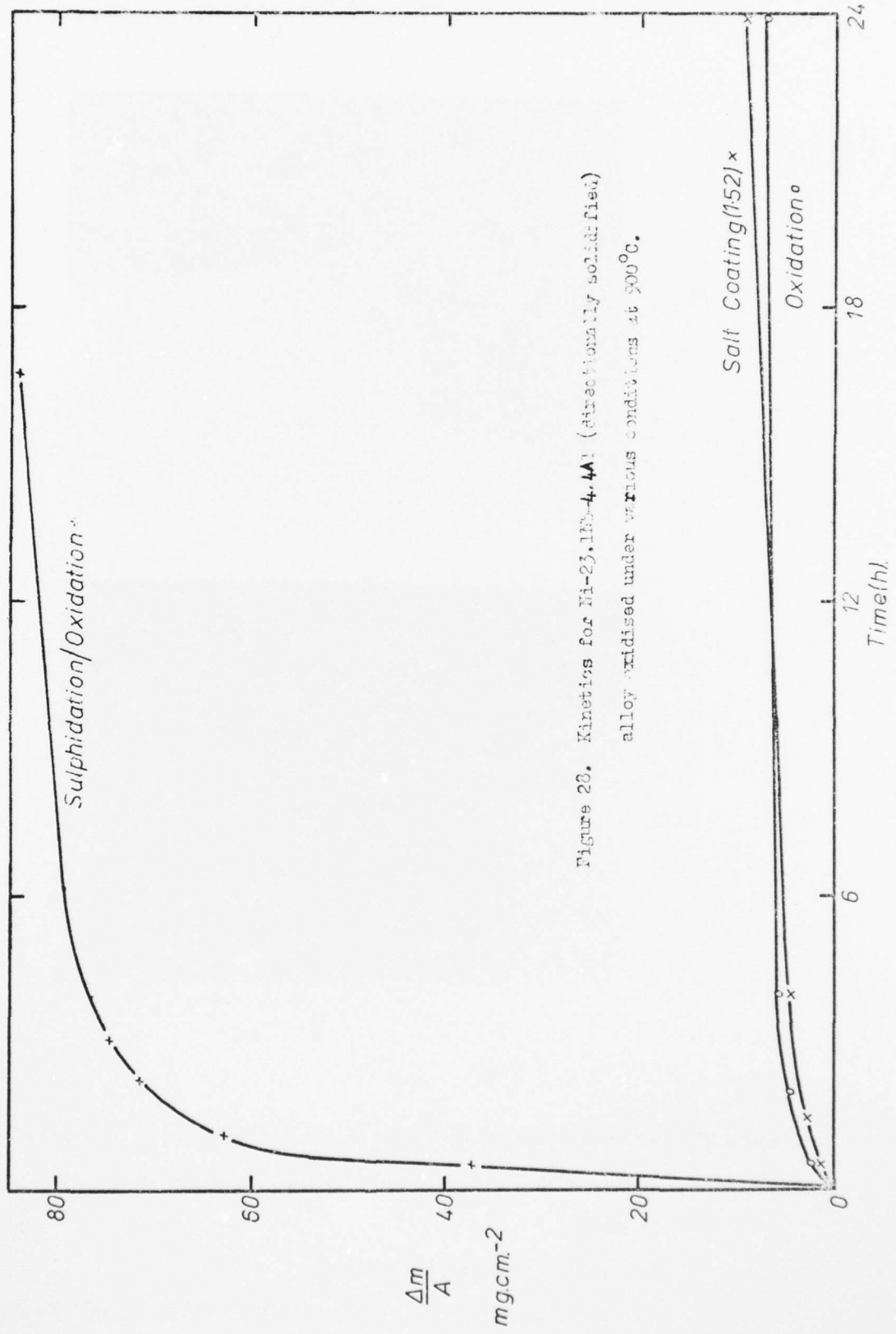


Figure 20. Kinetics for Ni-23.1Mo-4.4Al (directionally solidified) alloy oxidised under various conditions at 500°C.

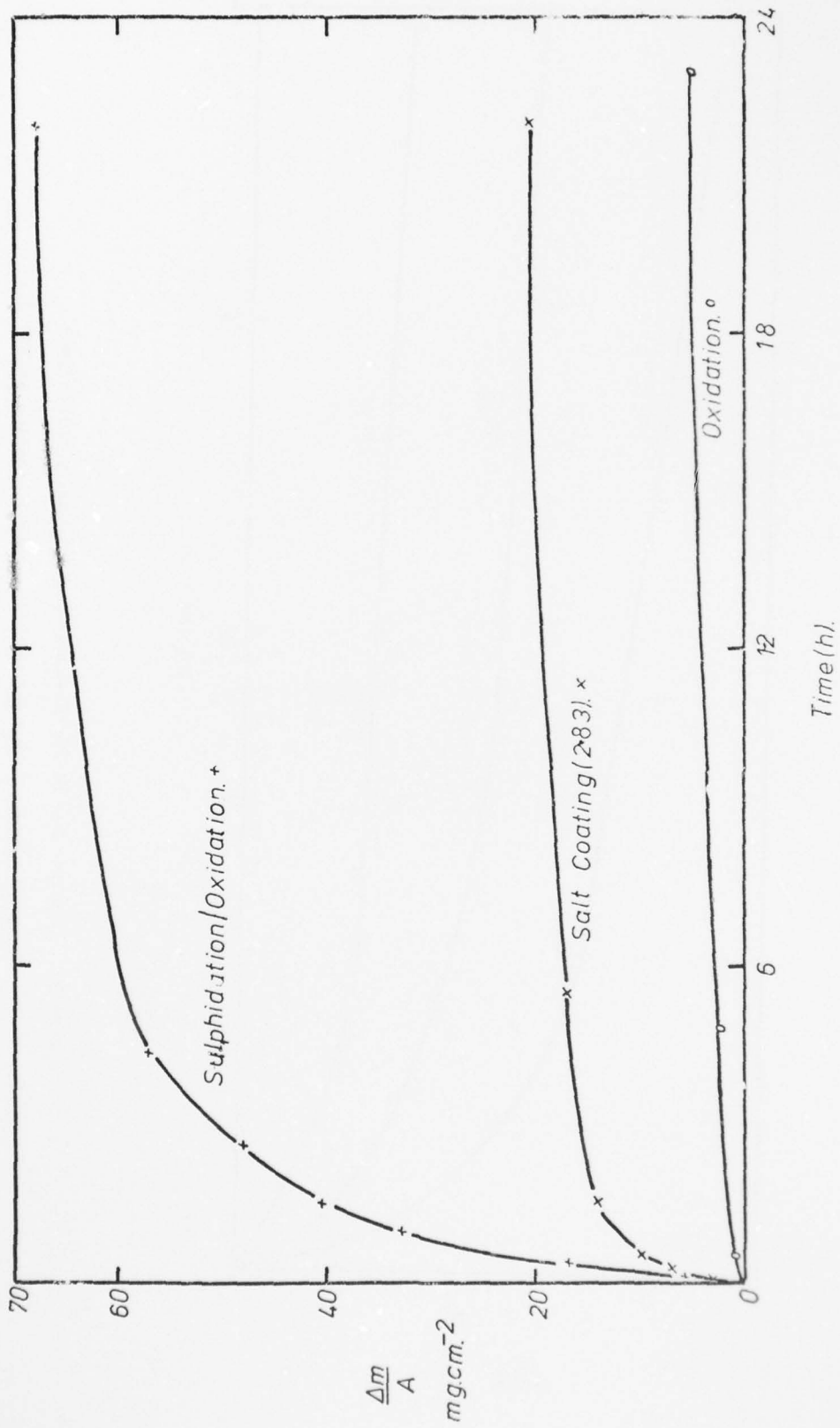


Figure 29. Kinetics for Ni-23.1Fe-4.4Al (directionally solidified) alloy oxidised under various conditions at 1000°C.

AD-A064 911

LIVERPOOL UNIV (ENGLAND) DEPT OF METALLURGY AND MAT--ETC F/G 11/6  
HIGH TEMPERATURE OXIDATION AND CORROSION OF IN-SITU COMPOSITE A--ETC(U)  
OCT 78 D M JOHNSON, D P WHITTLE, J STRINGER AFOSR-75-2785

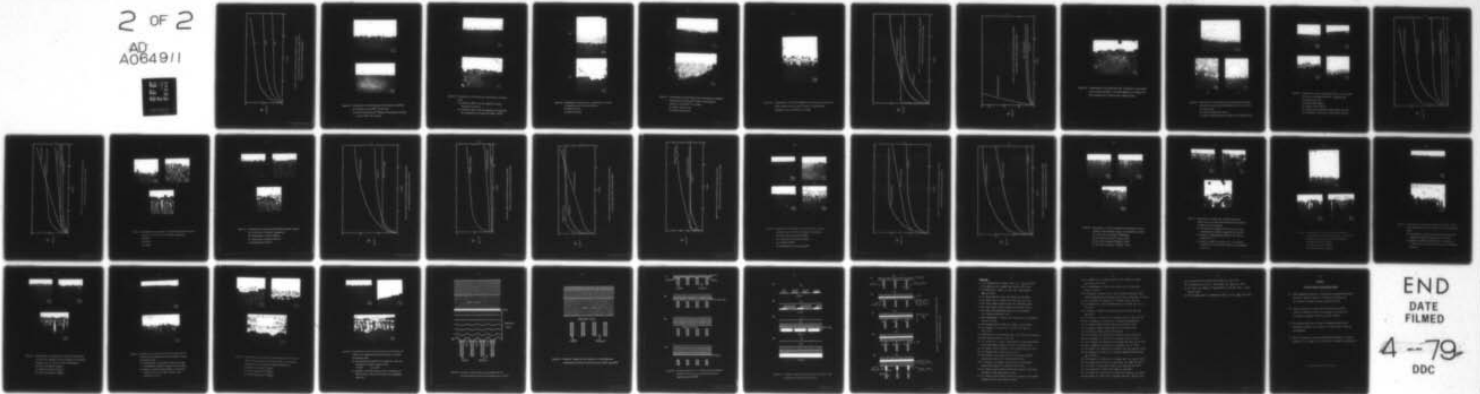
UNCLASSIFIED

AFML-TR-78-137

NL

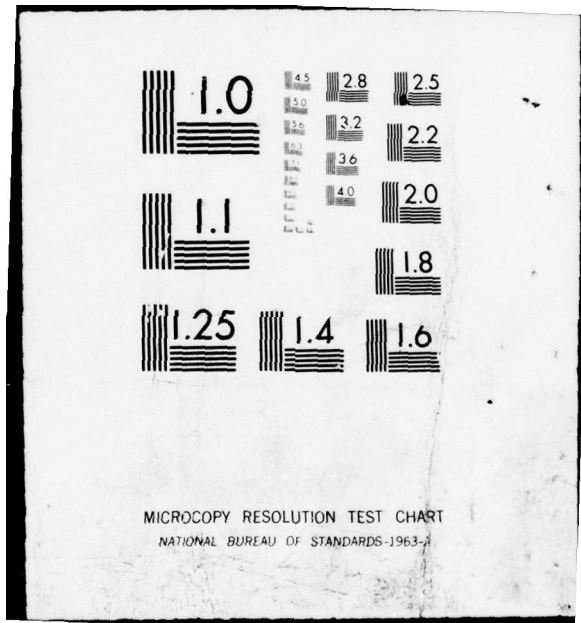
2 OF 2

AD  
A064911



END  
DATE  
FILMED

4--79  
DDC



MICROCOPY RESOLUTION TEST CHART  
NATIONAL BUREAU OF STANDARDS-1963-A

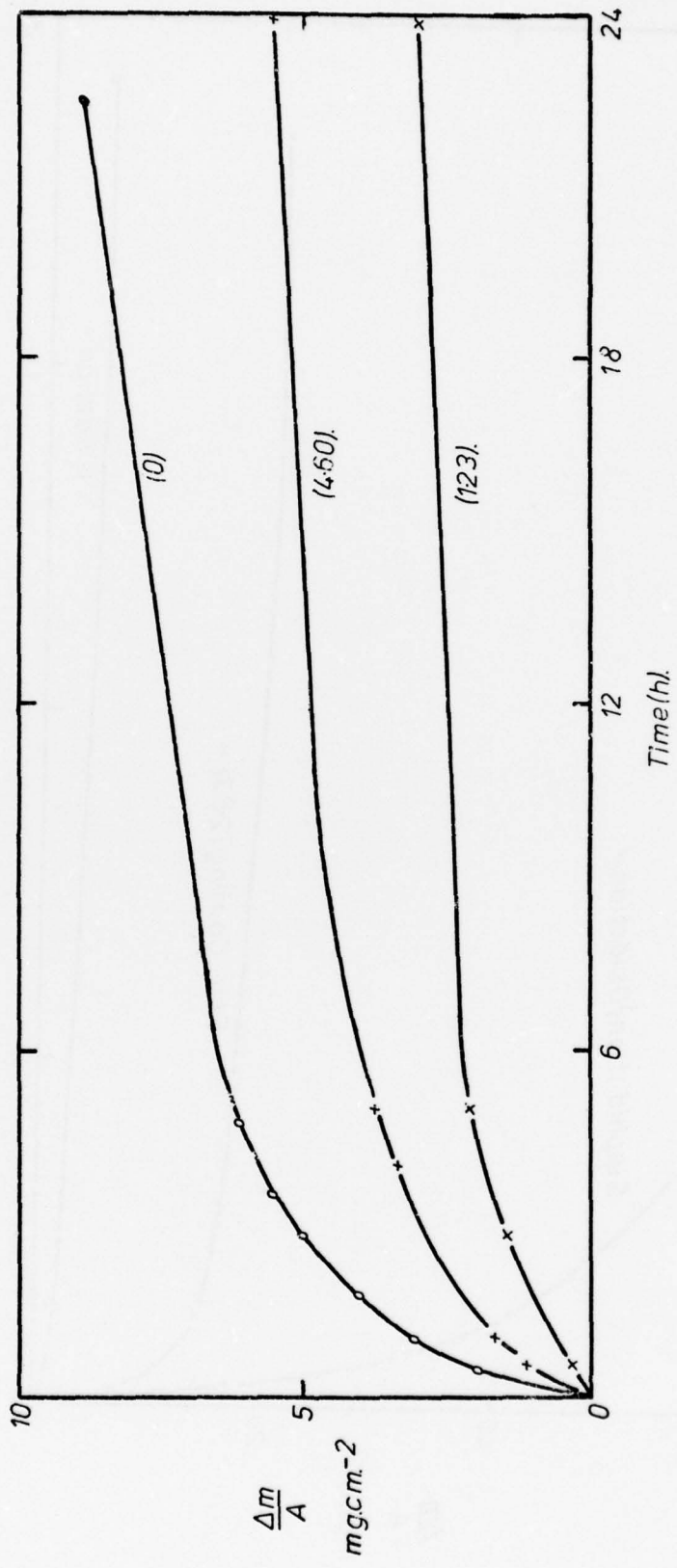


Figure 30. Kinetics for Ni-23.1Nb-4.4Al (directionally solidified) alloy oxidised with and without a Na<sub>2</sub>SO<sub>4</sub> coating at 870°C. (Thickness of coating in brackets in parenthesis).

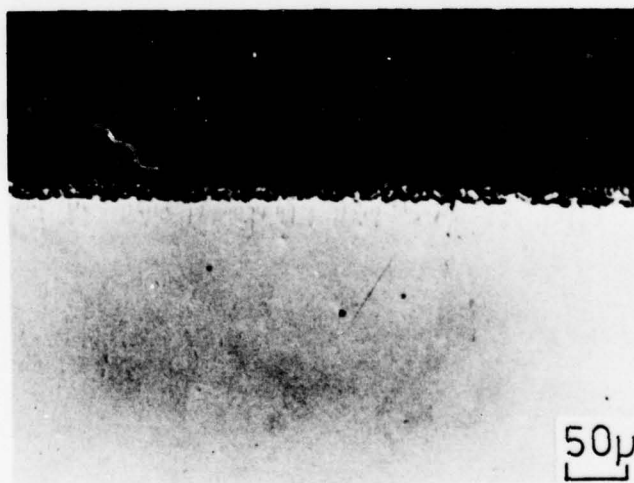


Figure 31. Cross-section of Ni-23.1Nb-4.4Al (directionally solidified)  
(a) oxidised in air at 870°C for 24 hours.  
(b) coated with 4.60 mg.cm<sup>-2</sup> Na<sub>2</sub>SO<sub>4</sub> and subsequently oxidised  
in air at 870°C for 24 hours.

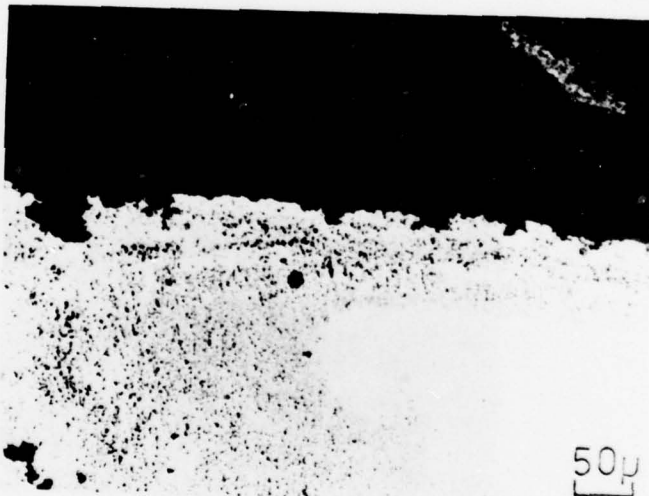
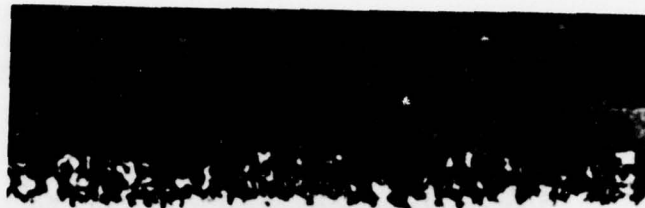


Figure 32. Cross-section of Ni-23.1Nb-4.4Al (directionally solidified) alloy

- (a) oxidised at 950°C in the Dean apparatus in  $\text{Na}_2\text{SO}_4$  atmosphere for 50 hours.
- (b) oxidised at 950°C in the Dean apparatus in a  $\text{Na}_2\text{SO}_4/10\%$  NaCl atmosphere for 168 hours with thermal cycling.

(a)



(b)



Figure 33. Cross-section of Ni-23.1Nb-4.4Al (directionally solidified) alloy which has been sulphidised/oxidised.  
(a) 900°C (17 hours).  
(b) 1000°C (22 hours).



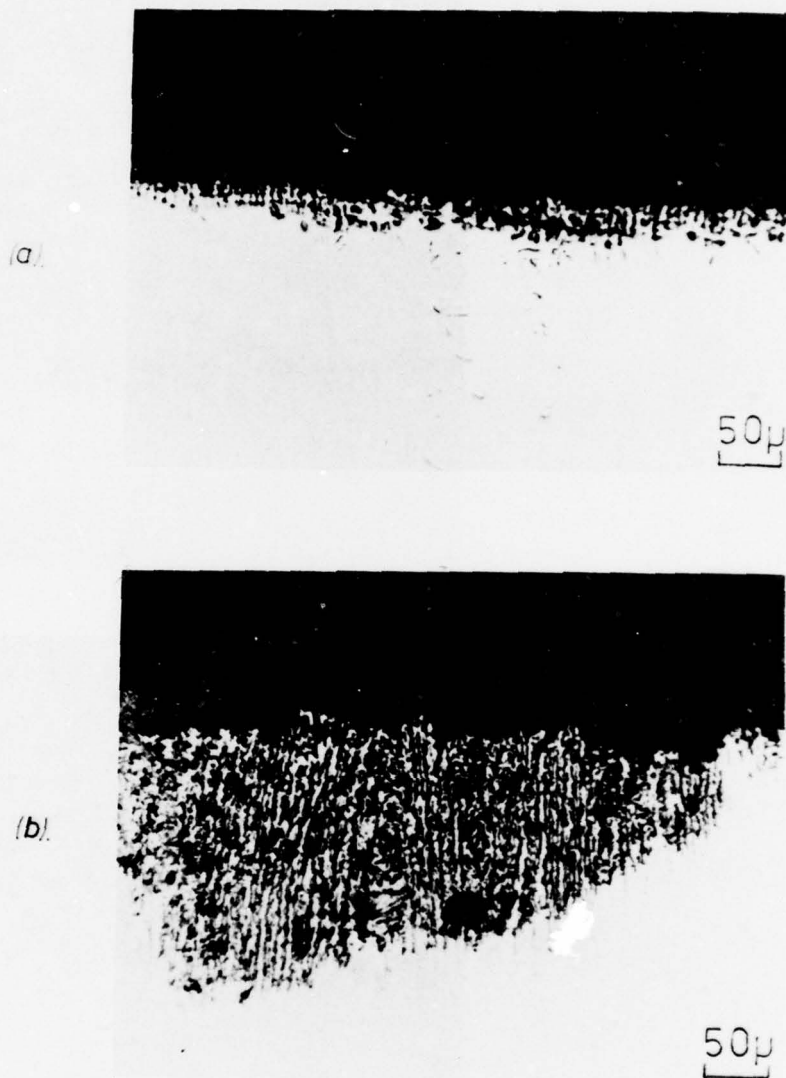


Figure 34. Cross-section of Ni-19.7Nb-6Cr-2.5Al (directionally solidified) alloy coated with  $2.22 \text{ mg.cm}^{-2} \text{ Na}_2\text{SO}_4$  and subsequently oxidised in air at  $900^\circ\text{C}$  for 24 hours.

(a) lightly attacked area

(b) heavily attacked area



Figure 35. Cross-section of Ni-19.7Nb-6Cr-2.5Al (directionally solidified) alloy coated with  $2.17 \text{ mg.cm}^{-2} \text{ Na}_2\text{SO}_4$  and subsequently oxidised in air at  $1100^\circ\text{C}$  for 24 hours.

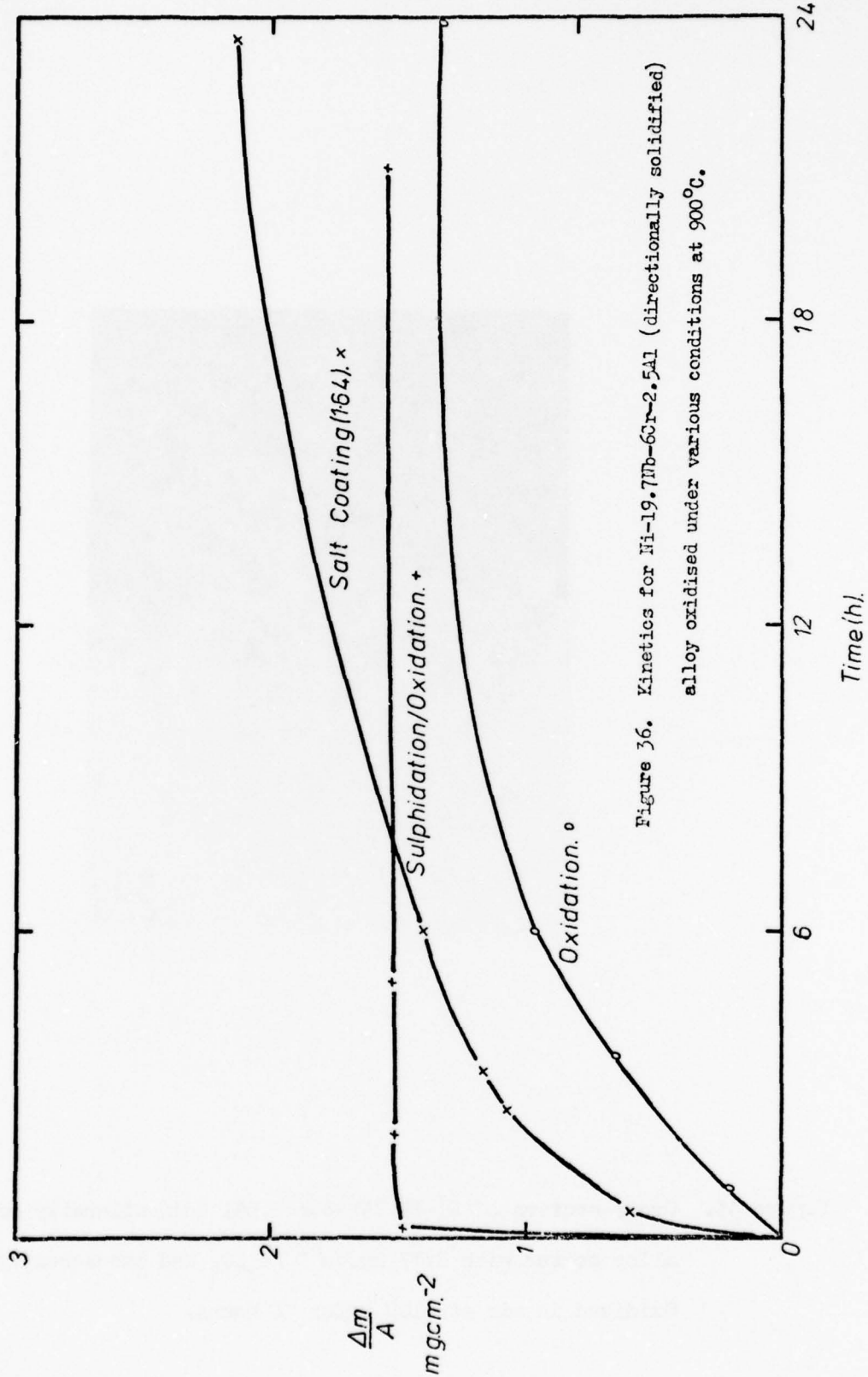


Figure 36. Kinetics for Ni-19.7Nb-60Cr-2.5Al (directionally solidified) alloy oxidised under various conditions at 900°C.

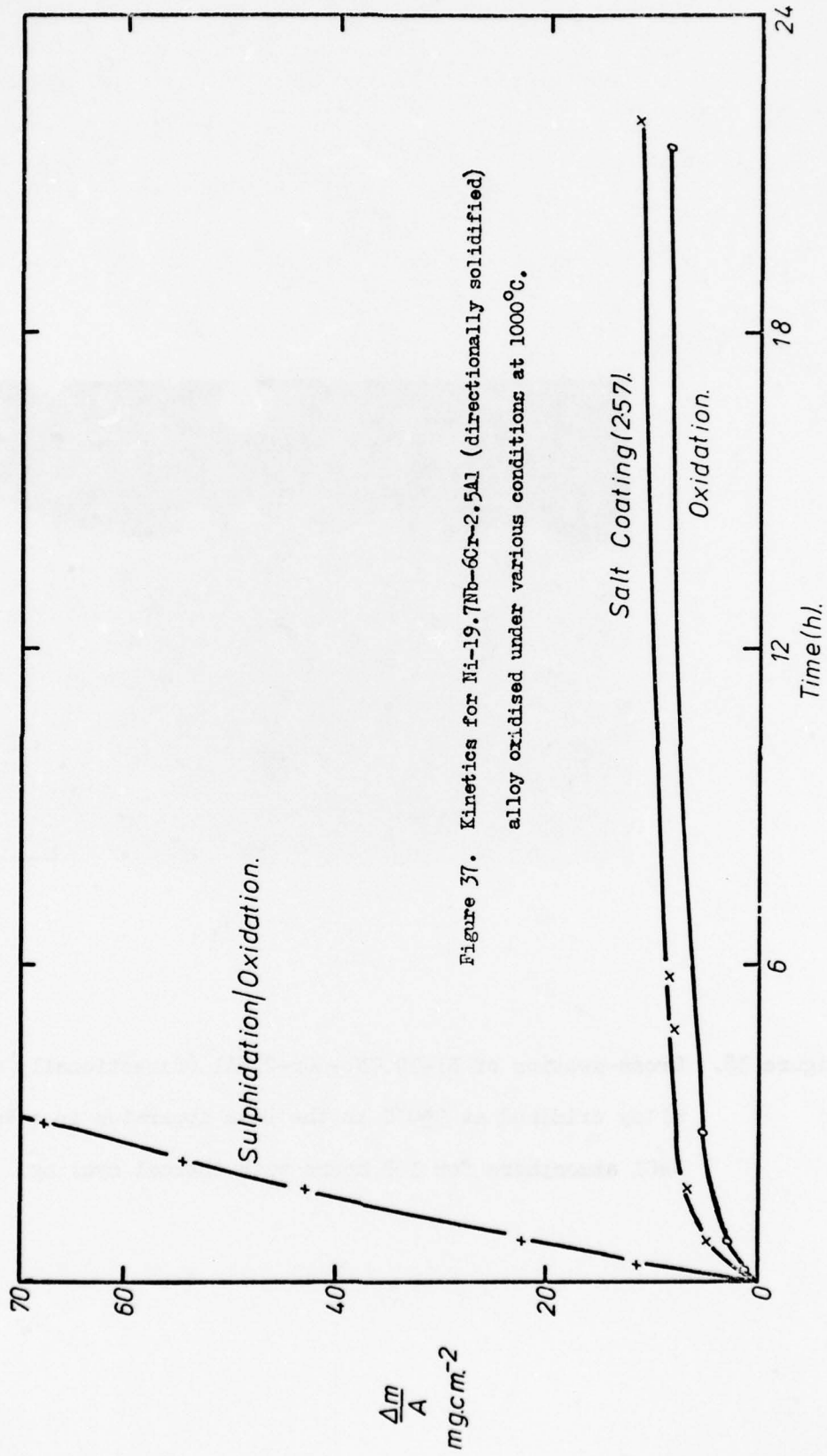


Figure 37. Kinetics for Ni-19.7Nb-60Cr-2.5Al (directionally solidified) alloy oxidised under various conditions at 1000°C.

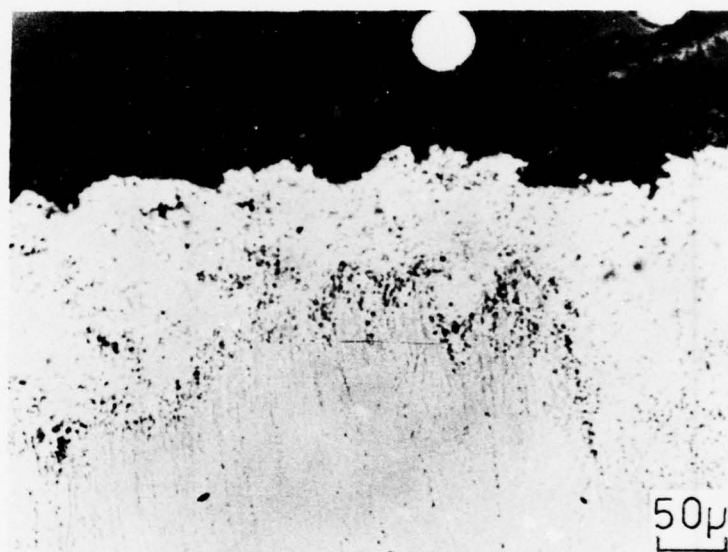


Figure 38. Cross-section of Ni-19.7Nb-6Cr-2.5Al (directionally solidified) alloy oxidised at 950°C in the Dean apparatus in a  $\text{Na}_2\text{SO}_4/10\%$  NaCl atmosphere for 168 hours with thermal cycling.

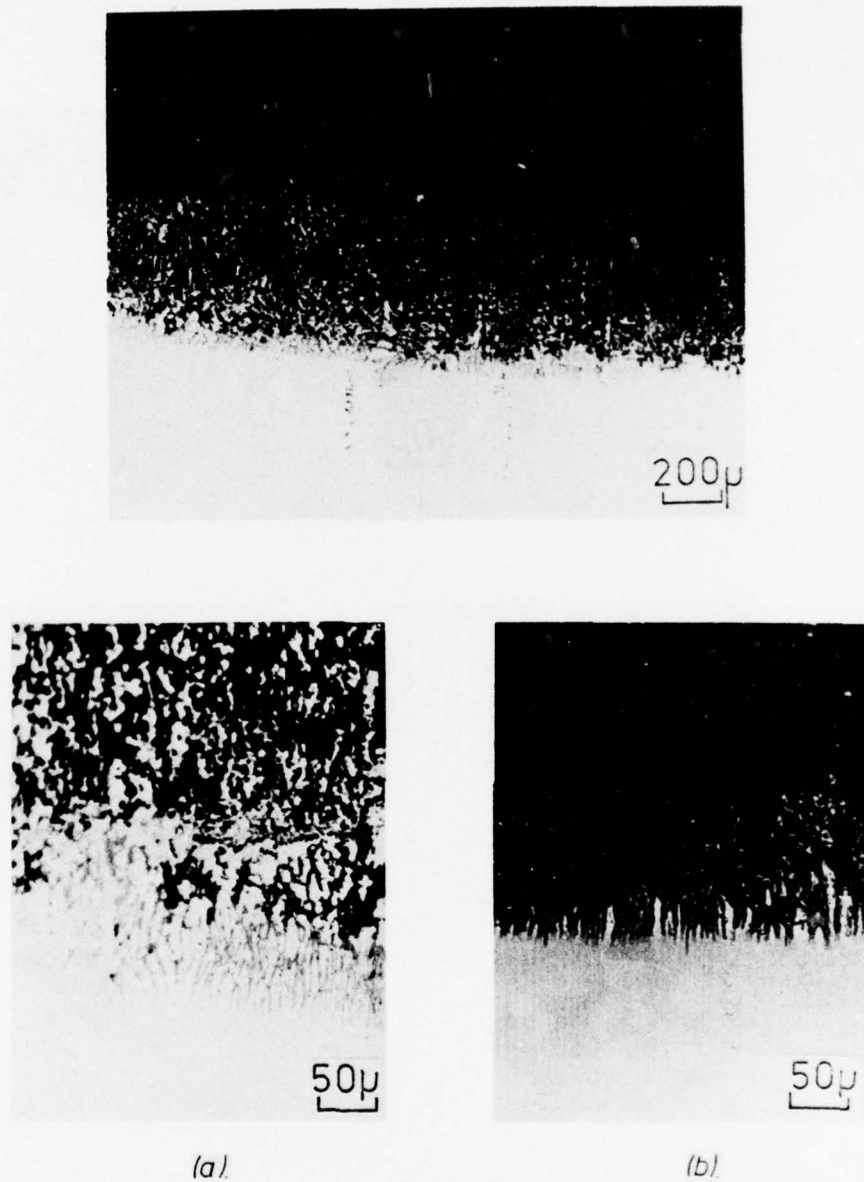


Figure 39. Cross-section of Ni-19.7Nb-6Cr-2.5Al (directionally solidified) alloy which has been sulphidised/oxidised at 1000°C for 3 hours.  
 (a) overall scale.  
 (b) unetched, showing the sulphides.  
 (c) etched, showing preferential oxidation of the  $\text{Ni}_3\text{Nb}$  lamellae.

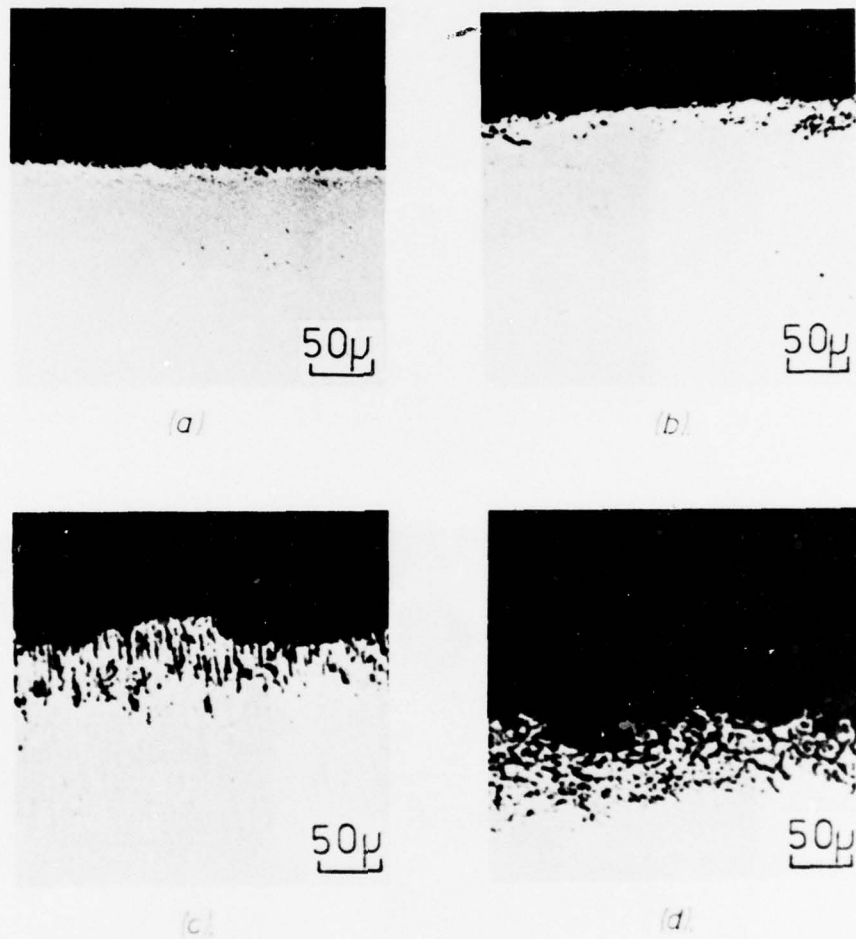


Figure 40. Cross-section of various Co-41Cr-2.4C eutectic alloys oxidised for 100 h in air between 900-1100°C, illustrating each morphological structure.

- (a) as-cast (900°C, Type I).
- (b) as-cast (1000°C, Type II).
- (c) directionally solidified 10.6 cm/hr (1000°C, Type III).
- (d) directionally solidified 31.5 cm/hr (1100°C, Type IV).

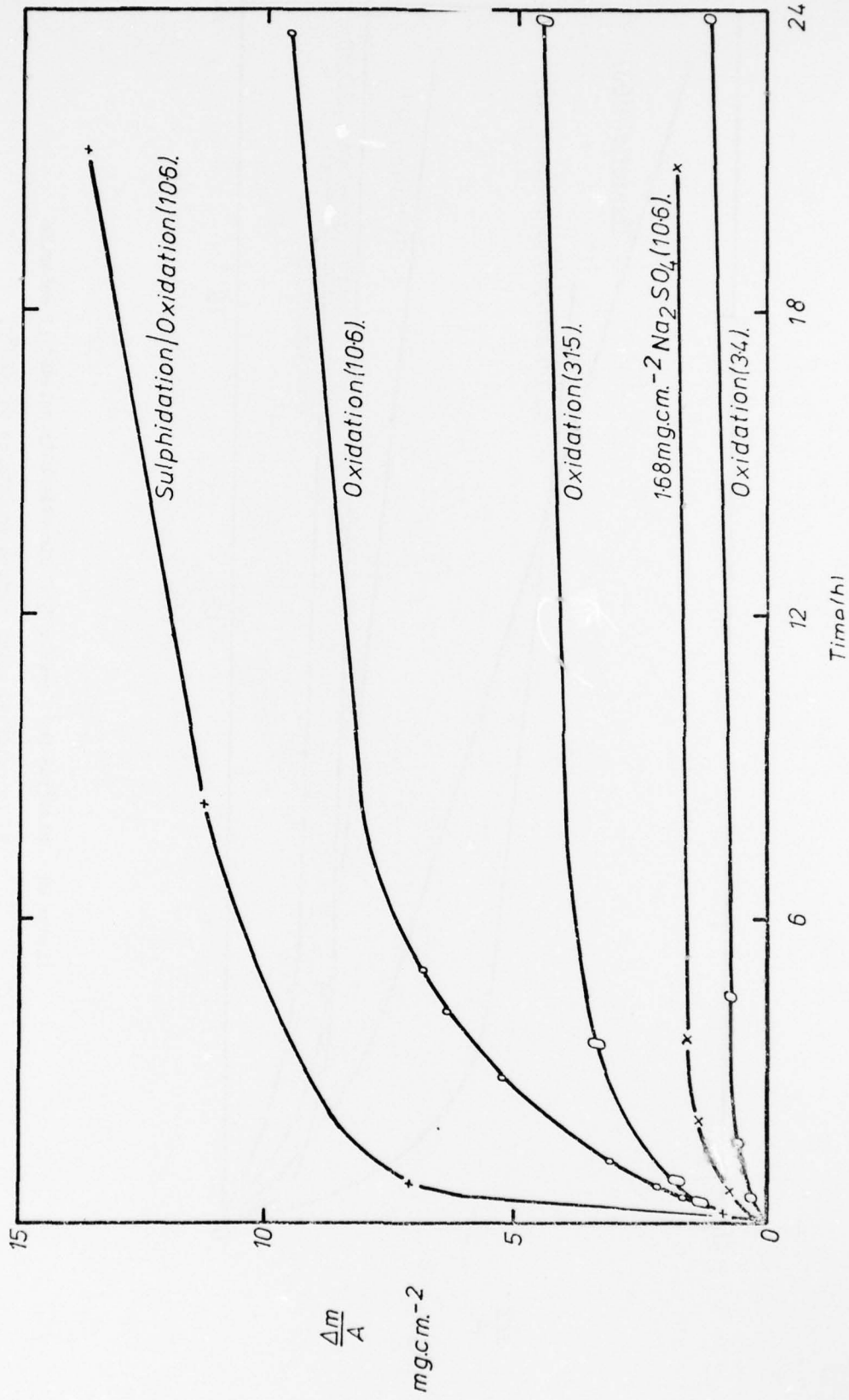


Figure 41. Kinetics for Co-41Cr-2.4C directionally solidified eutectic alloy oxidised under various conditions at 500°C.



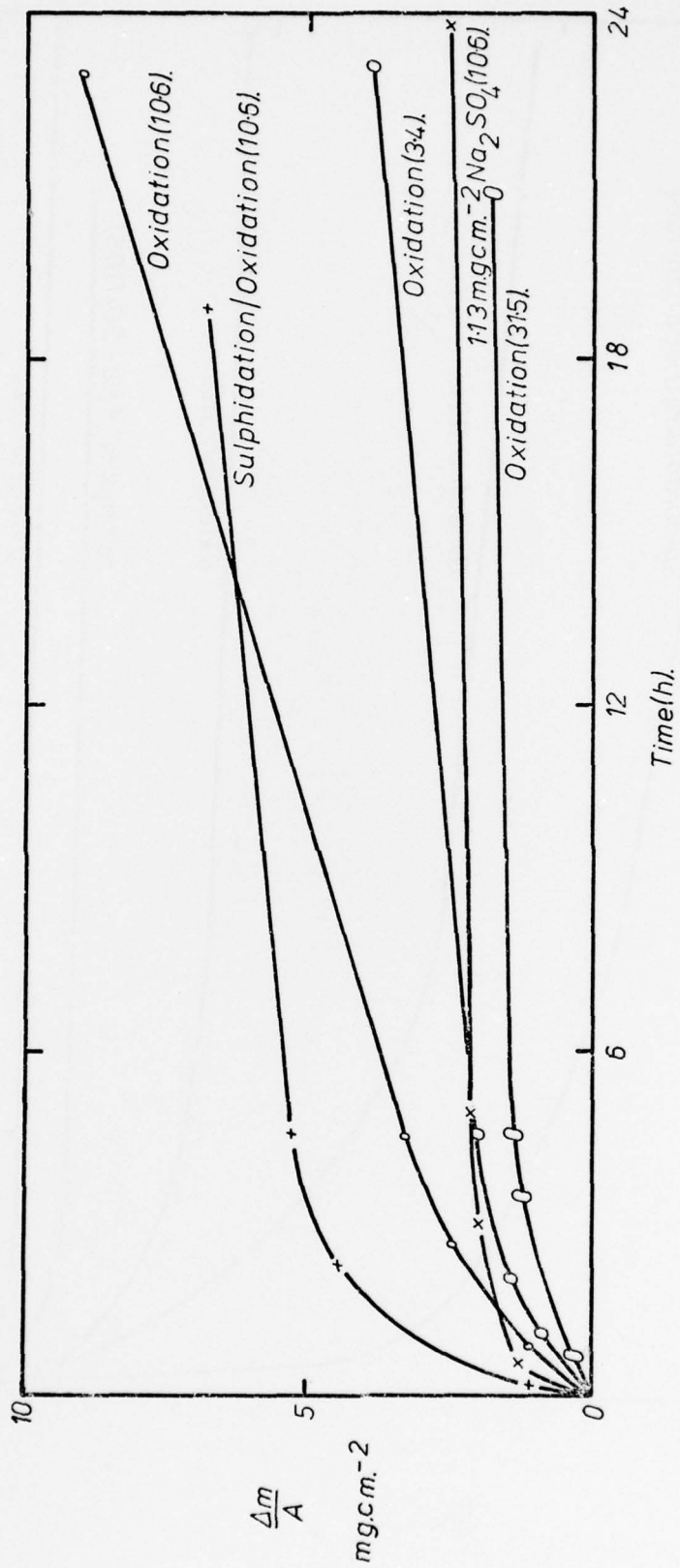


Figure 42. Kinetics for Co-4Cr-2.4C directionally solidified eutectic alloy oxidised under various conditions at 1000°C.

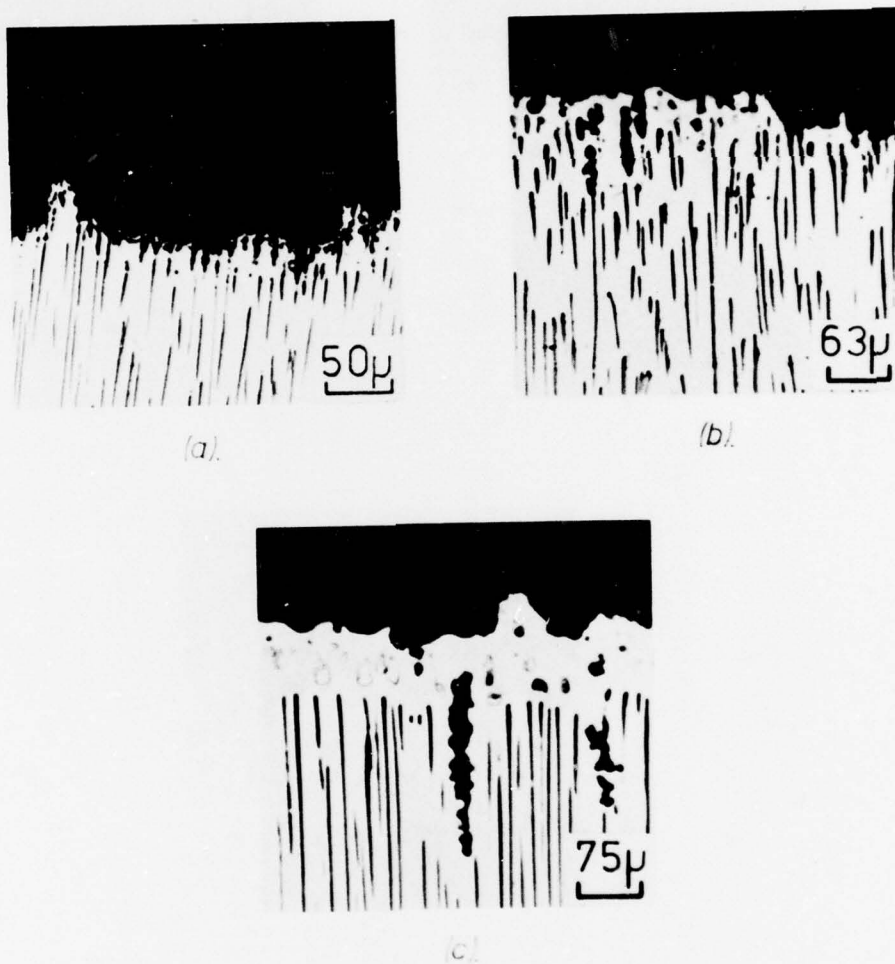


Figure 43. Cross-section of directionally solidified Co-15Cr-TaC specimens

oxidised in air for 100 h at different temperatures.

(a) 900°C.

(b) 1000°C.

(c) 1100°C.

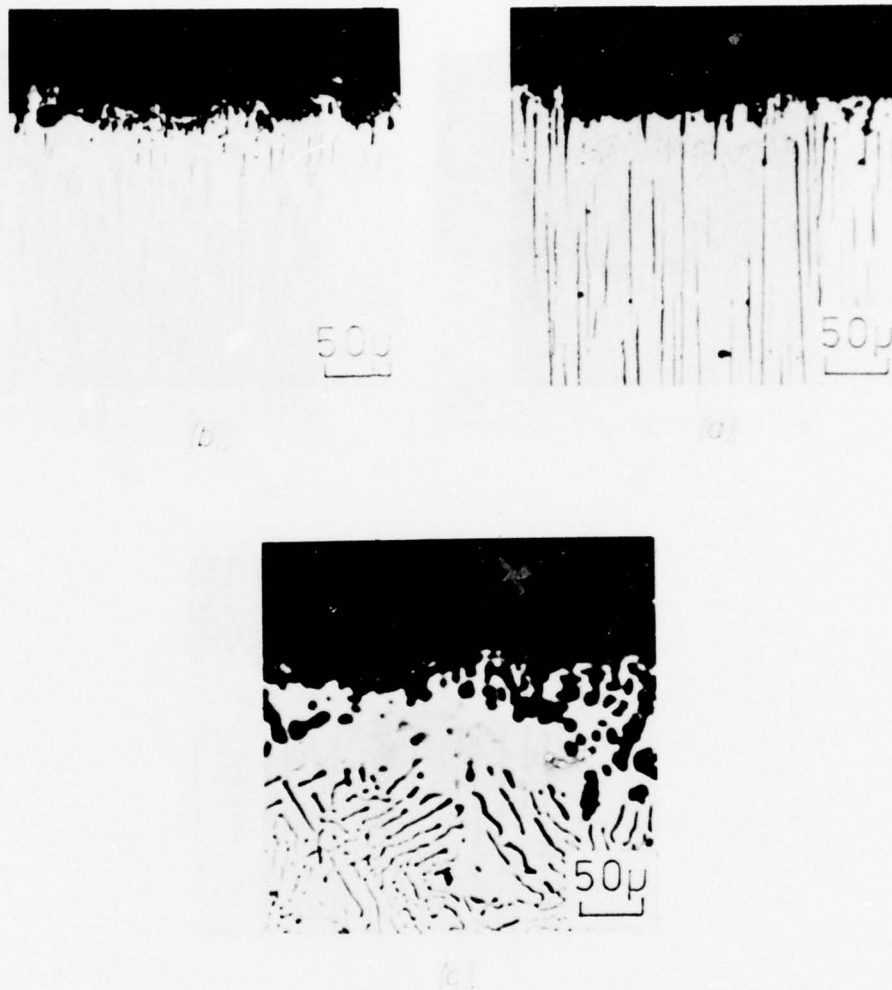


Figure 44. Cross-section of various Co-20Cr-10Ni-TaC specimens oxidised in air for 100 h at different temperatures.

(a) directionally solidified (900°C.).

(b) directionally solidified (1000°C.).

(c) furnace-cooled (1100°C.).

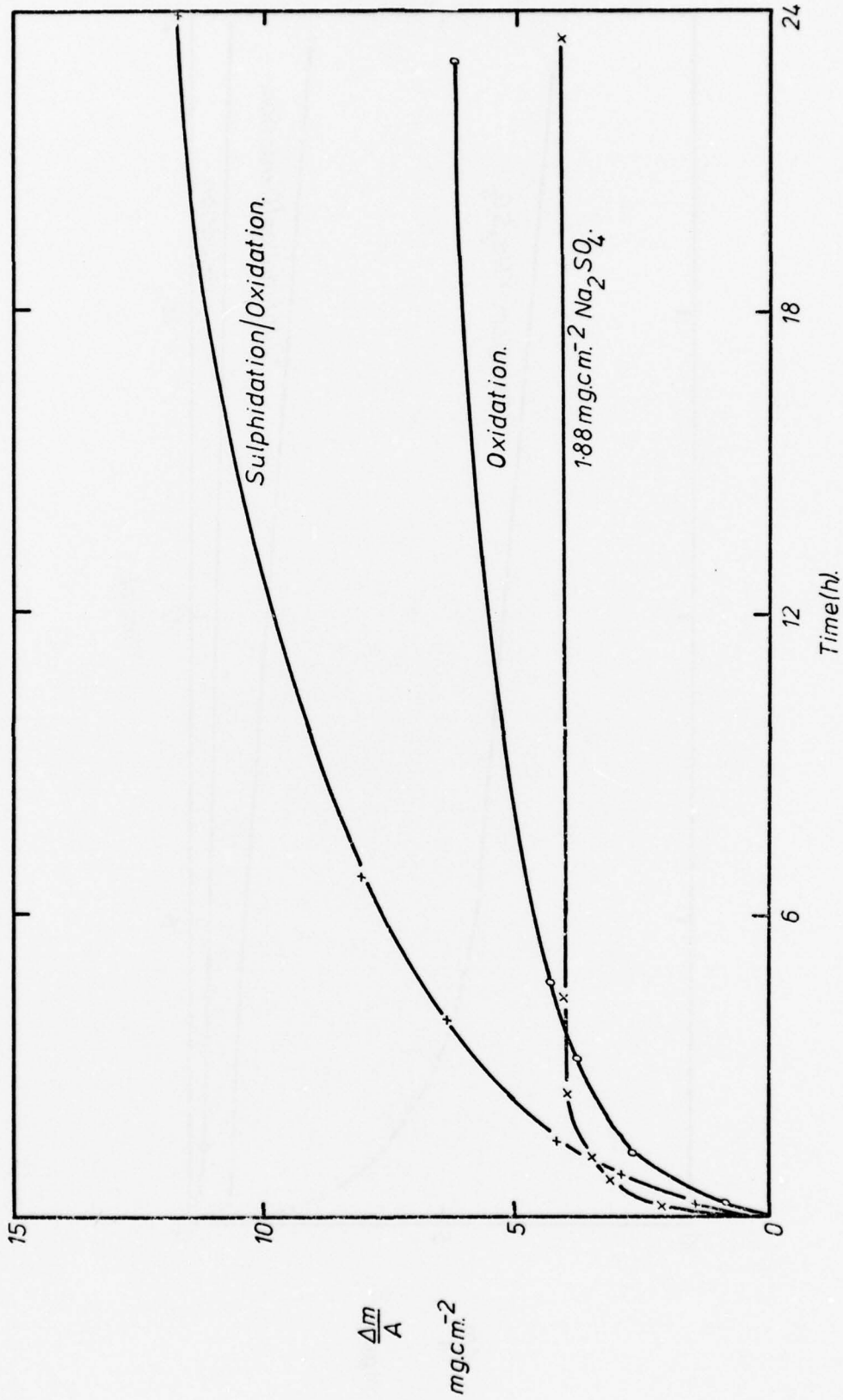


Figure 4.5a. Kinetics for Co-15Cr-7.5C directionally solidified eutectic alloy oxidised under various conditions at 900°C.

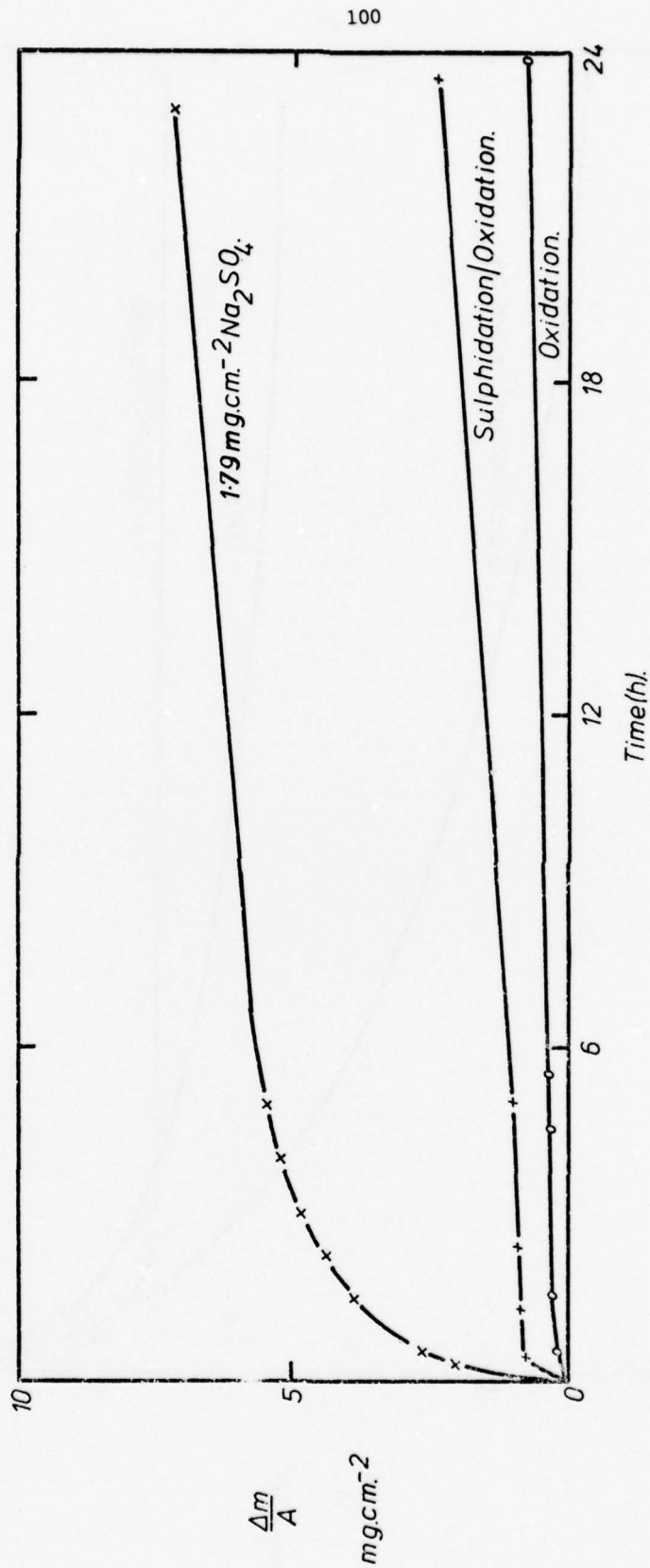


Figure 45b. Kinetics for Co-20Cr-10Ni-TaC directionally solidified  
eutectic alloy oxidised under various conditions at 900°C.

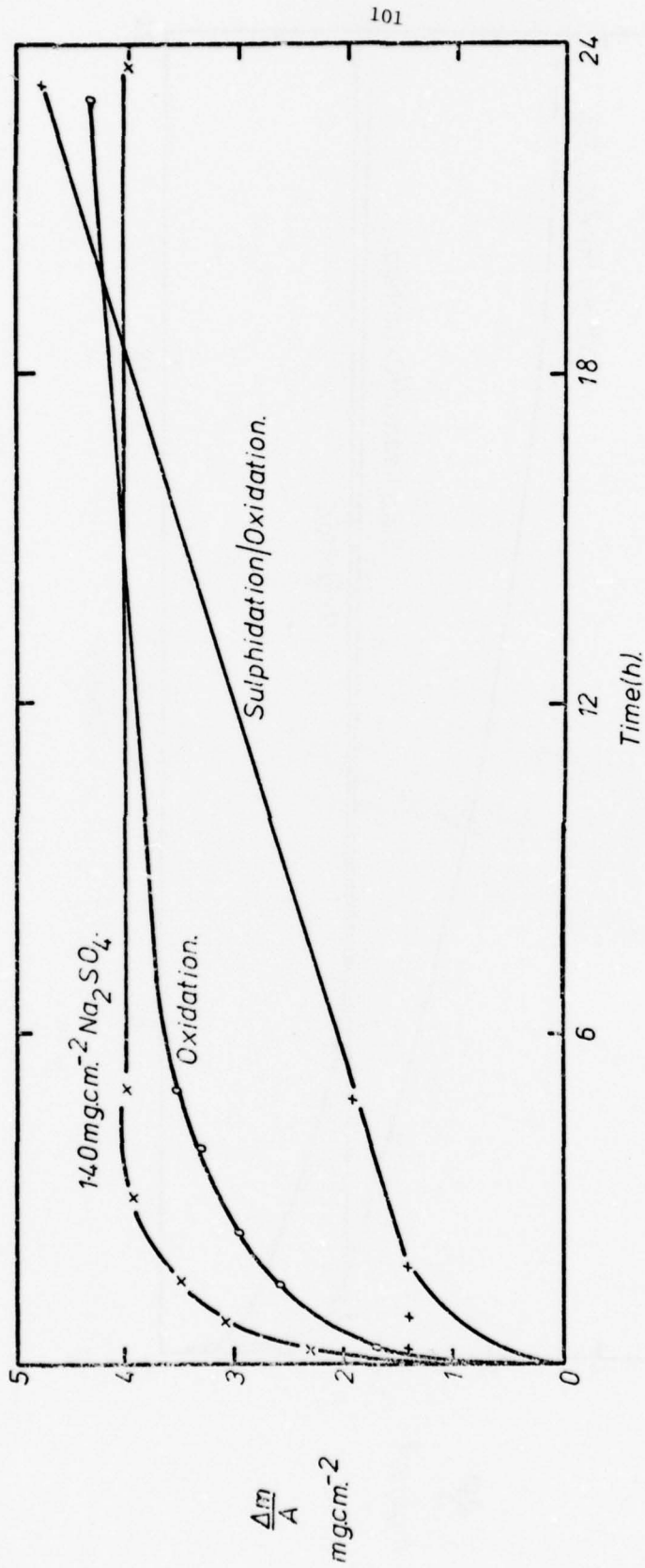


Figure 46a. Kinetics for Co-15Cr-7.5C directionally solidified eutectic alloy oxidised under various conditions at 1000°C.

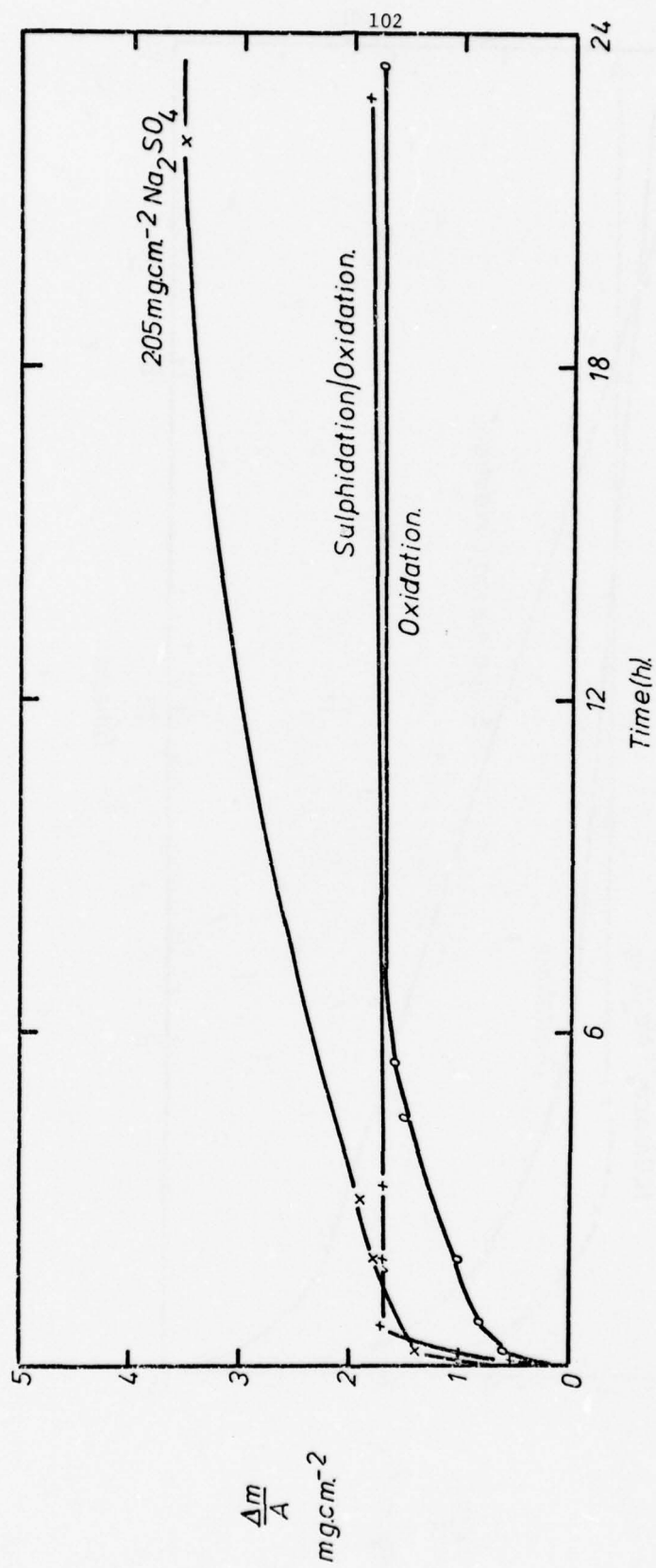


Figure 46b. Kinetics for Co-20Cr-10Ni-TaC directionally solidified eutectic alloy oxidised under various conditions at 1000°C.

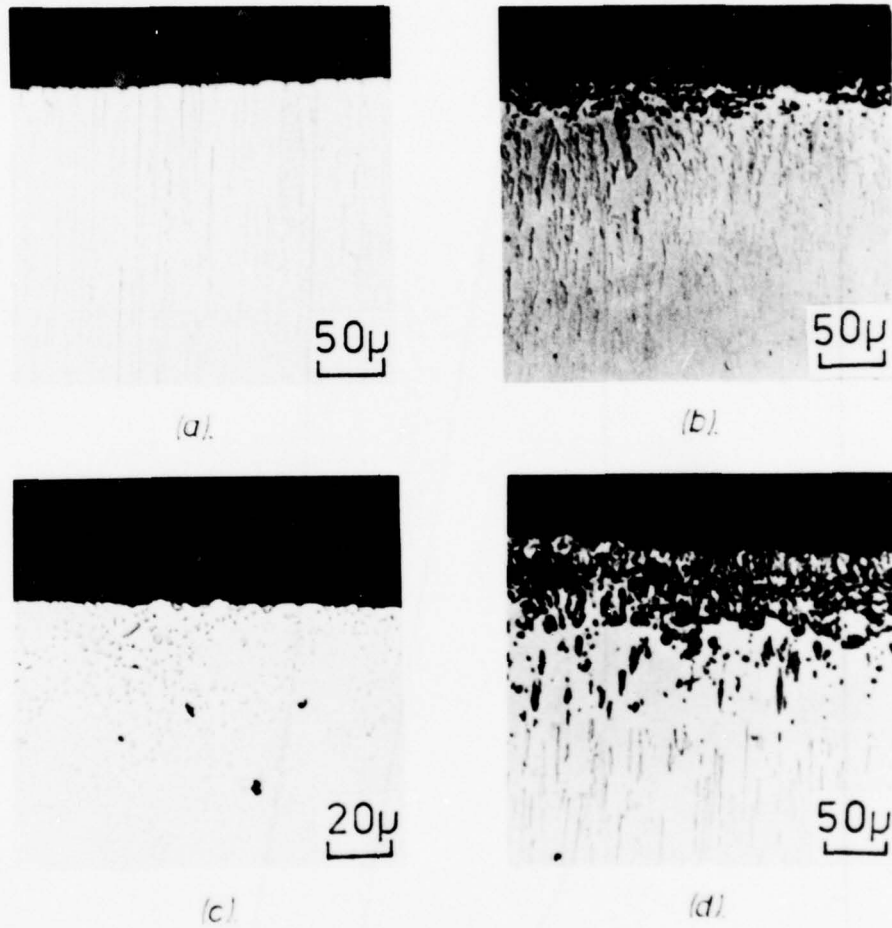


Figure 47. Cross-section of various Ni-12.3Cr-6.9Al-1.2C specimens oxidised in air for 100 h at different temperatures.

- (a) directionally solidified (900°C).
- (b) directionally solidified (1000°C).
- (c) as-cast (1100°C).
- (d) directionally solidified (1100°C).



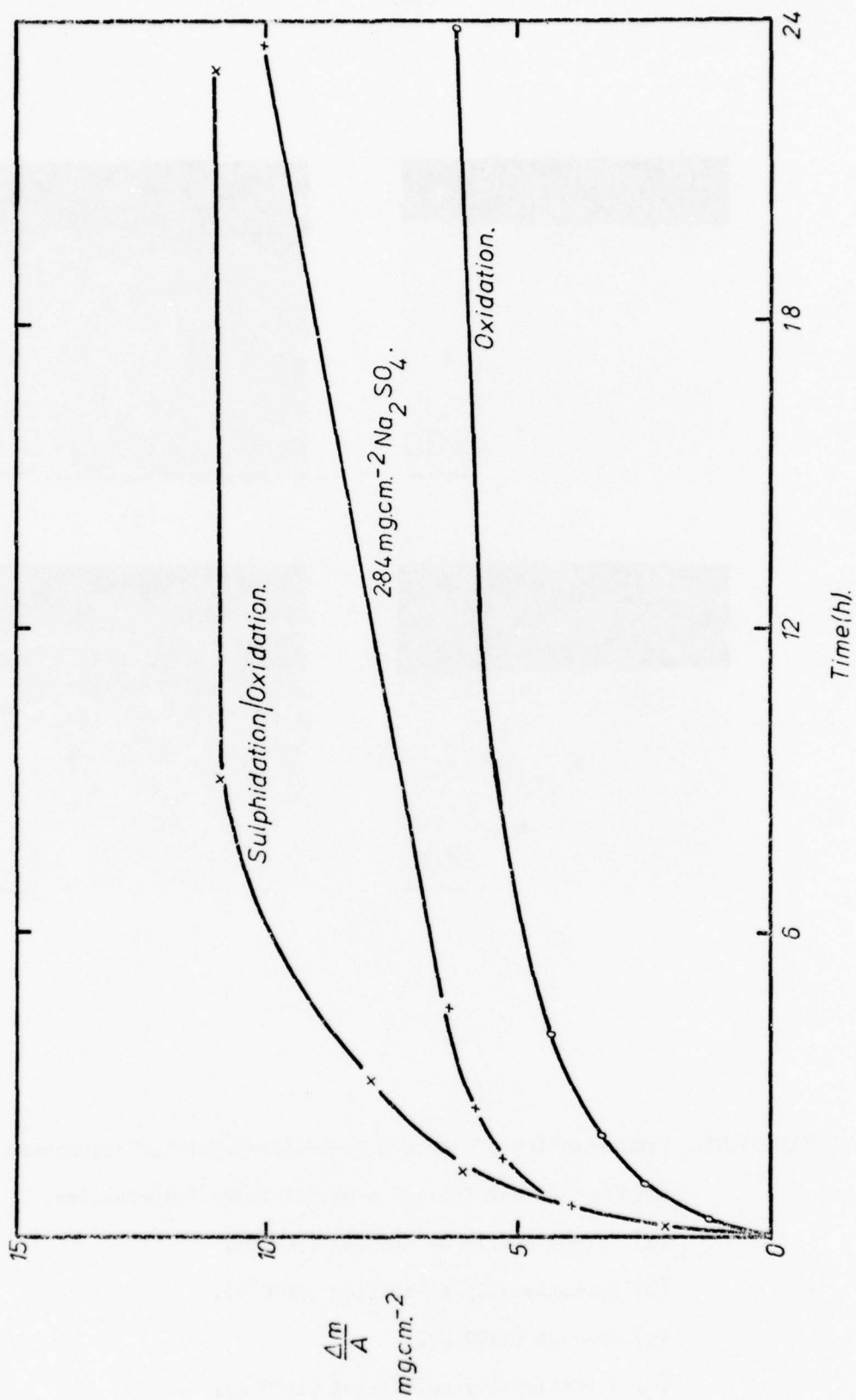


Figure 48. Kinetics for Ni-12.3Cr-6.9Al-1.8C directionally solidified alloy oxidised under various conditions at 900°C.

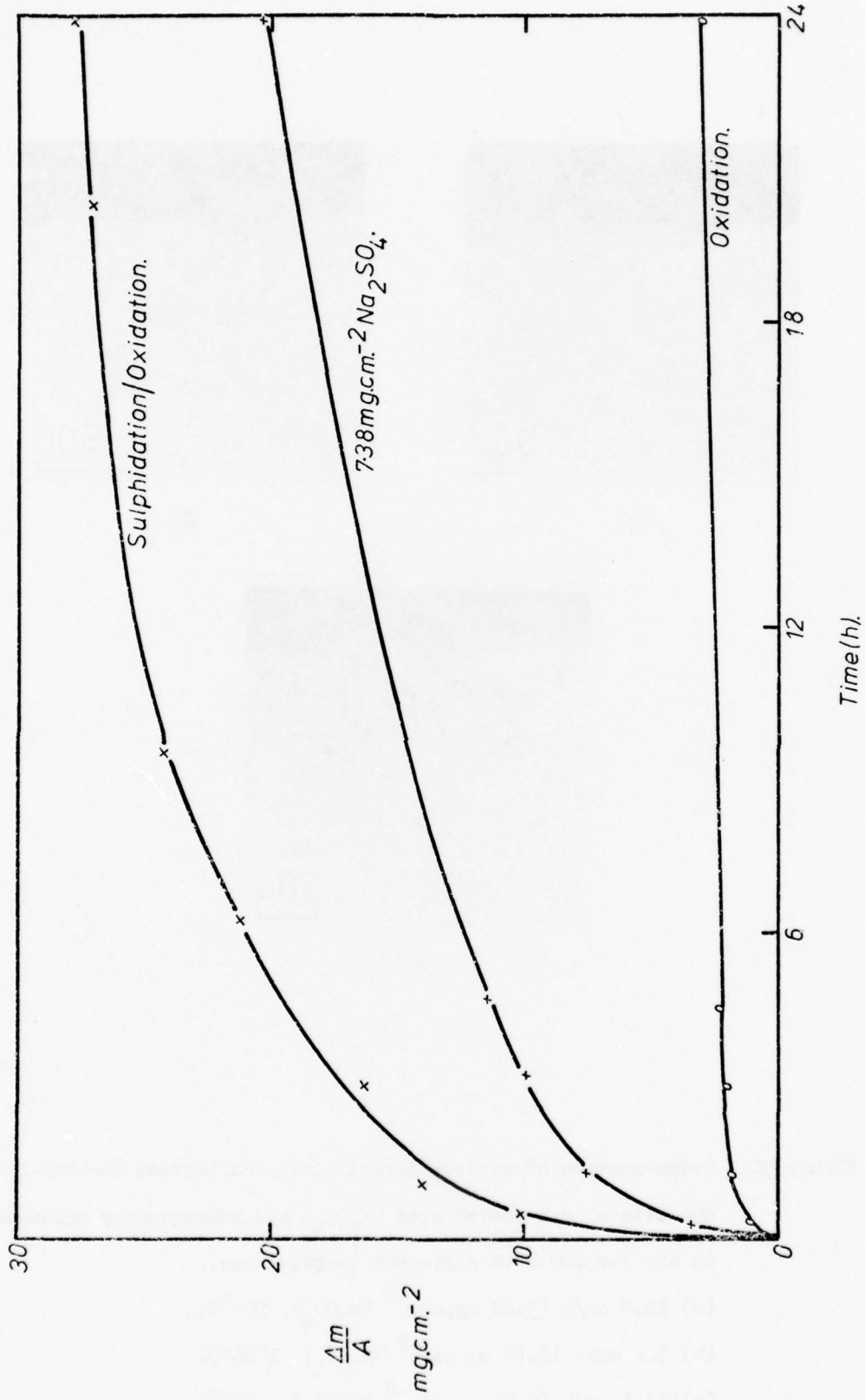


Figure 49. Kinetics for Ni-12.3Cr-6.9Al-1.8C directionally solidified eutectic alloy oxidised under various conditions at 1000°C.

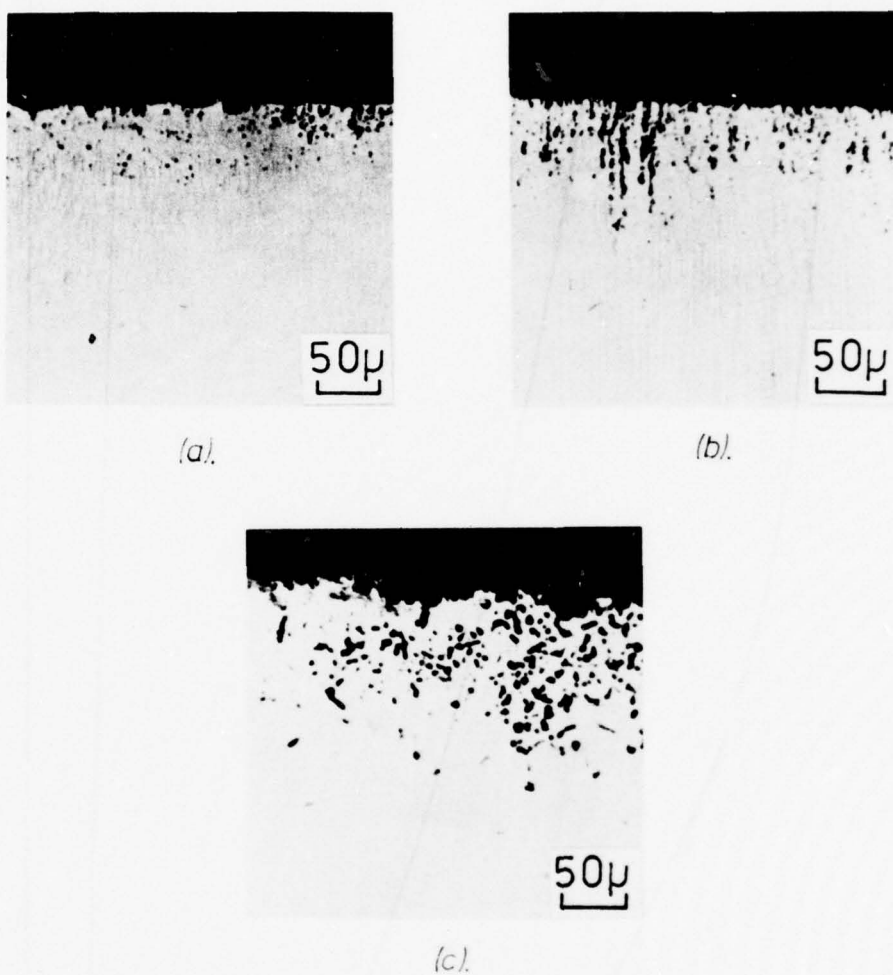


Figure 50. Cross-section of various directionally solidified Co-41Cr-2.4C eutectic alloys coated with  $\text{Na}_2\text{SO}_4$ , and subsequently oxidised in air for 100 h at different temperatures.

(a) 10.6 cm/h ( $3.62 \text{ mg.cm.}^{-2} \text{ Na}_2\text{SO}_4$ ),  $900^\circ\text{C}$ .

(b) 3.4 cm/h ( $2.60 \text{ mg.cm.}^{-2} \text{ Na}_2\text{SO}_4$ ),  $1000^\circ\text{C}$ .

(c) 31.5 cm/h ( $5.33 \text{ mg.cm.}^{-2} \text{ Na}_2\text{SO}_4$ ),  $1100^\circ\text{C}$ .

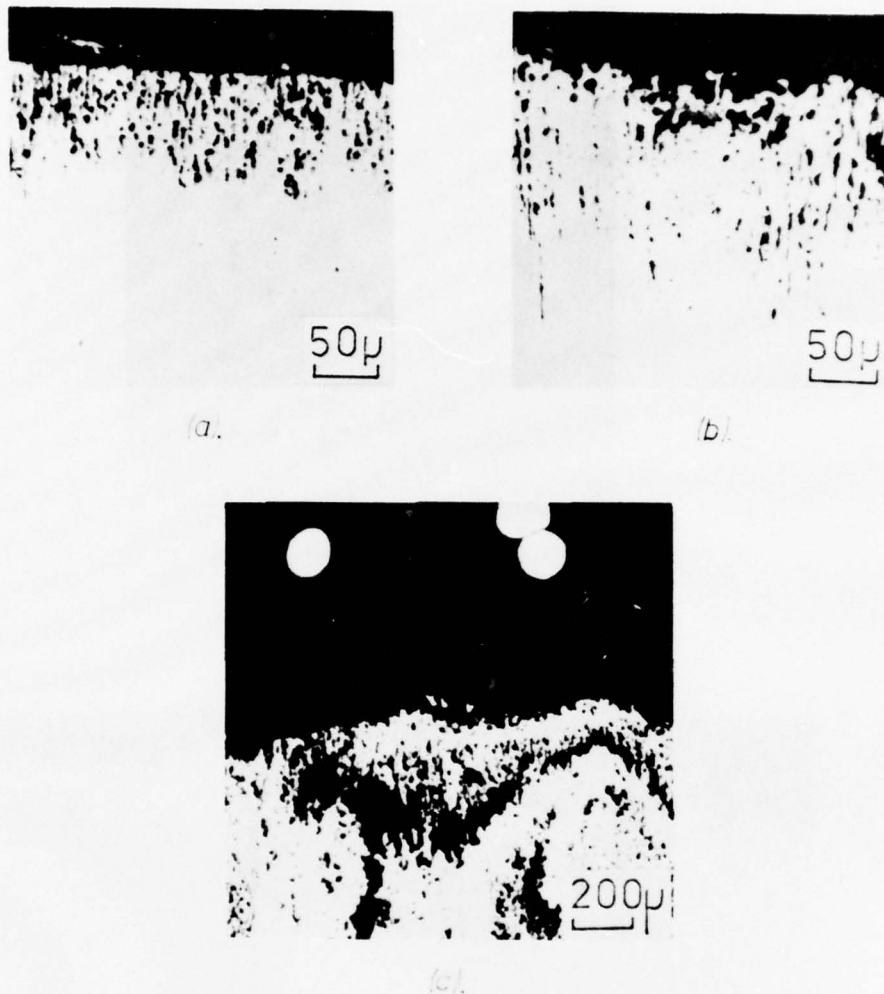


Figure 51. Cross-section of directionally solidified Co-41Cr-2.4C eutectic alloy (10.6 cm/h) specimens which have been subject to various hot-corrosion tests.

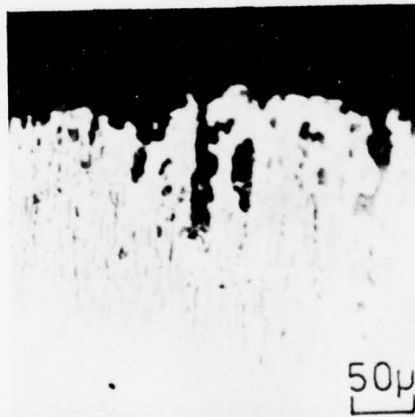
(a) pre-sulphidised in  $H_2/H_2S$  (90:10) mixture for 6 mins. and subsequently oxidised in oxygen for 45 h at  $1000^\circ C$ .

(b) exposed to condensing  $Na_2SO_4/10\% NaCl$  in the Dean rig at  $950^\circ C$  for 24 h.

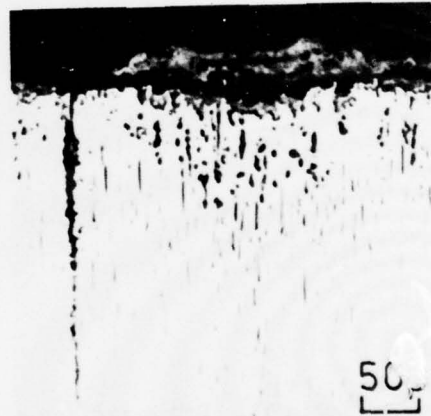
(c) exposed to condensing  $Na_2SO_4/10\% NaCl$  in the Dean rig at  $950^\circ C$  for 96 h, with cyclic cooling to room temperature every 24 h.



(a)



(b)



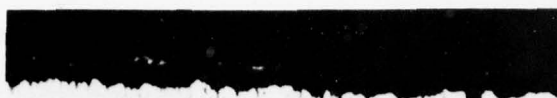
(c)

Figure 52. Cross-section of directionally solidified Co-15Cr-TaC eutectic alloy specimens coated with  $\text{Na}_2\text{SO}_4$  and subsequently oxidised in air for 100 hr at different temperatures.

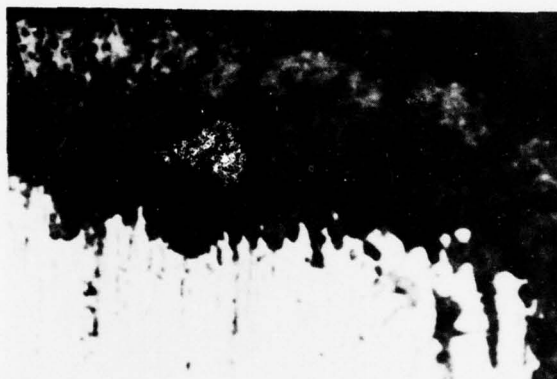
(a)  $900^\circ\text{C}$  ( $2.38 \text{ mg.cm.}^{-2} \text{ Na}_2\text{SO}_4$ ).

(b)  $1000^\circ\text{C}$  ( $4.59 \text{ mg.cm.}^{-2} \text{ Na}_2\text{SO}_4$ ).

(c)  $1100^\circ\text{C}$  ( $4.15 \text{ mg.cm.}^{-2} \text{ Na}_2\text{SO}_4$ ).



(a)



(b)

Figure 53. Cross-section of directionally solidified Co-15Cr-TaC eutectic alloy specimens which have been subject to various hot-corrosion tests.

- (a) pre-sulphidised in  $H_2/H_2S$  (90:10) mixture for 6 mins. and subsequently oxidised in oxygen for 24 h at  $1000^\circ C$ .
- (b) exposed to condensing  $Na_2SO_4/10\%$  NaCl in the Dean rig at  $950^\circ C$  for 240 h, with cyclic cooling to room temperature every 60 h.

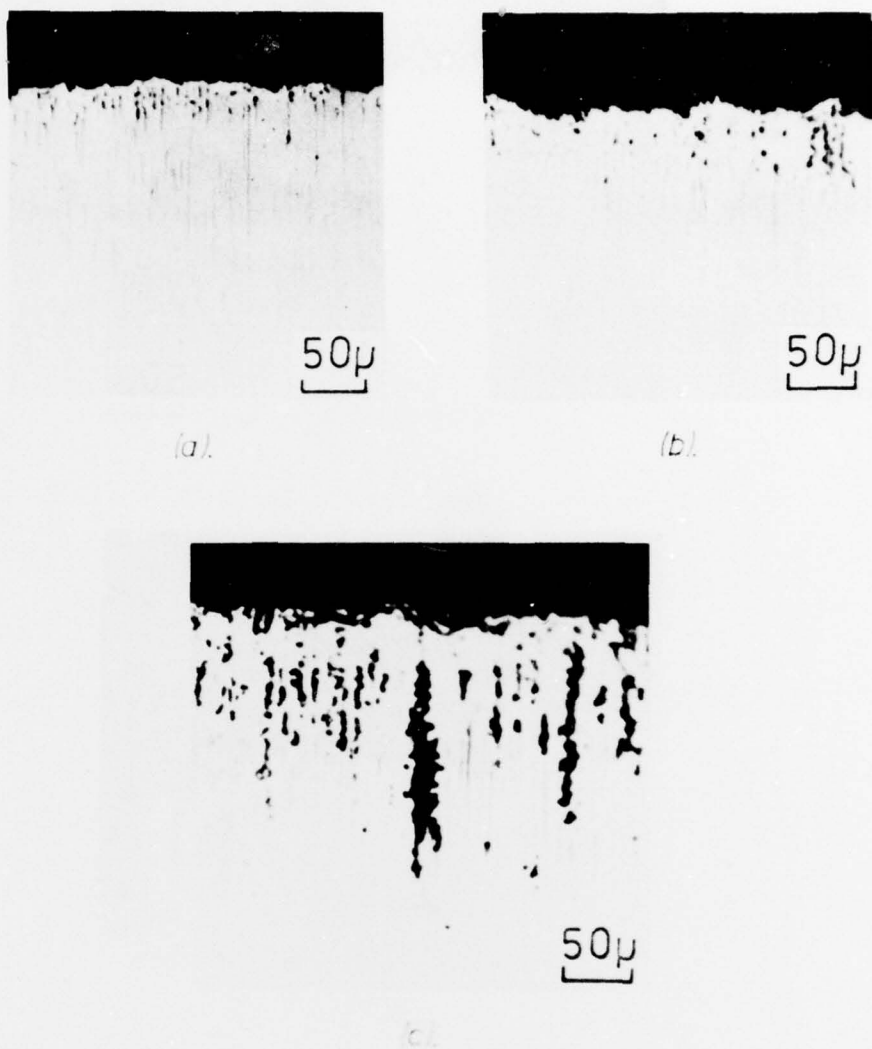


Figure 54. Cross-section of directionally solidified Co-20Cr-10Ni-TaC eutectic alloy specimens coated with  $\text{Na}_2\text{SO}_4$  and subsequently oxidised in air for 100 h at different temperatures.

- (a)  $900^\circ\text{C}$  ( $6.84 \text{ mg.cm.}^{-2} \text{ Na}_2\text{SO}_4$ ).
- (b)  $1000^\circ\text{C}$  ( $6.13 \text{ mg.cm.}^{-2} \text{ Na}_2\text{SO}_4$ ).
- (c)  $1100^\circ\text{C}$  ( $4.90 \text{ mg.cm.}^{-2} \text{ Na}_2\text{SO}_4$ ).



(a)



Figure 55. Cross-section of directionally solidified Co-20Cr-10Ni-TaC eutectic alloy specimens which have been subject to various hot-corrosion tests.

- (a) pre-sulphidised in  $H_2/H_2S$  (90:10) mixture for 6 mins. and subsequently oxidised in oxygen for 24 h at  $1000^\circ C$ .
- (b) exposed to condensing  $Na_2SO_4/10\%$  NaCl in the Dean rig at  $950^\circ C$  for 240 h, with cyclic cooling to room temperature every 60 h.



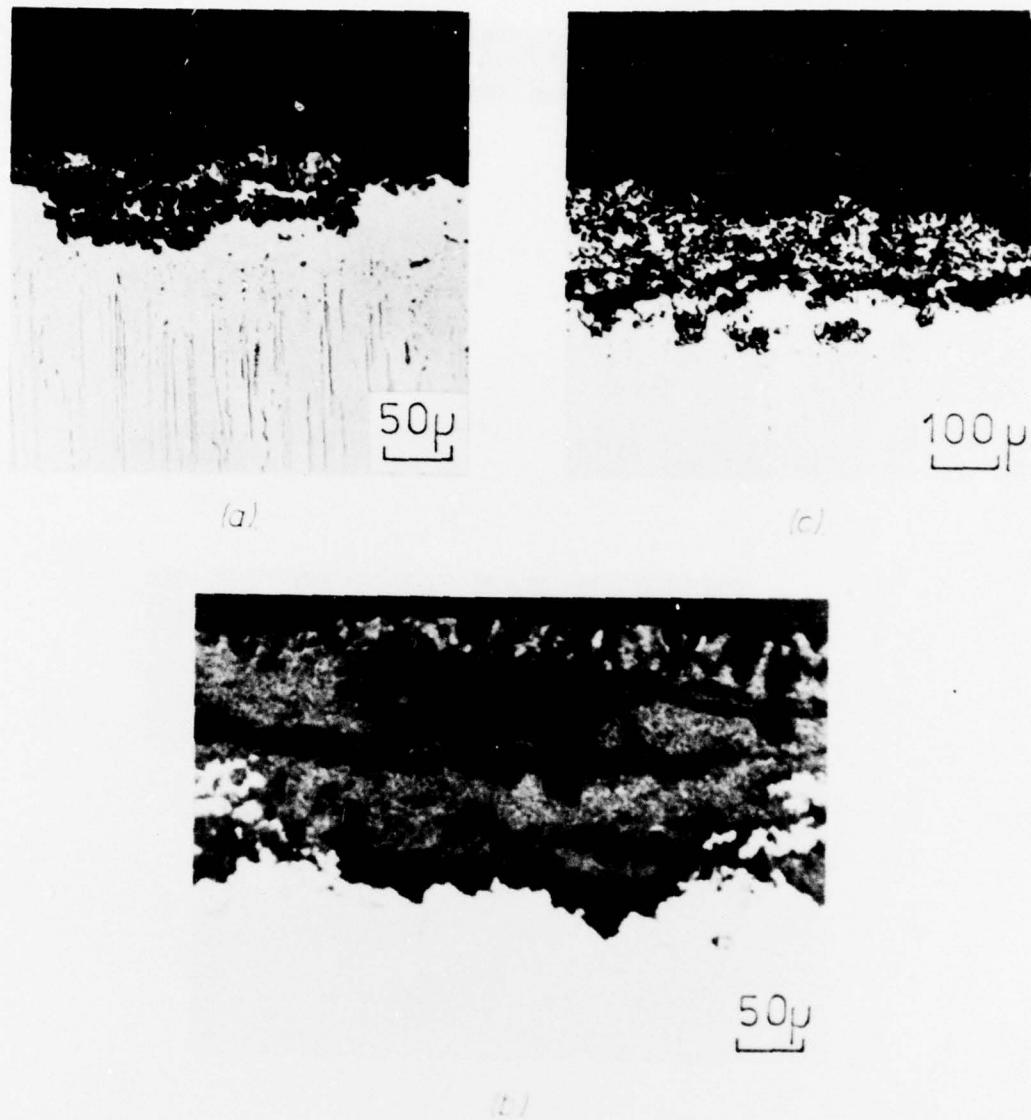


Figure 56. Cross-section of directionally solidified Ni-12.3Cr-6.9Al-1.8C eutectic alloy specimens coated with  $\text{Na}_2\text{SO}_4$  and subsequently oxidised in air for 100 h at different temperatures.

(a)  $900^\circ\text{C}$  ( $1.10 \text{ mg.cm.}^{-2} \text{ Na}_2\text{SO}_4$ ).

(b)  $1000^\circ\text{C}$  ( $2.67 \text{ mg.cm.}^{-2} \text{ Na}_2\text{SO}_4$ ).

(c)  $1100^\circ\text{C}$  ( $2.99 \text{ mg.cm.}^{-2} \text{ Na}_2\text{SO}_4$ ).

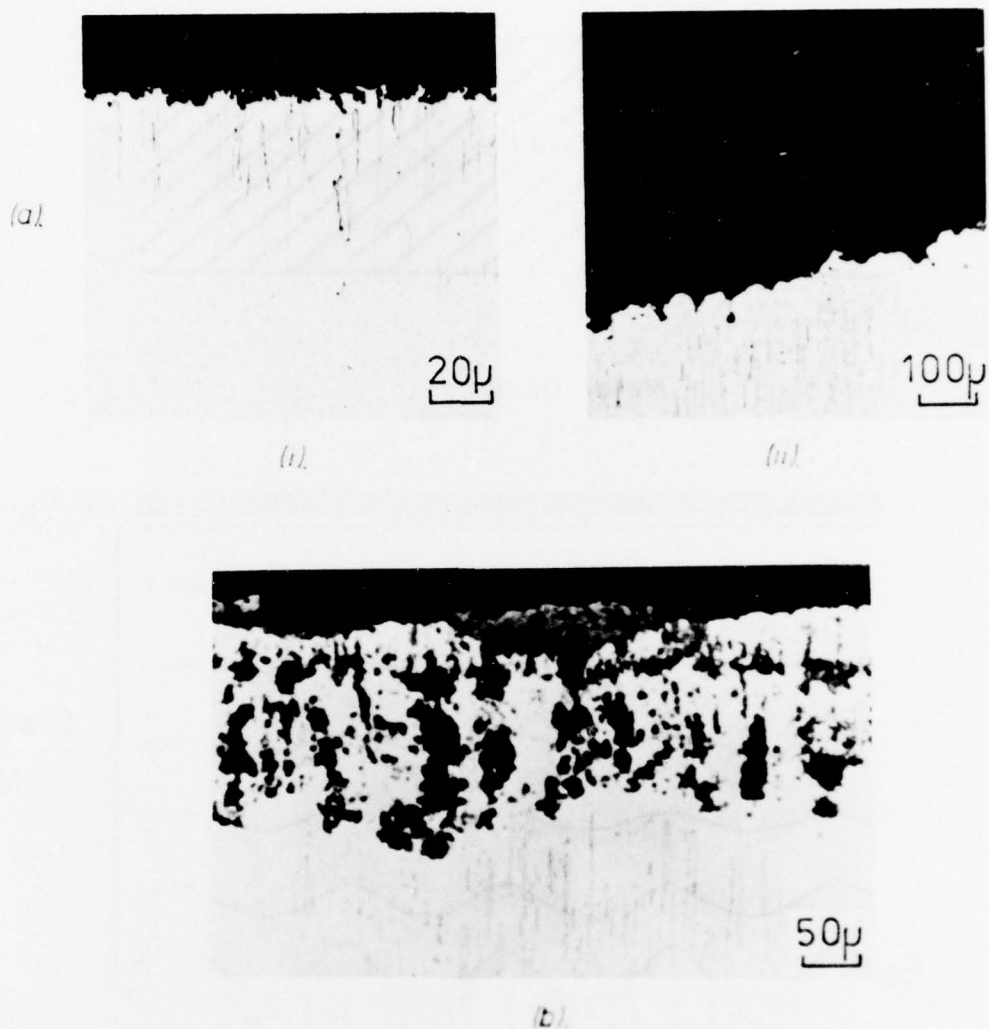


Figure 57. Cross-section of directionally solidified Ni-12.3Cr-6.9Al-1.8C eutectic alloy specimens which have been subject to various hot-corrosion tests.

(a) pre-sulphidised in  $H_2/H_2S$  (90:10) mixture for 6 mins. and subsequently oxidised in oxygen for 24 h.

(i)  $900^\circ C$             (ii)  $1000^\circ C$

(b) exposed to condensing  $Na_2SO_4/10\%$  NaCl in the Dean rig at  $950^\circ C$  for 240 h, with cyclic cooling to room temperature every 60 h.

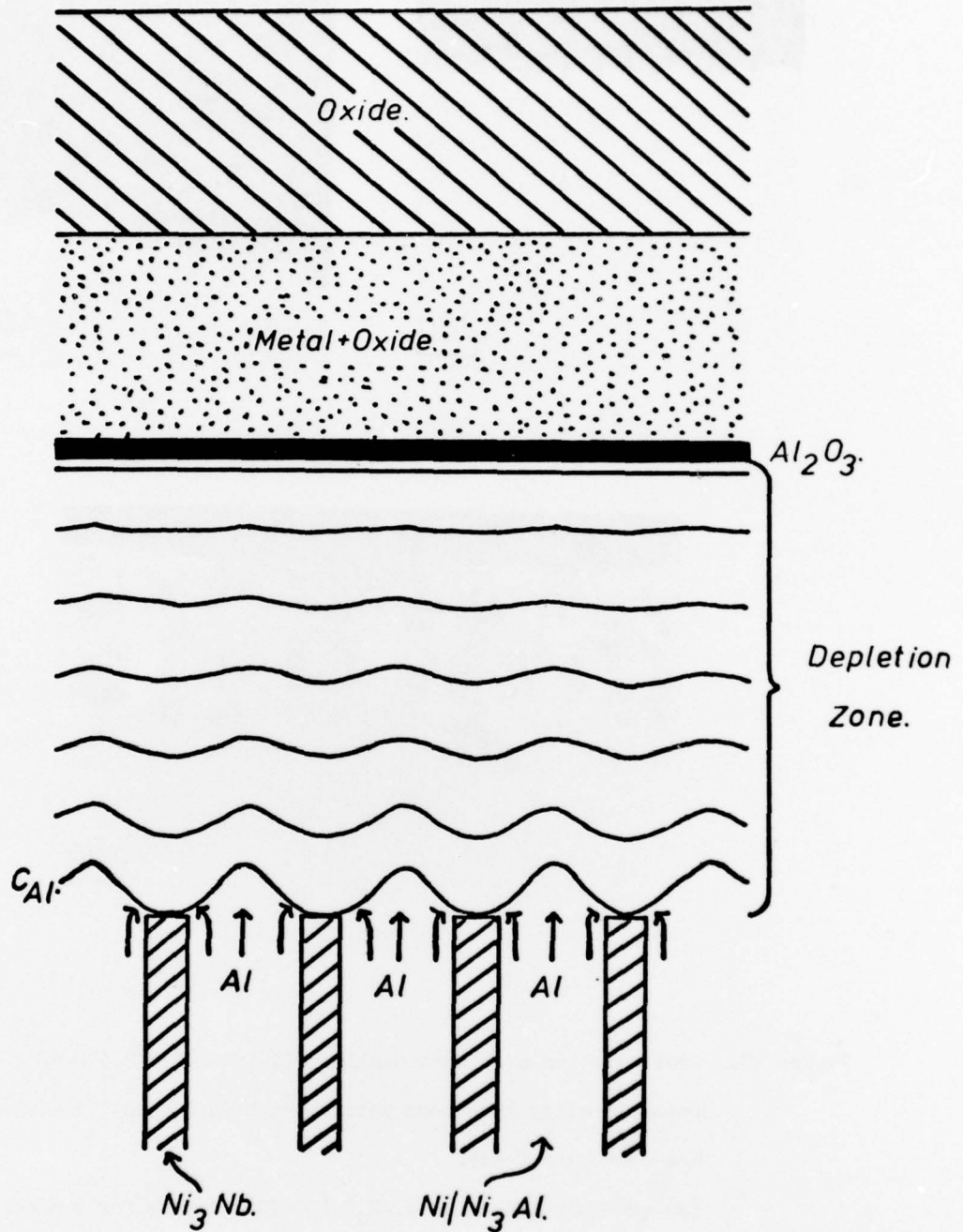


Figure 58. Schematic diagram showing  $Al_2O_3$  formation with the Ni-23.1Nb-4.4Al directionally solidified alloy at  $1100^\circ C$ .

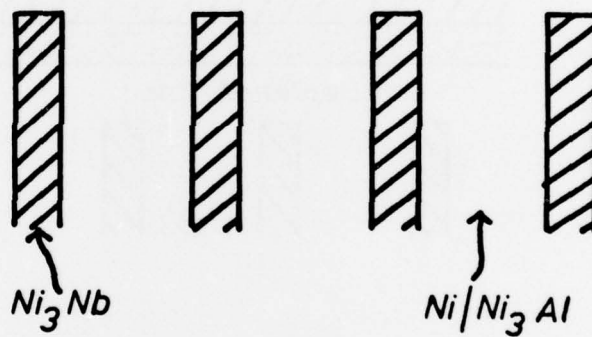
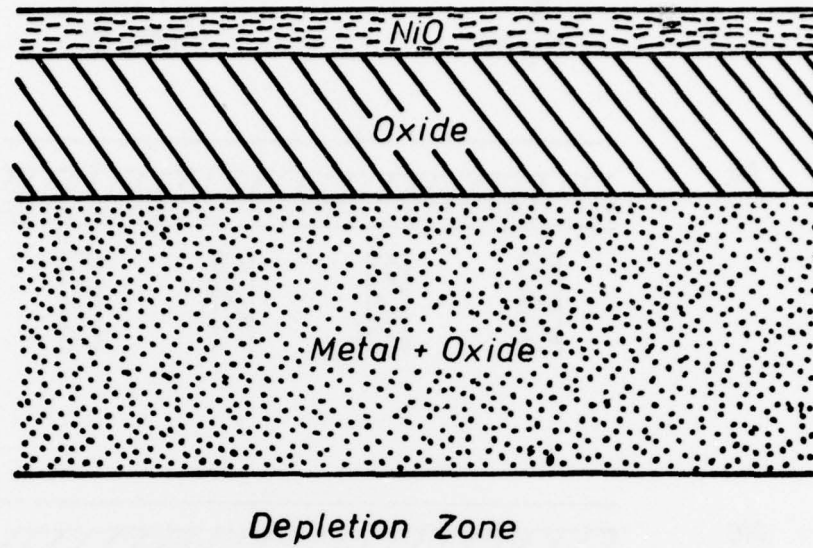


Figure 59. Schematic diagram for the oxidation of Ni-23.1Nb-4.4Al directionally solidified eutectic alloy at 900°C and 1000°C.

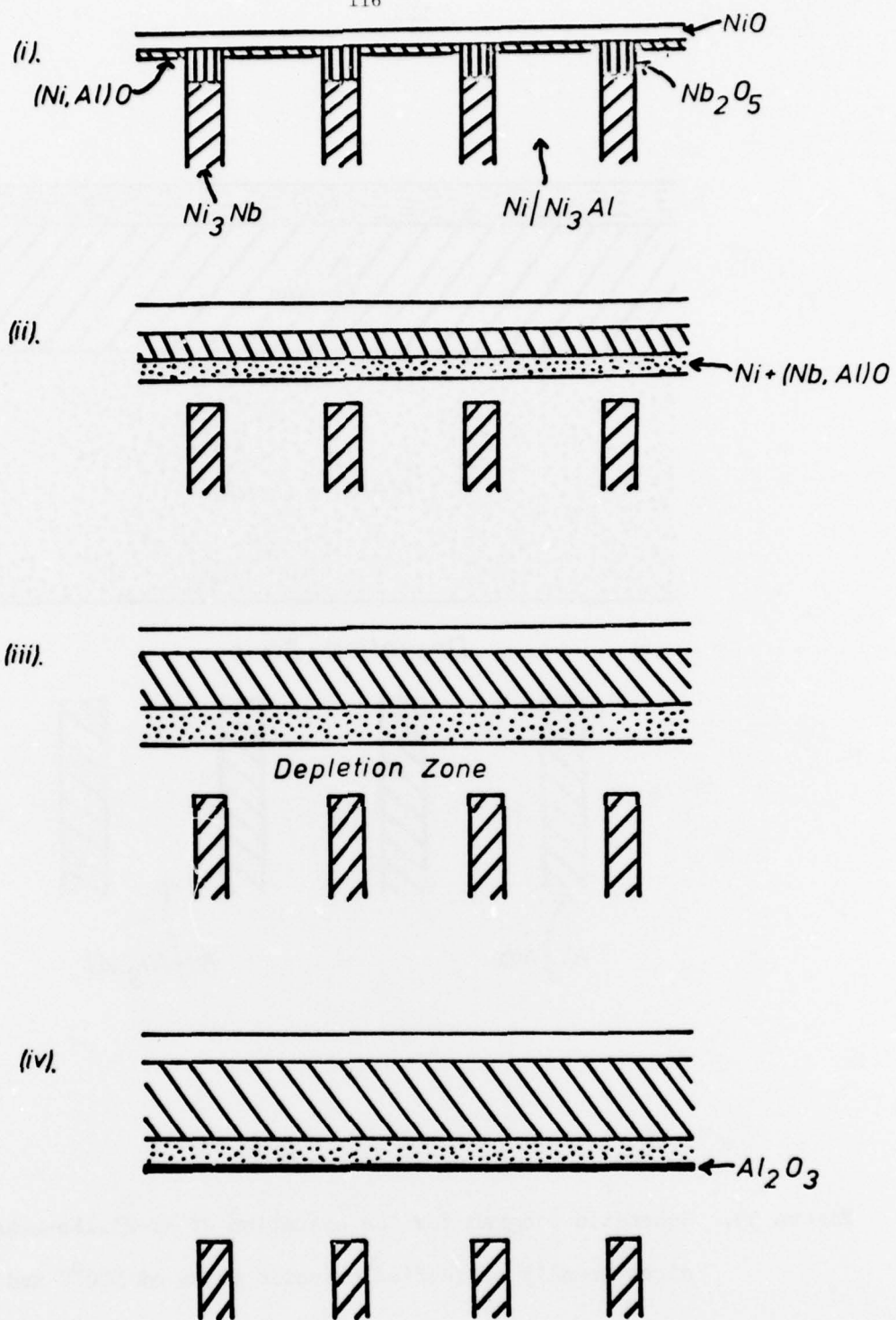


Figure 60. Schematic mechanism for the oxidation of the directionally solidified eutectic alloy Ni-23.1Nb-4.4Al within the temperature range 800-1100°C.

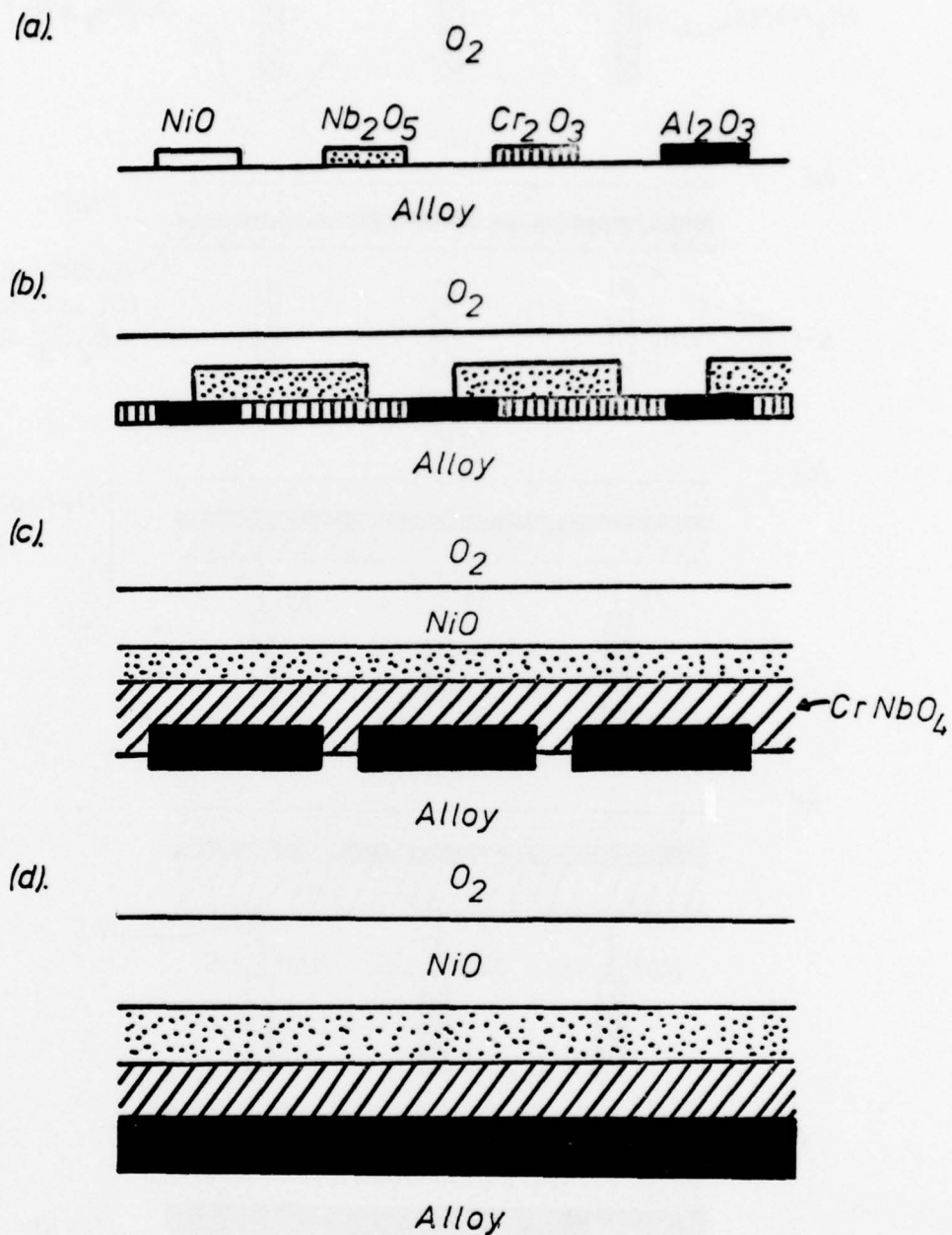


Figure 61. Schematic reaction mechanism for the oxidation of the quaternary Ni-19.7Nb-6Cr-2.5Al alloy.

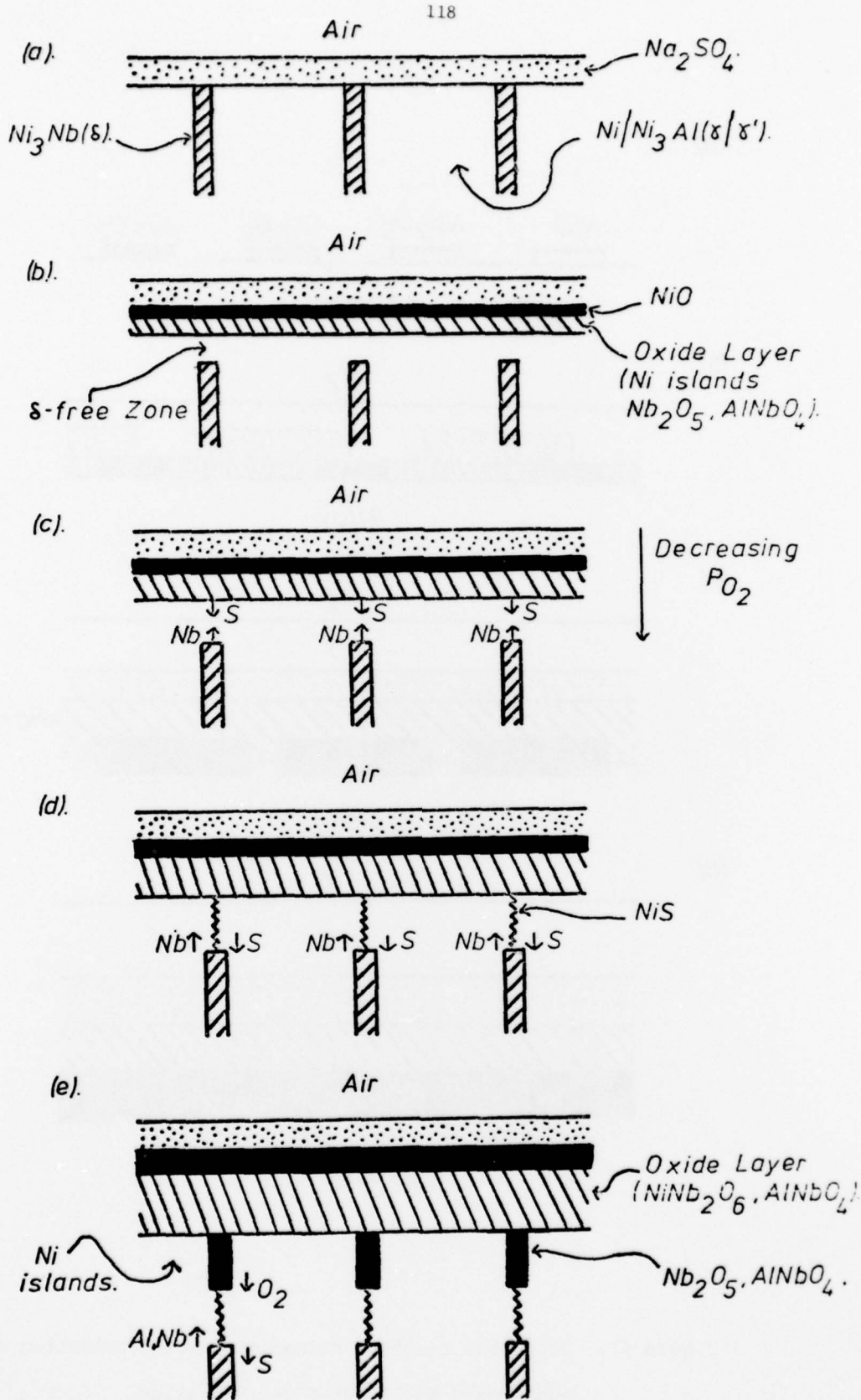


Figure 62. Schematic mechanism diagram for the hot-corrosion of both the ternary and quaternary alloys.

References

1. E.R. Thompson and F.D. Lemkey, *Trans. A.S.M.*, 61, 140 (1969).
2. F.D. Lemkey and E.R. Thompson, *Met. Trans.* 2, 1537 (1971).
3. H. Bibring and G. Siebel, *C.R. Acad. Sci., Paris Series C*, 268, 144 (1969).
4. J.L. Walters and H.E. Cline, *Met. Trans.*, 5, 1775 (1974).
5. E.R. Buchan and L.A. Tarchis, *Met. Trans.*, 5, 1413 (1974).
6. M.F. Henry, General Electric Report No. 73-C-RD-084 (1973).
7. M.G. Benz, General Electric Report No. 74-C-RD-191 (1974).
8. P.R. Sahn, "High Temperature Materials in Gas Turbines", p.73, Elsevier, Amsterdam (1974).
9. R.F. Vandermousen, P. Viatour, J.M. Drapier, and D. Coutsouradis, *Cobalt*, 39 (1973).
10. E.R. Thompson and F.D. Lemkey, *Met. Trans.*, 1, 2799 (1970).
11. E.R. Thompson, D.A. Koss, and J. Chesnutt, *Met. Trans.*, 1, 2807, (1970).
12. Conference on In-Situ Composites, Sept. 1972, Lakeville, Connecticut.
13. AGARD Conference Proc. No. 156 (1974).
14. E.J. Felten and F.S. Pettit, Paper presented to the Spring Meeting of the Metallurgical Society of A.I.M.E., Pittsburgh (1974).
15. J.G. Smeggil and M.D. McConnell, *Oxid. of Metals*, 8, 309, (1974).
16. J.G. Smeggil, *Oxid. of Metals*, 9, 31 (1975).
17. E.R. Thompson, F.D. George, and E.H. Kraft, United Aircraft Laboratories, Report No. N. 00019-70-C-0052 (1970).
18. E.R. Thompson, F.D. George, and E.H. Kraft, United Aircraft Laboratories, Report No. N. 00019-71-C-0096 (1971).
19. F.D. Lemkey, United Aircraft Laboratories, Report No. NAS 3-15562 (Prepared for NASA Lewis Research Centre).
20. F.D. Lemkey, United Aircraft Laboratories, Report No. NASA CR-2278 (Prepared for NASA Lewis Research Centre).



21. M.P. Arbuzov and V.P. Chaprina, *Izvest. V.U.Z., Fizika*, 75 (1969);  
*Met. Abst.* 4, 232 (1971).
22. R.F. Vandermousen, P. Vistour, J.M. Drapier, and D. Contsouradis,  
*Cobalt*, 39 (1973).
23. K. Fritscher, H. Gedanity, and G. Wirtn, Internal Report IB012-72/19,  
*Deutsche Forschung und Versuchsanstalt für Luft und Raumfahrt E.V.* (1973).
24. M.E. El Dahshan, D.P. Whittle and J. Stringer, *Cobalt*, 86 (1974).
25. P.A. Boiks and A.L. Moroz, *Poroshkovaya Met.*, 48 (1968); *Met. Abo.*, 1,  
503 (1968).
26. H. Bibring, G. Siebel and M. Rabinovitch, *Mem. Sci. Rev. Met.*, 69,  
431 (1972).
27. G.N. Irving, D.P. Whittle and J. Stringer, *Corr. Sci.*, 15, 337 (1975).
28. M.E. El Dahshan, D.P. Whittle and J. Stringer, Unpublished work.
29. J.G. Smeggil, General Electric Report No. 74-C-RD-026 (1974).
30. J.G. Smeggil, General Electric Report No. 74-C-RD-152 (1974).
31. F. Staub and E. Erdős, Private Communication.
32. M.E. El Dahshan, D.P. Whittle and J. Stringer, *Cobalt*, 182 (1972).
33. M.E. El Dahshan, D.P. Whittle and J. Stringer, *ibid*, 45 (1973).
34. M.E. El Dahshan, D.P. Whittle and J. Stringer, *Oxid. Met.*, 3, 179 (1974).
35. M.E. El Dahshan, D.P. Whittle and J. Stringer, *ibid*, 211 (1974).
36. D.M. Johnson, D.P. Whittle and J. Stringer, *Corr. Sci.*, 15, 649, (1975).
37. D.M. Johnson, D.P. Whittle and J. Stringer, *Werkstoffe und Korrosion*,  
26, 611 (1975).
38. D.M. Johnson, D.P. Whittle and J. Stringer, *Corr. Sci.*, 15, 721 (1975).
39. C.S. Giggins and F.S. Pettit, *J. Electrochem. Soc.*, 118, 1782 (1971).
40. F.H. Stott, G.C. Wood and M.G. Hobby, *Oxid. Metals*, 3, 103 (1971).
41. J.A. Goebel and F.S. Pettit, *Met. Trans.* 1, 1943 (1970).
42. J.A. Goebel, F.S. Pettit, and G.W. Goward, *Met. Trans.*, 4, 261 (1973).
43. S.K. Verma, D.P. Whittle, and J. Stringer, *Corr. Sci.*, 12, 545 (1972).

44. J.A. Goebel and F.S. Pettit, *Met. Trans.*, 1, 3421 (1970).
45. K. Kofstad and A.Z. Hed, *J. Electrochem. Soc.*, 116, 1542 (1969).
46. G.C. Wood, I.G. Wright, T. Hodgkiess and D.P. Whittle, *Werk. u. Korr.*,  
21, 900 (1970).
47. N.S. Bornstein and M.A. DeCrescente, *Trans. A.I.M.E.*, 245, 1947 (1969).

APPENDIXPublished Papers Acknowledging Support

- (1) "High Temperature Oxidation of Directionally Solidified Ni-Cr-Nb-Al ( $\gamma/\gamma'$ - $\delta$ ) Eutectic Alloys", J. Stringer, D.M. Johnson and D.P. Whittle, Oxidation of Metals, 12 (1978) 257-272.
- (2) "The Hot Corrosion of Directionally Solidified Ni-Cr-Nb-Al ( $\gamma/\gamma'$ - $\delta$ ) Eutectic Alloys", D.M. Johnson, D.P. Whittle and J. Stringer, Oxidation of Metals, 12 (1978) 273-291.
- (3) "The Oxidation Behaviour of Carbide Strengthened Directionally Solidified Eutectics", D.M. Johnson, D.P. Whittle and J. Stringer, in preparation.
- (4) "The Hot Corrosion of Carbide Strengthened Directionally Solidified Eutectics", D.M. Johnson, D.P. Whittle and J. Stringer, in preparation.